République Algérienne Démocratique et Populaire
Ministère de l'Enseignement Supérieur et de la Recherche Scientifique
Université A. MIRA-BEJAIA
Faculté de Technologie
Département de Génie Mécanique

THÈSE

Présentée par

LALAOUA Adel

Pour l'obtention du grade de

DOCTEUR EN SCIENCES

Filière : Génie Mécanique

Option : Énergétique et Rhéologie

Thème

Etude des instabilités dans les écoulements rotatifs : Application aux machines tournantes

Soutenue le : 28/10/2021 Devant le Jury composé de :

Nom et Prénom	Grade		
Mr SADAOUI Djamel	Professeur	Univ. de Béjaïa	Président
Mr NAIT BOUDA Faïçal	MCA	Univ. de Béjaïa	Rapporteur
Mme AMATOUSSE Nawel	Professeur	Univ. de Béjaïa	Examinateur
Mr DEBIANE Mohamed	Professeur	Univ. de USTHB	Examinateur
Mme MOKHTARI Faiza	Professeur	Univ. de USTHB	Examinateur
Mr NEBBALI Rezki	MCA	Univ. de Tizi Ouzou	Examinateur

Année Universitaire : 2020/2021

République Algérienne Démocratique et Populaire
Ministère de l'Enseignement Supérieur et de la Recherche Scientifique
Université A. MIRA-BEJAIA
Faculté de Technologie
Département de Génie Mécanique

THÈSE

Présentée par

LALAOUA Adel

Pour l'obtention du grade de

DOCTEUR EN SCIENCES

Filière : Génie Mécanique

Option : Énergétique et Rhéologie

Thème

Study of instabilities in rotating flows: Application to rotating machines

Soutenue le : 28/10/2021

Devant le Jury composé de :

Nom et Prénom	Grade		
Mr SADAOUI Djamel	Professeur	Univ. de Béjaïa	Président
Mr NAIT BOUDA Faïçal	MCA	Univ. de Béjaïa	Rapporteur
Mme AMATOUSSE Nawel	Professeur	Univ. de Béjaïa	Examinateur
Mr DEBIANE Mohamed	Professeur	Univ. de USTHB	Examinateur
Mme MOKHTARI Faiza	Professeur	Univ. de USTHB	Examinateur
Mr NEBBALI Rezki	MCA	Univ. de Tizi Ouzou	Examinateur

Année Universitaire : 2020/2021

بِسْمِ اللَّهِ الرَّحْمَنِ الرَّحِيمِ

اقْرَأْ بِاسْمِ رَبِّكَ الَّذِي خَلَقَ (1) خَلَقَ الْإِنْسَانَ مِنْ عَلَقٍ (2) اقْرَأْ وَرَبُّكَ الْأَكْرَمُ (3) الَّذِي عَلَّمَ بِالْقَلَمِ (4) عَلَّمَ الْإِنْسَانَ مَا لَمْ يَعْلَمْ (5) " **صدق الله العظيم**

بِسْمِ اللَّهِ الرَّحْمَنِ الرَّحِيمِ

قَالَ رَبِّ اشْرَحْ لِي صَدْرِي (25) وَيَسِّرْ لِي أَمْرِي (26) وَاحْلُلْ عُقْدَةً مِنْ لِسَانِي (27) يَفْقَهُوا قَوْلِي (28)

صدق الله العظيم

اهـــــداء

أهدي هذا العمل المتواضع:

إلى روح ابي العزيز وروح امي الغالية وروح اخي الغالي نبيل رحمهم الله جميعا و اسكنهم فسيح جنانه.

إلى أعز ما أملك في الوجود زوجتي الغالية نهاد التي أمدتني بزاد الإرادة والعزيمة وسبل النجاح.

إلى اخوتي (موسى. عمار. ضيف) و ا يتخالعزيزة (حبيبة).

إلى روح أخي العزيز براهيم، وزوجته زينة وابناءهم ايناس و**بومدين** واية.

الى اسراء تسنيم و اسلام ابناء اختي الغالية صليحة

الى عمي سعيد وحماتي سليمة والدي نهاد.

إلى كل من شجعني على تخطي الصعاب.

إلى زملائي وجميع الأساتذة الكرام.

إلى شهداء الواجب الوطني الذين سقطوا في ميدان الشرف.

تحيا الجزائر المجد والخلود لشهدائنا الابرار.

TABLE OF CONTENTS

Acknowledgements

First of all, I thank God the almighty for the grace, sustenance, strength and the knowledge given to me to complete this work.

I would like to express my profound appreciation and gratitude to Dr. Naït Bouda Faïçal who was exceptional in his support, advice, motivation, encouragement, and guidance, whose untiring efforts allowed the realization of this thesis.

Furthermore, I would like to thank Pr. SADAOUI Djamel, Pr. AMATOUSSE Nawel, Pr. DEBIANE Mohamed, Pr. MOKHTARI Faiza Ep. MERAH and Dr. NEBBALI Rezki for taking the time to review this thesis and serving as members of my doctoral committee. Their advices, recommendations, and comments are of great importance for the completion of this dissertation. I would like to extend my thanks to all the members of the Mechanical Engineering Department and the faculty of Technology of the university of Bejaïa for their support.

Most importantly, I am grateful to my wonderful wife Nihad. She has been patient, understanding, encouraging, and constantly interested in what I do, helping me through the inevitable frustrations of this long work. I also want to thank the members of my family, sisters (Zina, Habiba and Saliha) and brothers (Ibrahim, Moussa, Amer and Dhaïf) and specially: Ines, Boumediene, Aya, Israa and Islam; for their continued support in prayers, motivation, patience, encouragement, and endurance throughout the period I spent on this work.

During the course of this PhD, the guidance and support of certain individuals has proved very beneficial to my completion of the work. Special thanks goes to all my friends and colleagues, past and present, such as Ouali M'heni, Aiche Fazia, Guedifa Reda, Hamel rachid, Bezghoud Sidi Mohamed, Djebbour Ali, Kerboub Youcef, Hellalbi Amine and particularly Merah Karim, Adnane Elmahfoud and Azzam Tarik for all their support, the relationship established and their encouragement during this research. I would like to thank my friends and colleagues for keeping me sane over the years of study.

Finally, I wish to thank Belkajouh Tarik, Djeziri Amer and Ifferoudjen Reda for their emotional support and encouragement throughout the entire time I have spent studying for the PhD.

Special mention to my country, Algeria, with the hope that we someday find the road to science.

List of tables

Table **Page**

List of figures

Figure **Page**

List of Abbreviations

English letters

R_1 : Inner radius (m);

R_2 : Outer radius (m);

$R_{2min}=R_1+d_0$: radius of the outer cylinder for $\alpha=0$ (m);

$R_{2max}=R_{2min}+Htg\alpha$: Radius of the conical outer cylinder for $\alpha \neq 0$ (m);

H : Height of cylinder (m);

d : Annular gap (m);

(U, V, W) : Radial, axial and azimutal velocity components (m/s);

T : Temperature (°C)

TCF : Taylor Couete Flow;

TCPF : Taylor-Couette-Poiseuille flow;

CCF : Circular Couette Flow;

TVF : Taylor Vortex Flow;

WVF : Wavy Vortex Flow;

MWVF : Modulated Wavy Vortex Flow;

TTVF : Turbulent Taylor Vortex Flow;

LSF : Laminar Spirals Flow

SCF : Spherical Couette Flow;

CTCF : Conical Taylor-Couette flow;

HVBK model : Hall-Vinen- Bekharevich-Khalatnikov model;

PIV : Particle Image Velocimetry;

MHD : Magneto-Hydro Dynamic;

MRI : Magneto-Rotational Instability;

Greek Symbols

α : Apex angle (°);

r , θ, z : Radial, axial and azimuthal directions;

ρ : Density (kg/m^3)

$\eta=R_1/R_2$: Radius ratio;

$\Gamma=H/d_0$: Aspect ratio;

$\delta=d/R_1$: Ratio of the gap to the radius of the inner cylinder;

Ω_1 : Angular velocity of the inner cylinder (rad/s);

Ω_1 : Angular velocity of the outer cylinder (rad/s);

$\mu= \Omega_{1/} \Omega_2$: Rotation rate

υ : Kinematic viscosity (m^2/s);

ω_θ : Azimuthal vorticity;

$\Gamma = ru_\theta$: Angular momentum (m^2/s);

$B_1(k_m r)$: Bessel function of order 1

$\beta=(R_2-R_1)/R_1$: Gap width for spherical Couette flow;

$\Lambda=2d$: Axial wavelength (mm);

$\Delta = \nabla^2$:The Laplacian operator in the cylindrical coordinates:

y_p : Distance to the wall from the adjacent cell centroid (mm);

τ_w : Wall shear stress (Pa);

C_f : Skin friction coefficient;

ΔT : Temperature gradients (°C);

Dimensionless numbers

Ta : Taylor number;

Ta_c : Critical Taylor number

Re : Reynolds number;

Re_c : Critical Reynolds number;

Gr : Grashof number

$Ri = Gr/Re^2$: Richardson number

$Re_z = Re_{axial}$: Reynolds number related to the Poiseuille flow;

Ha : Hartmann number;

Subscripts

i/in : Inner

o/out : Outer

CHAPTER I

General Introduction

« As far as the laws of Mathematics refer to reality, they are not certain; as far as they are certain, they do not refer to reality »

Albert. Einstein

Chapter I: General introduction

The objective related to the study of rotating flows lies, among other things, in the prediction of instabilities that occur during their development from the stable laminar state to the developed turbulent state. Therefore, a satisfactory explanation of the phenomena of instability and an overall understanding of their evolution would make it possible to establish a theory capable of predicting most secondary movements in connection with the emergence of chaos and the onset of turbulence. This is the major concern of physical hydrodynamics to date. In addition, the development of new calculation codes has led, in recent decades, to the advent of computational power-based numerical simulations to address physical processes with increasingly complex characters. Therefore, with the use of calculation codes, it is possible to choose simple prototype situations to draw the different properties and thus a better understanding of the physical phenomena involved. Examples include flat flow, flow between parallel walls, flow in circular or rectangular pipe, flow around cylinder, sphere or disk, etc....

On the other hand, the examination of flows between two coaxial cylinders, between coaxial spheres, between coaxial cones or combination between them remain difficult to understand because of the three-dimensional and unsteady nature of the transition process, which is phenomenologically more complex than the simple geometries mentioned above. Further, this flow problem occupies a privileged place because of the importance and role played in the conditions of instability and the gradual degradation of order towards the disorder in hydrodynamics of chaos.

Furthermore, the study of rotating flows is currently the subject of several works and constitutes a great phenomenological wealth, particularly in the analysis of fundamental physical processes; laminar-turbulent transition. Moreover, Rotating flows occur in many technical systems and in nature, such as rotating tube heat exchangers, chemical mixing filtration, bearing chambers, flotation cells and extractors, pumps for the oil and water industries as well as in the drilling of oil wells, where mud flows between the drilling rod and the well casing, to remove the cuttings and wastewater treatment. Among the most widely used rotating flow systems, the device known as Taylor-Couette, fluid evolving in an annular gap between two rotating bodies, which is most famous for its role in the development of hydrodynamic stability theory and for the wide variety of flow regimes that it can exhibit depending on the Reynolds or Taylor number. Moreover, it is this type of flow system that has been adopted to model natural phenomena in atmospheric physics

(meteorology), citing the example of Hadley circulation cell (Fig. I.1) and in astrophysics to study the atmospheric dynamics of planets, an example of the great red spot of Jupiter (Fig. I.2). Also, in Geophysics, as part of the study of the dynamo effect governing the Earth's mantle (Fig. I.3).

On the industrial side, the Taylor-Couette system plays an important role because of its many and diversified links with technology and engineering applications. There are many applications, including the technology using turbines that are integrated into alternators in power plants, turbines found in turboreactor engines in Avionics (Fig. I.4) and centrifugal pumps used in the chemical and pharmaceutical industries (Fig. I.5). Another area of great importance is the systematic use in tribology to establish optimal lubrication conditions for gearbox bearings in the automotive, aerospace and power generation industries (Fig. I.6). It is also used in filtration systems to purify wastewater or body fluids such as blood (Fig. I.7). Recently, this flow system has been used in an important research area like biomedical, a Paracorporeal Respiratory Assist Lung (PRAL), to treat a prevalent lung disease, Chronic Obstructive Pulmonary Disease (COPD). The PRAL is comprised of an annular hollow fiber membrane bundle that is rotated to increase the gas exchange efficiency of the device and pump blood. Thus, the proprieties of Taylor-Couette flow is utilized to provide CO2 removal at a low blood flow rate for the treatment of respiratory failure, particularly acute exacerbations of Chronic Obstructive Pulmonary Disease (Fig. I.8). It is also a subject of widespread practical interest owing to its direct connection with engineering applications including, rheology of blood (hemorheological) (Fig. I.9), cooling of electric motors (Fig. I.10), and as a crystallization separate process system (Fig. I.11). Furthermore, the Taylor– Couette flow reactor is employed as a new method to produce a single- or few-layer graphene oxide from bulk graphite with high yields in a significantly shortened reaction time (Fig.I.12).

The main objective of our study is to numerically simulate the fluid flow between two concentric bodies, the inner element rotates and the outer one is kept stationary. In general, works on the Taylor-Couette flow are carried out in complex situations with a geometric modification or with a superposition of another type of flow. Studies carried out with geometric modifications belong to the class of confined flows. The flow patterns and the instabilities between rotating bodies and combinations of them are investigated. These can be regarded as part of the large domain of the flows in rotating systems. Special emphasis is placed on the first onset and the further development of instabilities. For a better understanding of these different flow structures we have striven to illuminate the situation by the use of simple models. For these we have varied the geometry but retained certain boundary conditions to provide a suitable basis of comparison. All the bodies tested, cylinders, spheres, and cones are bodies of revolutions with symmetry about the axis of

rotation. Therefore, the aim of this research is to provide further details on the flow features in the annulus between different coaxial bodies.

This thesis is organized into seven chapters as follow:

Chapter one is the introductory chapter and is intended to summarize the background and the motivation for which this research study was carried out, the aims and objectives of this present research as well as an outline of the structure of the thesis.

Chapter two provides a concise literature review of the available research to date on the flow behaviour as well as documentation on the theories of fluid instability in concentric rotating bodies. We also propose to perform an analysis of the effect of different parameters on the occurrence of various instabilities in order to derive some physically interesting properties. Thus, we discuss the thermal, rheological, dynamic and geometric effects influencing the evolution of the laminar-turbulent transition in the Taylor-Couette flow. Thereafter, we propose to carry out a synthesis of previous works on the appearance of different hydrodynamic instabilities in modified Taylor-Couette flows (by a variation of the cylindrical geometry to spherical, conical and ellipsoid configuration) in order to analyze and clarify the existing analogies between the different rotating flow systems.

Chapter three gives an overview of current CFD modeling techniques including the basic principles of CFD. The numerical methodology, including the numerical scheme, the governing equations (continuity and momentum equations), and convergence criteria employed for this study are discussed.

Chapter four describes the CFD modeling of the effect of the cylinders-spheres combinations on the onset of different instabilities of a fluid confined between two concentric bodies. The modeling strategy was developed by studying three types of flow configurations: cylindrical Taylor-Couette flow (with fixed endcaps), flow between two concentric cylinders with hemispheres on the lower end wall, and flow between two coaxial spherocylinders (cylinders with hemispheres on the upper and lower end surfaces). Thus, chapter details the CFD geometry and problem formulation, the mesh generation, the discretization scheme for the pressure and the moment equations, the boundary conditions, the convergence criteria as well as the discussion of the obtained results from the CFD predictions. The work presented in Chapter IV has been published in the European Physical Journal Plus.

Chapter five discusses, the influence of the working fluids confined inside an infinite aspect ratio Taylor-Couette system on the onset of cellular pattern. The main goal of this work is to show how the change in cellular pattern operates when changing the working fluid by simulating and comparing four different liquids namely hydrogen, helium, lithium and water. The work presented in Chapter V has been published in the Journal of the Brazilian Society of Mechanical Sciences and Engineering.

Chapter six concerns the numerical investigation of the fluid motion in an annulus between cylinder-cone combinations. The transitional phenomena occurring in this flow are discussed under the effect of opening angles of the outer cylinder. The main goal it is to show how operates the change in the structure of the movement when changing the geometry of the flow through angular deviation, i.e., from coaxial rotating cylinders to an inner cylinder rotating in a conical container. The work presented in Chapter VI has been published in the European Physical Journal Applied Physics.

Chapter seven presents a three-dimensional computational fluid dynamic of the flow of an electrically conducting fluid, liquid sodium, in an annulus between two concentric rotating spheres subjected to a dipolar magnetic field. The work presented in Chapter IV has been published in Topical Problems of Fluid Mechanics.

Finally, conclusions are drawn on the research work in this thesis, specifically, the different modelling strategy has been exposed. From the conclusions, recommendations for further work are made.

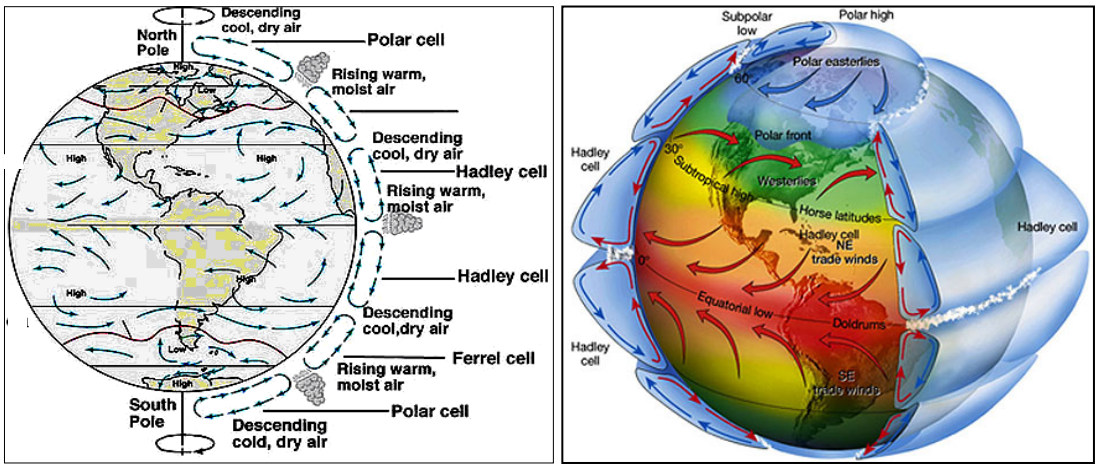

Figure I.1: Hadley circulation cell.

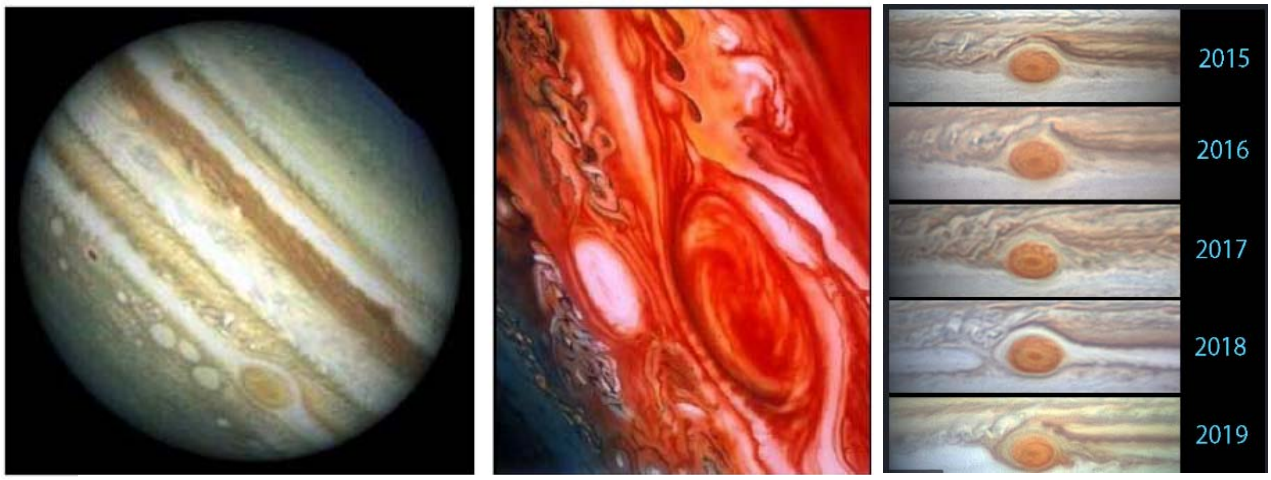

a) b) c)

Figure II.2: (a) Picture of Jupiter showing its three White Ovals and its great Red spot .

(b) Zoom on the great Red spot and a White Oval.

(c) Development of the great Red spot.

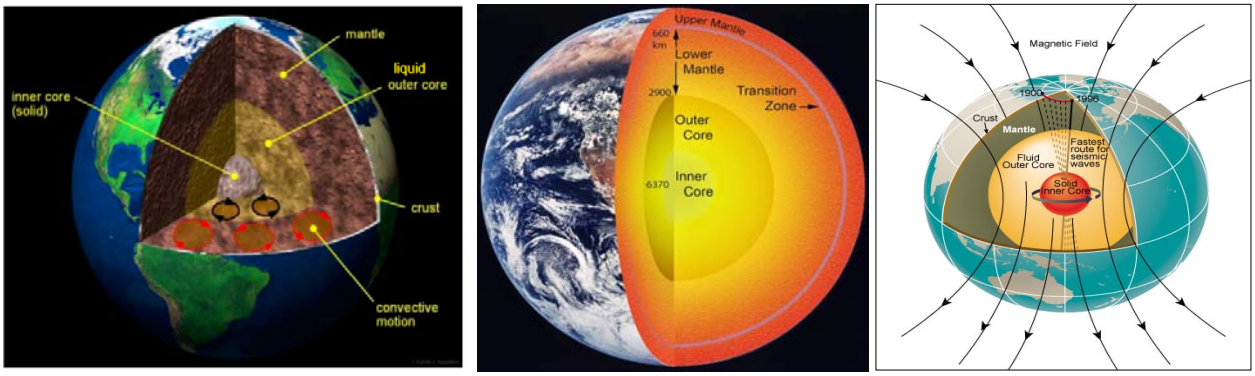

Figure II.3: Dynamo effect governing the Earth's mantle

a) Schematic of a turboreactor b) Turboreactor Rolls-Royce c) Lab-scale prototype of a turboreactor

Figure I.4: Turboreactor (stator-rotor).

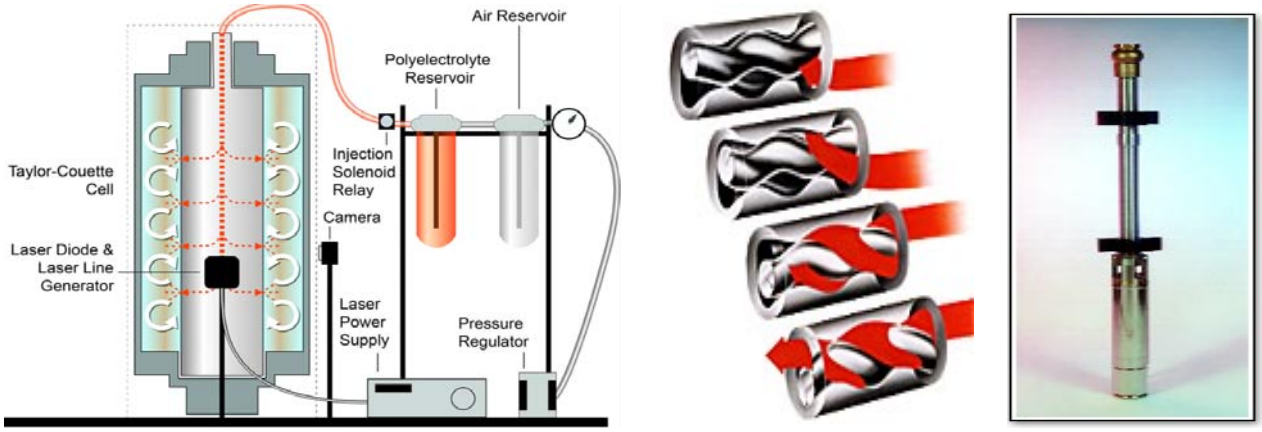

Figure I.5: Centrifugal pumps used in the chemical and pharmaceutical industries.

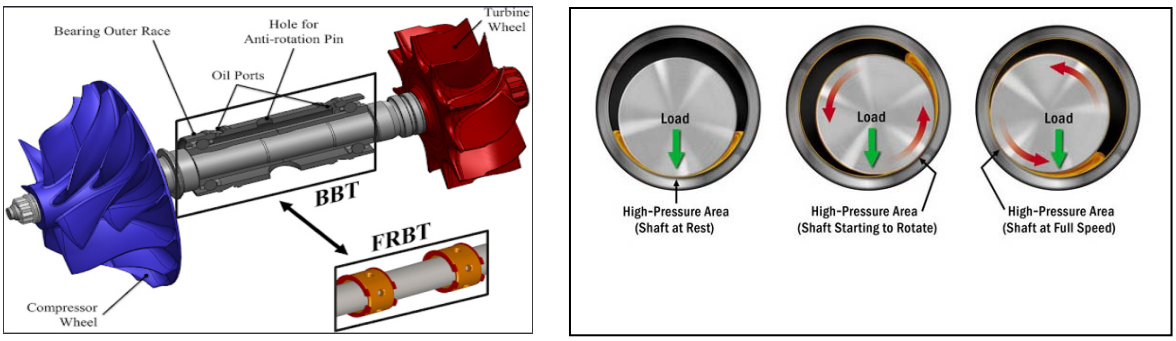

a) Bearing consisting of two concentric cylinders b) Bearing consisting of two eccentric cylinders

Figure I.6: Tribology of gear transmission bearings in rotating machines.

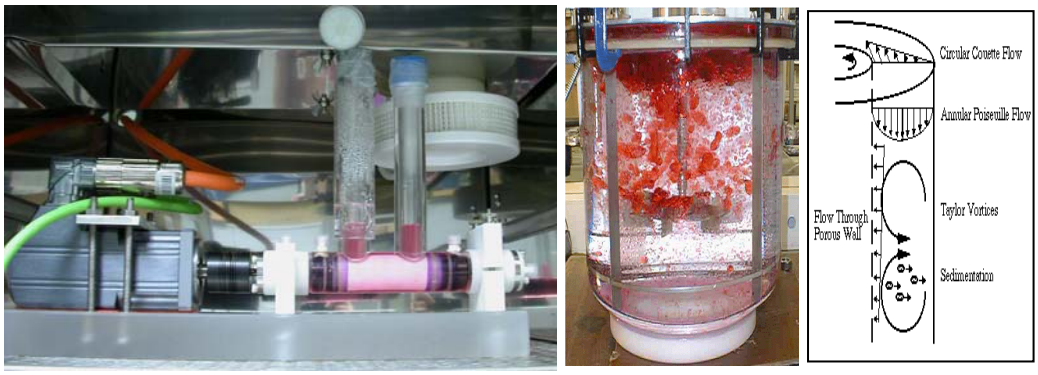

Figure I.7: Filtration system using Taylor-Couette flow reactor with porous inner cylinder.

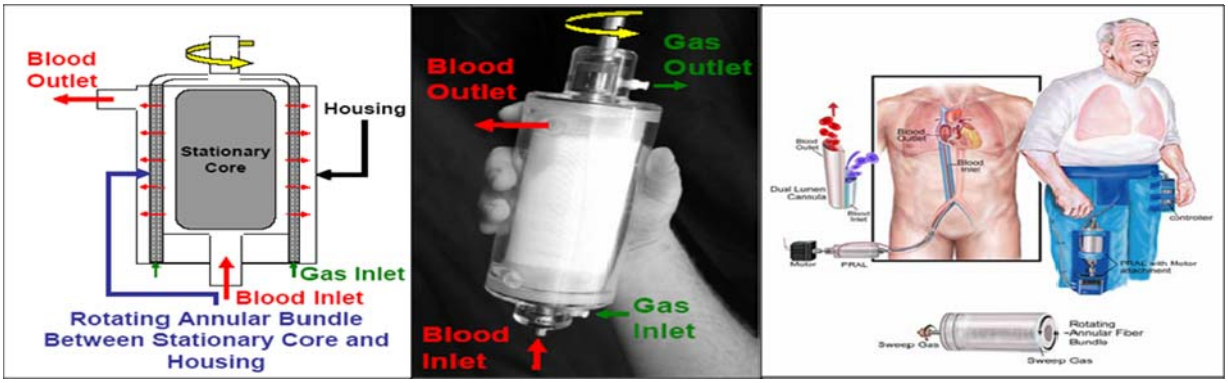

a) Schematic of PRAL b) PRAL prototype c) Schematic of PRAL connected to patient

Figure I.8: Paracorporeal Respiratory Assist Lung (PRAL): *A Paracorporeal Respiratory Assist Lung is configured with an annular cylindrical hollow fiber membrane (fiber bundle) that is rotated at rapidly varying speeds. Blood is introduced to the center of the device and is passed radially through the fiber bundle. The bundle is rotated at rapidly changing velocities with a rotational actuator. The rotation of the fiber bundle provides centrifugal kinetic energy to the fluid giving the device pumping capabilities and may create Taylor vortices to increase mass transfer. Rotation of the fiber bundle increases the relative velocity between the fluid and the hollow fibers and increases the mass transfer. The porosity of the fiber bundle may be varied to enhance gas exchange with the blood.*

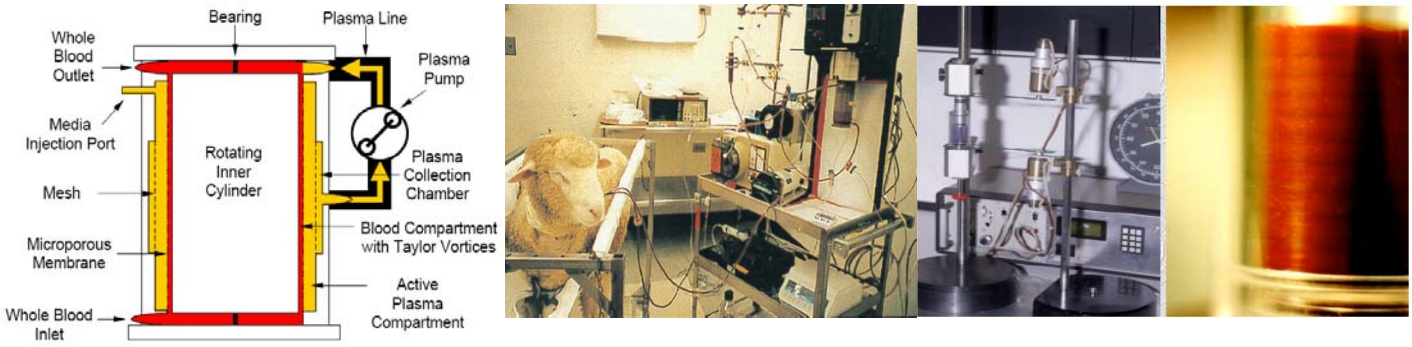

Figure I.9: Experimental set up for hemorheological studies (Schematic, device of Taylor-Couette system and Taylor vortices for blood). *Bands of dark and light red are distinguishable. Dark red regions have high concentration of red blood cells. Distance between two dark red regions equals gap width.*

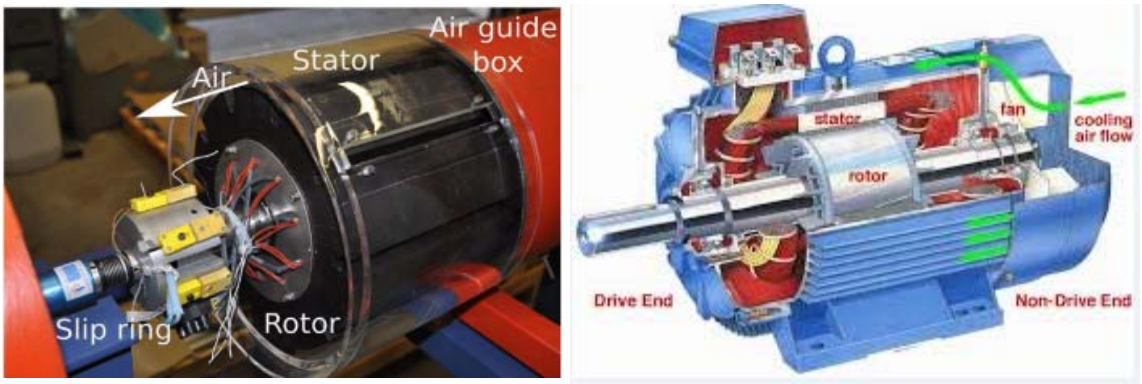

Figure I.10: Cooling of electric motors.

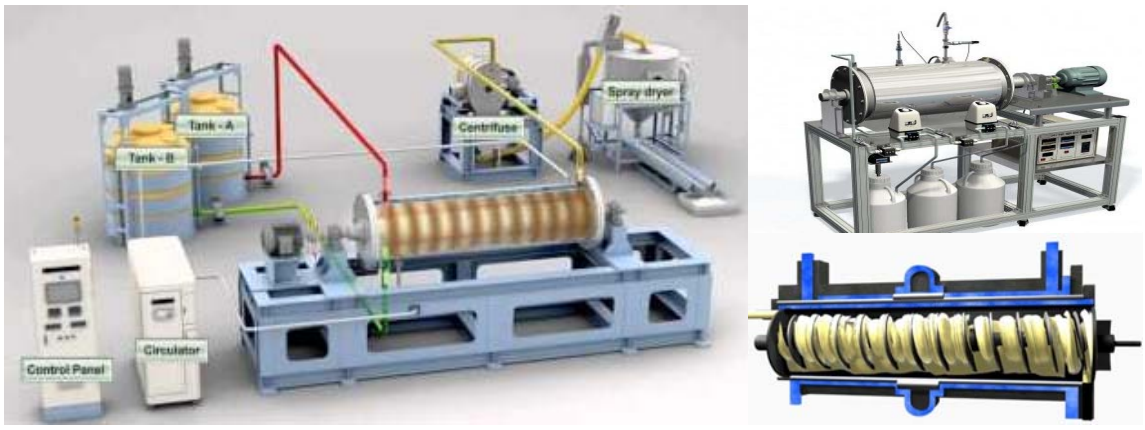

Figure I.11: Continuous Crystallization Separate Process System" known as Taylor-Couette Crystallizer".

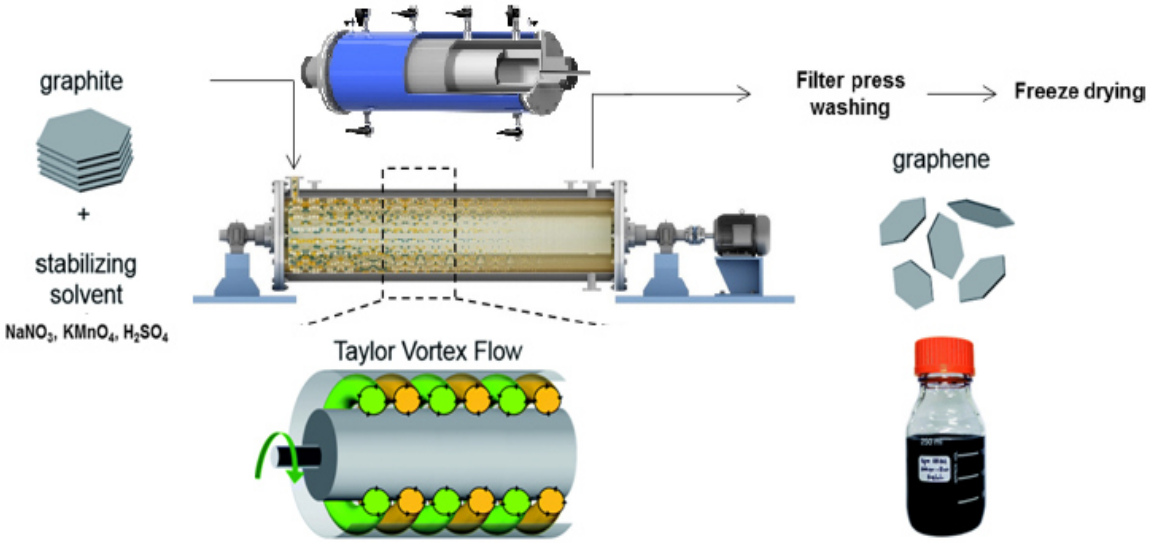

Figure I.12: Oxidation reaction of graphite flakes in the Taylor-Couette flow reactor.

CHAPTER II

Literature Review

« Its seems doubtful whether we can expect to understand fully the instability of fluid low without obtaining a mathematical representation of the motion of a fluid in some particular case in which instability can actually be observed, so that a detailed comparison can be made between the results of analysis and those of experiment. »

Geoffrey. Ingram. Taylor

CHAPTER II : LITERATURE REVIEW

II.1 Introduction

People have been investigating the hydrodynamic stability of rotating fluids between two cylinders, both experimentally and analytically, for more than one hundred years. Why did such an apparently "simple problem" become so popular? In fact, investigators were amazed to see the wealthy variety of flow patterns that occur, for example, when the speed of the inner cylinder is increased and the outer cylinder is at rest. One attractive feature of these patterns is their degree of symmetries, both spatially and temporally. For example, the circular Couette flow (CCF) and Taylor vortex flow (TVF) are axisymmetric along the axis of the cylinders and are time-independent when the speed of the inner cylinder is low. However, as the angular velocity of inner cylinder increases, the flow pattern becomes more and more complicated, breaking more and more symmetries both spatially and temporally. With the increase of the inner cylinder speed, the Taylor vortex flow is replaced by wavy vortex flow (WVF), which is non-axisymmetric and time-dependent. Eventually the flow becomes turbulent, containing large-scale structures with many degrees of symmetry. This model problem then appears as an ideal example of a system that progressively approaches turbulence, which is still one of the challenging problems in the field of fluids.

II.2 Historical investigations of the Taylor-Couette flow

The history of Taylor-Couette flow is a long and storied one. The literature concerning pattern forming bifurcations driven by inner and/or outer cylinder rotation and their role in the supercritical transition to turbulence is extensive (see, e.g., the book by Koschmieder [1], the bibliography compiled by Tagg [2], the review articles by Tagg [3] and by Di Prima and Swinney [4], and the expansive study by Andereck et al. [5]).

The first theoretical discussion of the flow between concentric cylinders is attributed to Newton in 1687 [6]. In 1848, Stokes [7] investigated the flow between two rotating cylinders. He showed that the azimuthal velocity v_θ as a function of the radial position r is given by:

$$v_\theta(r) = Ar + \frac{B}{r}, \qquad \text{(II.1)}$$

where

$$A = -\Omega_1 \frac{\eta^2 - \mu}{1 - \eta^2} \text{ and } B = \Omega_1 R_1^2 \frac{1 - \mu}{1 - \eta^2} \qquad \text{(II.2)}$$

R_1 and R_2 are the radii of the inner and outer cylinders, respectively, Ω_1 and Ω_2 are their angular frequencies of rotation, $\mu = \Omega_1/\Omega_2$, and $\eta = R_1/R_2$. The axial and radial components of velocity v_z and v_r are zero. Today, this flow is known as circular Couette flow (CCF).

The final two decades of the 19th century saw a great number of researchers turning their attention to the study of flows between concentric cylinders. In 1881, Margules derived a formula that allowed the measurement of fluid viscosity by measuring the torque exerted by the fluid on one of the cylinders in a Taylor-Couette configuration as the other was rotated at constant speed [8]. Later, Couette and Mallock conducted experiments in apparatus driven by electric motors publishing their initial results in 1888. Mallock's paper is mostly concerned with measurements of the viscosity of water, which he measured by rotating the outer cylinder and measuring the torque on the inner cylinder [9]. In this paper, Mallock notes the presence of a secondary flow due to the finite size of his apparatus. In 1896, Mallock discussed the effect of inner vs. outer cylinder rotation and system size on his viscosity measurements, as well as his efforts to minimize end wall effects [10].

Couette [11] described a series of experiments in which he measured the viscosities of water and air using a concentric cylinder apparatus of his own design in which the outer cylinder was driven by an electric motor.

Motivated by meteorological considerations, Lord Rayleigh [12]derived a general criterion for the stability of rotating, inviscid flows. Rayleigh's argument proceed as follows: A rotating fluid in equilibrium will flow in such a way that the centrifugal force is balanced by the radial pressure gradient, i.e. $\partial p/\partial r = \rho v(r)^2/r$. Suppose that a fluid element originally at $r = R_1$ is moved outward to a new radial position R_2. The flow will be stable if the fluid element experiences a restoring force that tends to move it back toward its original position. For an incompressible fluid this requires that $v(R_2)^2/R_2 > v(R_1)^2/R_1$ for all $R_2 > R_1$. Mathematically, this can be expressed in terms of the angular velocities ($\Omega = v/r$) as:

$$\frac{d(rv)^2}{dr} = \frac{d}{dr}(r^2\Omega)^2 \rangle 0 \qquad \text{(II.3)}$$

Rayleigh applied this criterion to the inviscid flow between concentric cylinders and arrived at the conclusion that such flows are always unstable when the inner cylinder rotates and the outer cylinder is stationary and always stable when the outer cylinder rotates and the inner cylinder is stationary. The more general case can be evaluated by inserting the velocity profile derived by Stokes (Equation II.1) into Equation II.3, resulting in the constraint that when the flow is stable.

$$\frac{\Omega_2}{\Omega_1} \rangle \left(\frac{R_1}{R_2}\right)^2 \qquad \text{(II.4)}$$

If we denote that $\mu = \Omega_2/\ \Omega_1$ and $\eta = R_1/R_2$, this relation can be illustrated with the stability diagram in Figure II.1. Here it can be seen that the Taylor-Couette flow of an inviscid fluid will be unstable for all counter-rotating flows or whenever the ratio of the angular velocity of the outer cylinder to that of the inner cylinder is less than the square of the radius ratio

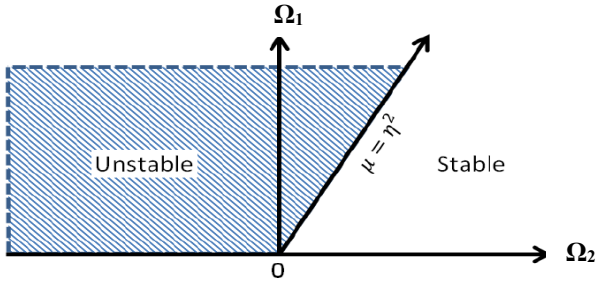

Figure II.1: Rayleigh's stability criterion for inviscid Taylor-Couette flow. Adapted from ref. [5].

In 1921 Geoffrey Ingram Taylor, inspired by the theoretical work of Lord Rayleigh and others, began work on a concentric cylinder apparatus [13, 14]. He successfully applied linear stability theory to the viscous flow between concentric cylinders and was able to calculate the critical condition for instability in terms of the rotation rates of the cylinders, their radii, and the fluid viscosity in the narrow gap approximation, i.e. as the radius ratio η=1. Taylor concluded that viscosity played a stabilizing role in some flows that would otherwise be unstable according to Rayleigh's criterion (Equation II.4). Taylor predicted that flows where the outer cylinder rotation dominates (i.e., when the cylinders co-rotate and the angular velocity of the outer cylinder is greater than that of the inner cylinder, so that $\mu > +1$, or when the inner cylinder is held fixed, so that $\mu = \pm\infty$) should be linearly stable at all rotation rates and derived more detailed stability criteria for general co- and counter-rotating flows. Taylor's results are summarized in Figure II.2.

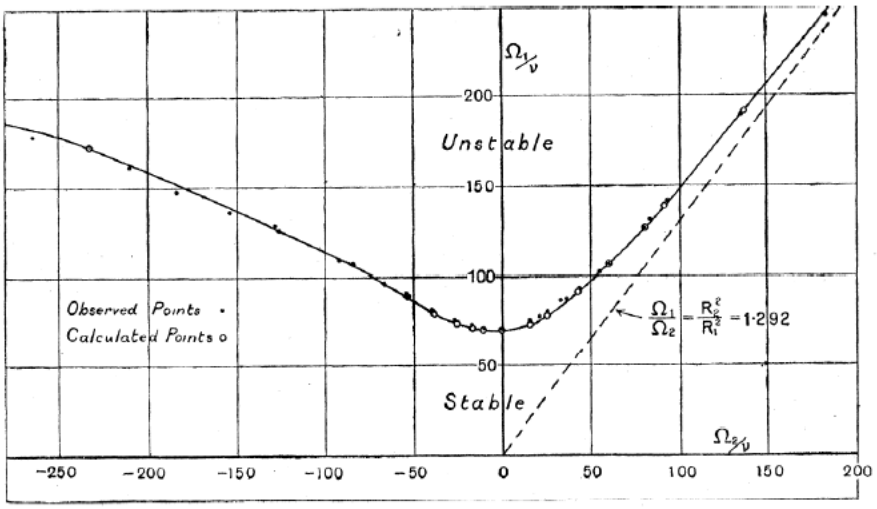

Figure II.2: Stability diagram for Taylor-Couette flow. Open circles correspond to the theoretically predicted stability boundary. Closed circles correspond to the experimentally observed stability boundary. Adapted from ref. [14].

Wendt [15] reported the first measurements of the velocity and pressure distributions inside the gap, as well as measurements of the torque transferred between the cylinders for a range of aspect and radius ratios.

The understanding of Taylor's flow remained at the same stage for several decades until Chandrasekhar's work in 1954 [16]. He presented the solution of the stability problem for any value of the rotational rate ($\mu=\Omega_2/\Omega_1$) assuming a small annular space between cylinders. A few years later, in 1958, Chandrasekhar [17] presented the first study of the problem of stability between two rotating cylinders for a large annular space ($\eta=0.5$). In 1965, Coles [18] at Caltech was beginning what would become a monumental, decade-long study of flow transitions in Taylor-Couette flows. Coles's study was originally inspired by the lack of experimental data on the transition to turbulence in the absence of the Taylor instability. His initial experiments were carried out in a large apparatus and used air as the working fluid. Coles performed detailed hot wire measurements for cases where one cylinder rotated and the other was at rest, as well as cases where both cylinders rotated. Coles reported that the transition to turbulence dominated by centrifugal instability was governed by the emergence of a series of progressively more complicated patterns, which were reflected by the hot wire spectra. He called this route to turbulence "transition by spectral evolution". Moreover, his extensive study showed that for a given Re_i above the linear stability boundary as many as 26 states with differing azimuthal and axial wave numbers could be observed. These states are now collectively known as wavy Taylor vortices (WVF) and (along with other supercritical flow regimes of Taylor-Couette flow) have been the subject of intense study in the decades since Coles's pioneering work.

Gollub and Swinney [19] and Fenstermacher et al. [20] studied the temporal properties of the flow field for increasing Reynolds numbers beyond the first critical Reynolds number by using an optical heterodyne technique to measure the time dependence of the radial component of velocity at a fixed point. Furthermore, Andereck et al. [5] conducted an experimental investigation in which both cylinders were rotated in different directions and both cylinders were rotated in the same direction. They observed several flow regimes, including Taylor vortex flow, wavy vortex flow, Modulated Wavy Vortex Flow (MWVF), Laminar Spirals Flow (LSF), interpenetrating spirals, spiral turbulence, turbulent Taylor vortex flow, and various combinations of these flows. These flow regimes are shown in Figure II.3.

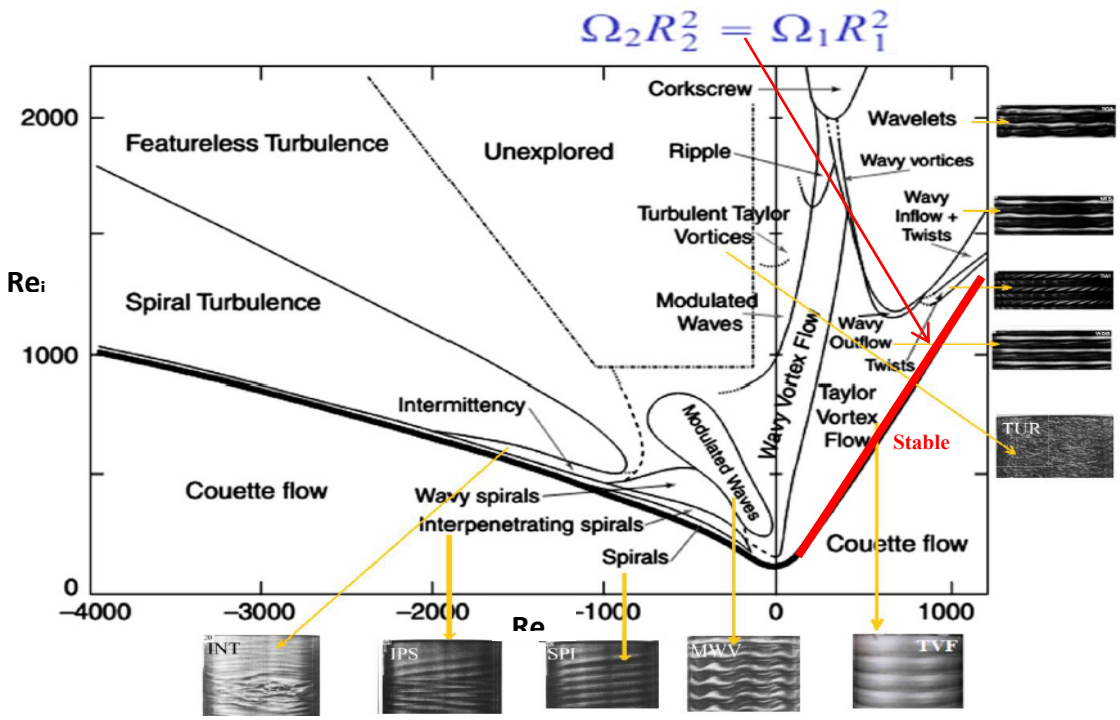

Figure II.3: Flow regimes between independently rotating concentric cylinders. Adapted from ref. [5].

In addition, Lathrop et al. [21] examined the behaviour of the Taylor -Couette system over the Reynolds number range $800 \leq Re \leq 1.23 \times 10^6$ using high-precision torque measurements, local wall shear stress measurements, and flow visualization. They found that, above a non-hysteretic transition Reynolds number, $Re = 1.3 \times 10^4$, the closed system behaves like open wall-bounded shear flows (pipe flow, duct flow and flow over a flat plate) at high Reynolds numbers. Czarny et al. [22] performed a direct numerical simulation using a three-dimensional spectral method of a short finite-length annular flow (η=0.75 and Γ=6) driven by counter-rotating cylinders. The numerical model predicted two different flow regimes, wavy vortices and interpenetrating spirals. Moreover, Heise et al. [23] and Abshagen et al. [24] studied the nonlinear dynamics of Taylor vortex flow (TVF) and wavy vortex flow (WVF) in an attempt to understand several bifurcation processes exhibited in the TCF for the wide gap problem. Manneville and Czarny [25] studied the aspect ratio dependency of Taylor vortices for the wide gap problem. Abshagen et al. [26] also carried out experimental investigation on the multiplicity of states in Taylor-Couette flow, which appeared due to the axial localization of the azimuthal traveling wave for wide gap problems. This led López et al. [27] to conduct a numerical analysis in an attempt to better understand the multiplicity of states found in Abshagen et al. [26]. In the work of Martinand et al. (28), stability analysis had been used in the Taylor vortex flow and the wavy vortex flow for radius ratio 0.55 and Re ranging between 69 and 210. This study had reported that the cause of the transition between Taylor vortex flow and wavy vortex flow is not the same in the narrow gap and wide gap problems. More

recently, Razzak et al. [29] investigated the possible sources of nonaxisymmetric disturbances and their propagation mechanism in Taylor-Couette flow for wide gap problems using a direct numerical simulation with a radius ratio of 0.5 and the Reynolds number (Re) ranging from 60 to 650. Their results show that an axisymmetric Taylor-vortex flow occurs when Re is between 68 and 425. Above Re = 425, transition from axisymmetric to non-axisymmetric flow is observed up to Re = 575 before the emergence of wavy-vortex flow, as illustrated in Figure II.4**.**

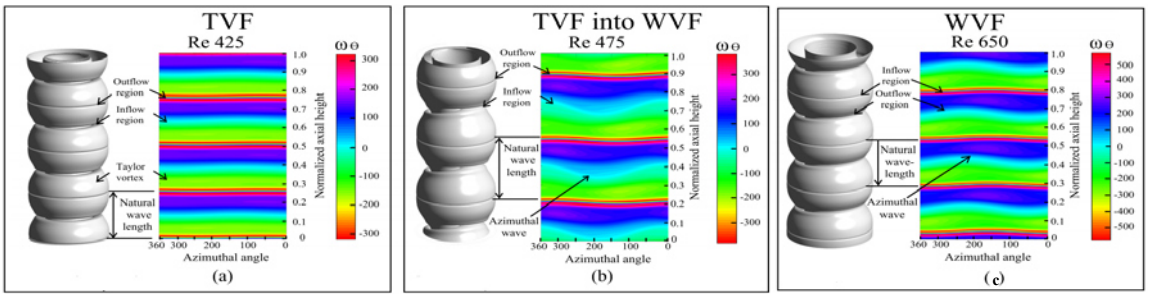

Figure II.4: The azimuthal vorticity (ω_θ) contour around 360° at the mid annulus location: (a) ω_θ contours in the TVF, (b) ω_θ contours in the transition of TVF into WVF, and (c) ω_θ contours in the WVF. Adapted from Ref. [29].

II.3 Theories of fluid instability in concentric cylinders

In this section, some of the known theories of fluid instability in concentric cylinders are reviewed. Since the work of Rayleigh and Taylor on instability, theories predicting the growth of the Taylor vortices and the mechanism of flow instability with further increase of speed were proposed by many investigators. These theories include: (II.3.1) Rayleigh criterion (II.3.2) The linear stability theory, (II.3.3) The energy method, (II.3.4) The weak nonlinear stability theory**,** and (II.3.5) Non-linear theory.

II.3.1 Rayleigh criterion for instability

The first hydrodynamic stability criterion for inviscid fluids was derived by Rayleigh in 1917 [12] who formulated a stability criterion for the mean viscous flow between two concentric rotating cylinders which was based on the inviscid perturbation equations. Rayleigh considered a basic swirling flow of an inviscid fluid which moves with angular velocity Ω about the axis of rotation. The equations of motion allow Ω to be an arbitrary function of the distance r from the axis, provided the velocities in the radial and axial directions are zero. Rayleigh did not establish his criterion for stability by an analytical discussion of the relevant perturbation equations but by a simple physical argument.

The kinetic energy of the fluid contained in two elemental rings with r = R_1, and r = R_2, with equal volumes dV can be expressed as:

$$\frac{1}{2}\rho(\Gamma_1^2 R_1^{-2} + \Gamma_2^2 R_2^{-2})dV \qquad (II.5)$$

where Γ (= ru_θ) is the angular momentum of a fluid element per unit mass.

Assuming the fluids contained in the two elementary rings are interchanged, as the angular momentum of an element of the inviscid fluid is constant, the resulting kinetic energy is:

$$\frac{1}{2}\rho(\Gamma_1^2 R_2^{-2} + \Gamma_2^2 R_1^{-2})dV \qquad (II.6)$$

The change in the kinetic energy as a result of the interchange is:

$$\frac{1}{2}\rho(\Gamma_1^2 R_2^{-2} + \Gamma_2^2 R_1^{-2})dV - \frac{1}{2}\rho(\Gamma_1^2 R_1^{-2} + \Gamma_2^2 R_2^{-2})dV \qquad (II.7)$$

The change in the kinetic energy is therefore proportional to

$$(\Gamma_2^2 - \Gamma_1^2)(R_1^{-2} - R_2^{-2}) \qquad (II.8)$$

Suppose that $R_2 > R_1$, then the change in kinetic energy is negative provided $\Gamma_2^2 > \Gamma_1^2$ and positive if $\Gamma_2^2 < \Gamma_1^2$. Thus, if Γ^2 decreases with r anywhere, this would increase the kinetic energy and would imply instability. On the other hand, if Γ^2 increases with r, this would lower the kinetic energy and would imply stability. This is simply Rayleigh's criterion which states that the necessary and sufficient condition for a distribution of angular velocity $\Omega(r)$ to be stable (to axisymmetric disturbances) is when the condition

$$\frac{d}{dr}(r^2\Omega)^2 \rangle 0 \qquad (II.9)$$

is satisfied everywhere in the flow field and that the distribution of angular velocity $\Omega(r)$ is unstable if $(r^2\Omega)^2$ decreases with increasing r anywhere inside the flow field.

This can be expressed as the stability criterion:

$$(R_2^2\Omega_2)\rangle(R_1^2\Omega_1) \qquad (II.10)$$

However, Rayleigh's stability criterion can only be applied to the case of inviscid flow or when the effect of viscosity is assumed not to affect the onset of instability. In addition, Rayleigh's physical arguments were based on axisymmetric disturbances to the flow. At a low rotational speed, viscosity damps the perturbations, thereby preventing the formation of vortices. For such a case, the flow develops as a basic Couette flow for the case of a fluid between two concentric rotating cylinders. This implies that another theory is needed to deal with viscous fluid flow. This gives rise (drove) to the development of a linear instability theory where transition to instability is governed by the critical Taylor number, depending on the radius ratio of the cylinders and on the rotational speeds.

II.3.2 Linear theory of instability

Taylor [14] was the first to successfully apply linear stability theory to a specific incompressible fluid dynamic problem and succeeded in obtaining quantitative agreement between theory and experimental results for the onset of the flow instability between two

concentric rotating cylinders. In contrast to Rayleigh's analysis, Taylor considered an incompressible viscous fluid in steady motion between two infinitely long concentric cylinders, which are rotated about a common axis with constant angular velocity Ω_1 at $r = R_1$ and Ω_2 at $r = R_2$ where $R_2 > R_1$. One of the aims was to determine the velocity distribution within the annulus. Taylor assumed a Bessel function series solution for the streamwise velocity perturbation u_1 as:

$$u_1 = \sum_{m=1}^{\infty} a_m B_1(k_m r) \qquad (II.11)$$

where $B_1(k_m r)$ is a Bessel function of order 1 and k_m is the m^{th} wavenumber. This satisfies the conditions $u_1 = 0$ at R_1 and R_2. Taylor substituted the solution of Equation II.11 into the momentum perturbation equations to obtain the complete solution for v_1 and w_1.

A system of linear homogenous equations in a_m, $1 \leq m \leq \infty$, was obtained by Taylor after the application of the boundary conditions $u_1 = v_1 = w_1 = 0$ at $r = R_1$ and $r = R_2$ Taylor was able to eliminate all the unknowns from the equations of disturbed motion since the number of the unknowns is the same as that of the equations. The resulting equation takes the form of an infinite determinant equating to zero, which can be regarded as an equation to determine the growth rate q of a given initial harmonic type disturbance. Taylor used the solution as a criterion for the stability of a given initial disturbance and concluded that if the value of q is real, then the motion is stable or unstable according as whether q is negative or positive. Similarly, if q is complex, the motion is unstable, if the real part of q is positive. The motion is then an oscillation of increasing amplitude.

Taylor theoretically expressed the threshold at which the flow in coaxially rotating cylinders becomes unstable as:

$$Ta_c = \frac{\pi^4 (1 + d/2R_1)}{0.057(1 - 0.652\, d/R_1) + 0.00056(1 - 0.652\, d/R_1)^{-1}} = 1706 \qquad (II.12)$$

In equation II.12, the term $0.652d/R_1$ is a correction factor due to the fact that d, the distance between the cylinders, is not negligible compared with R_1. This correction allows neglecting higher-order terms of the ratio d/R_1 and may be expected to hold until d/R_1 exceeds one third. This resulting value of 1706 in equation II.12 is now referred to as the first critical Taylor number Ta_{c1} at which the first transition occurs from circular Couette Flow (CCF) to Taylor Vortex Flow (TVF). Taylor established that, below the first critical Taylor number, the flow is stable with no vortical structure. When the Taylor number (Ta) of the flow exceeds the first critical Taylor number ($Ta > Ta_c$), the flow is unstable and forms axisymmetric toroidal vortices.

The mathematical description of the vortex instability by Taylor is based on the assumption that the distance between the inner and the outer cylinder is small compared to the inner cylinder radius, R_1, so that $\eta \rightarrow 1$.

After Taylors first success in the calculation of the critical Taylor number by using linear stability theory, many authors such as Jeffreys [30], Chandrasekhar [16, 31], Di Prima [32], and Di Prima and Swinney [4], have made significant improvements to the linear stability theory both analytically and numerically. Jeffreys [30] was the first to propose an alternative solution approach for the linear perturbation model by Taylor. He reduced the equations of linear theory of Taylor instability to a single sixth-order differential equation for the case of a narrow gap d/R_1. He showed the value of the first critical Taylor number to be approximately equal 1709 for the case $\Omega_2/\Omega_1 \rightarrow 1$, where Ω_2/Ω_1 is the ratio of the rotation rates of the outer and inner cylinders. Moreover, Chandrasekhar [16] and Di Prima [32] derived another expression for the first critical Taylor number as a function of the gap width d and the inner cylinder radius R_1, when d is much smaller than R. This expression is given as:

$$Ta_c = 1695\left(1 + \frac{d}{R_1}\right) \qquad (II.13)$$

Chandrasekhar [31] obtained two simple equations for the computation of the critical Taylor number depending on the value of μ as:

$$Ta_c = \frac{3416}{1+\mu}\left[1 - 7.61 * 10^{-3}\left(\frac{1-\mu}{1+\mu}\right)^2\right] \qquad (\mu \rightarrow 1, \eta \rightarrow 1) \qquad (II.14)$$

$$Ta_c = Ta_{c0}(1-\mu)^4 \qquad (\mu \rightarrow \infty, \eta \rightarrow 1) \qquad (II.15)$$

where $Ta_{co} = 1182$ and $\mu = \Omega_2/\Omega_1$.

The case of wide gaps ($\eta < 1$) when $\Omega_2 = 0$ was studied numerically by Roberts [33] who found the critical Taylor number to vary with the gap d as:

$$Ta_c = 4931\eta^2 - 10087\eta + 6895.2 \qquad (II.16)$$

II.3.3 Energy theory of instability

The energy theory method helps to understand the physical processes that lead from a linear instability to a non-linear instability in flows. The energy theory method has been used in the study of flow instabilities by Schmid and Henningson [34], Betchov and Criminale (Jr) [35], Lin [36], Joseph [37], and Drazin and Reid [38]. This method involves observing the rate of increment of the disturbance energy of the flow system with time. The critical condition is determined by the maximum Reynolds number at which the disturbance energy in the system monotonically decreases with time. Dou [39] observed that the critical Reynolds number

obtained using the energy method by Betchov and Criminale (Jr) [35], Schmid and Henningson [34], and Drazin and Reid [38] is much lower than that obtained in experiment.

In the flow system, it is considered that turbulent shear stresses interact with the velocity gradient and a flow disturbance gets energy from mean flow in such a way. Thus, a small flow disturbance can be amplified by the large energy gradient. When disturbances are amplified, they suppress the mean flow energy, when disturbances are decaying, the mean flow internal energy increases.

Although it is possible to understand the transition process from the energy theory method, the mechanism is still not fully understood and the agreement with the experimental data is still not satisfying. As such, Dou [39] proposed another mechanism for flow instability and transition to turbulence in wall-bounded shear flows (which include the plane Poiseuille flow, the pipe Poiseuille flow, and the plane Couette flow). This mechanism suggests that the energy gradient in the transverse direction plays a role in the amplification of a disturbance, whereas the energy loss in streamline direction serves the function of damping the disturbance. The related analysis obtains consistent agreement with the experimental data at the critical condition for wall-bounded shear flows.

Recently, Dou et al. [40] utilized the new energy gradient theory mechanism to study the instability of Taylor-Couette flow between concentric cylinders. The aim of their investigation was to demonstrate that the mechanism of instability in the Taylor-Couette flow can be explained via the energy gradient concept. They gave detailed derivation for the calculation of the energy gradient parameter in the flow between concentric rotating cylinders. Their calculated results for the critical condition of primary instability (with semi-empirical treatment) are found to be in very good agreement with the experiments in the literature. Their results also show that a mechanism of spiral turbulence generation observed for counter-rotation of two cylinders can be explained using the energy gradient theory and that the energy gradient theory can serve to relate the condition of transition in Taylor-Couette flow to that in plane Couette flow.

II.3.4 Weakly non-linear theory

The linear theory only considered the infinitesimal disturbances in the flow. As such, only the initial growth of the disturbance can be determined. The linear theory of hydrodynamic stability can easily predict correctly the critical Taylor number, but it cannot predict the establishment of a new equilibrium flow, the Taylor vortex flow, above the critical Taylor number. The exponential growth of the disturbances considered in linear theory cannot be sustained long in time and, in a real flow, the growth rate is suppressed by viscous effects. Therefore, it is necessary to solve the nonlinear equations, which means that the higher order

terms cannot be neglected, as suggested by Deng [41]. Stuart [42] extended the linear theory to larger amplitude disturbances by studying the mechanics of disturbance growth taking the non-linearity of the hydrodynamic system into account. Davey [43] made use of a weakly non-linear approach to obtain a Landau-type equation that describes the time evolution of the vortex velocity field. A good agreement was found between Davey's result and the one obtained by Donnelly [44] over the range of the Taylor numbers above the critical value for which the perturbation theory is expected to be valid.

II.3.5 Non-linear theory

Jones [45] proposed an approach that is valid near the stability boundary for the onset of wavy vortex flow for two radius ratios, $\eta = 0.8757$ and $\eta \rightarrow 1$ at a large Taylor numbers. They employed the Galerkin method for the solution of the partial differential equations in two spatial variables with prescribed boundary values. In the Galerkin method, the stability problem is solved by finding the eigen-values of the matrices related to the differential equations. They applied their techniques only for the case where the inner cylinder is rotating and the outer cylinder is at rest. The results obtained using their method show agreement with the results of Zarti and Mobbs [46].

II.4 The main flow regimes in Taylor-Couette flow

The understanding of the flow regime prevailing in an annular enclosure in which the inner and outer cylinders co-rotate or counter-rotate, as well as the scenario of one rotating while the other is stationary is reasonably well established in the literature. As the inner cylinder rotates, it induces a centrifugal force that moves the fluid radially outward. This motion is resisted by the radial pressure gradient due to the stationary outer cylinder wall. At equilibrium, when the angular speed of the inner cylinder is moderate, the centrifugal force is balanced by the radial pressure gradient and the resulting swirling flow pattern between the two concentric rotating cylinders is the laminar two-dimensional flow known as the circular Couette Flow (CCF). If the inner cylinder is rotated fast enough, the centrifugal forces overcome the radial pressure gradient and the system makes a transition from the two-dimensional flow regime to more complex flow regime. This section gives a concise review of the most common flow regimes in concentric rotating cylinders and their characteristics as identified by various researchers. This review is limited to the cases in which the inner cylinder is rotating while the outer cylinder is stationary. Based on the three parameters (η, Γ, and Ta or Re), several flow regimes that exist in an incompressible fluid between two concentric rotating cylinders have been identified. These parameters have a crucial influence on the nature of the flow dynamics and scaling of the system as well as the transition

threshold. The main parameters influencing the formation of different transition regimes of Taylor-Couette flow are:

- The radius ratio $\eta = R_1/R_2$.
- The aspect ratio $\Gamma = H/(R_2 - R_1) = H/d$, where H is the length or height of the cylinders.
- The Taylor number or Reynolds number defined as:

$$\mathrm{Re} = \frac{\Omega_1 R_1 d}{\nu} \qquad (II.17)$$

$$Ta = Re^2 \frac{d}{R_1} \qquad (II.18)$$

Stuart [42] defined the Taylor number as follow:

$$Ta_s = \sqrt{Ta} = Re\sqrt{\frac{d}{R_1}} \qquad (II.19)$$

II.4.1 Circular Couette Flow (CCF)

For low rotation rates, fluid elements in Taylor-Couette flows simply follow circular paths as would be expected from symmetry considerations. This featureless flow is called circular Couette flow (CCF). This is the perfectly azimuthal, undisturbed laminar base flow. The velocity profile is approximately linear in r for narrow gaps. From the Navier-Stokes equations we can describe the velocity fields. The following simplifying assumptions can be assumed:

- Stationary, axisymmetric and invariant problem according to cylinder height, i. e.

$$\frac{\partial}{\partial t} = \frac{\partial}{\partial z} = \frac{\partial}{\partial \theta} = 0 \qquad (II.20)$$

The velocity field is written $\vec{V}(u_r = U = 0, u_\theta = V, u_z = W)$

And the conservation equations, after simplification from the above assumptions, are written:

- Continuity: $\nabla \vec{V} = 0$ *(II.21)*
- Navier-stokes equation according to r : $-\rho \frac{V^2}{r} = -\frac{\partial p}{\partial r}$ *(II.22)*
- Navier-stokes equation according to θ : $0 = \mu \Delta V - \mu \frac{V^2}{r} \Rightarrow \frac{\partial^2 V}{\partial r^2} + \frac{1}{r}\frac{\partial V}{\partial r} - \frac{V}{r^2} = 0$ *(II.23)*
- Navier-stokes equation according to z : $0 = -\frac{\partial p}{\partial z} + \mu\left[\frac{\partial^2 W}{\partial r^2} + \frac{1}{r}\frac{\partial W}{\partial r}\right]$ *(II.24)*

Interpretation:

- Equation (II.22) expresses the balance of the centrifugal force - pressure gradient. The pressure gradient tends to push the fluid inwards (r decreasing), while the centrifugal force drives the fluid outwards.

- Equation (II.23) translates the conservation of the kinetic moment. From this equation, the azimuth velocity field can be determined.
- Equation (II.24) reflects the equilibrium of axial pressure - axial viscous diffusion. It gives us the axial component of velocity.

It is possible to determine the analytical solution of such a flow from the azimuthal component of the velocity, i.e. from Equation (II.23)

$$\frac{\partial^2 V}{\partial r^2}+\frac{1}{r}\frac{\partial V}{\partial r}-\frac{V}{r^2}=0 \Rightarrow \frac{\partial^2 V}{\partial r^2}+\frac{\partial}{\partial r}\left(\frac{V}{r}\right)=0 \Rightarrow \frac{\partial}{\partial r}\left(\frac{1}{r}\frac{\partial}{\partial r}(rV)\right)=0 \Rightarrow \frac{1}{r}\frac{\partial}{\partial r}(rV)=constant$$

Finally, the velocity is of the form: $V = Ar + \frac{B}{r}$ *(II.25)*

and with the boundary conditions we find: $V = -\frac{R_1^2}{R_2^2 - R_1^2} r + \frac{R_1^2 R_2^2}{R_2^2 - R_1^2}\frac{1}{r}$ *(II.26)*

The velocity expression shows that the centrifugal force $F=\rho V^2/r$ is higher on the side close to the inner cylinder $r = R_1$, and therefore when the rotational speed Ω_1 of the inner cylinder exceeds a certain critical value Ω_{1c}, the laminar flow becomes unstable.

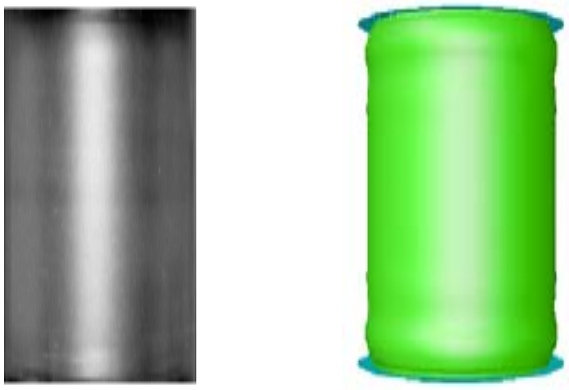

(a) (b)

Figure II.5: Circular Couette flow. (a) Experimental visualization and (b) Numerical simulations.

II.4.2 Taylor Vortex Flow (TVF)

The Taylor vortex flow is a steady axisymmetric vortex flow, in which toroidal vortices encircle the inner cylinder and are stacked in the axial direction. The boundaries between neighboring vortices are flat and perpendicular to the cylinder axis. The flow pattern is shown by the flow visualization and numerical simulation in Figure II.6(b and c). The axial wavelength which corresponds to the height of a pair of rollers is approximately equal to twice the gap (Λ=2d), as shown in Figure II.6(a). The vortical motion of the TVF grows as the Taylor/ Reynolds number increases. The upper limit of the TVF regime is marked by the appearance of azimuthal travelling waves on these vortices.

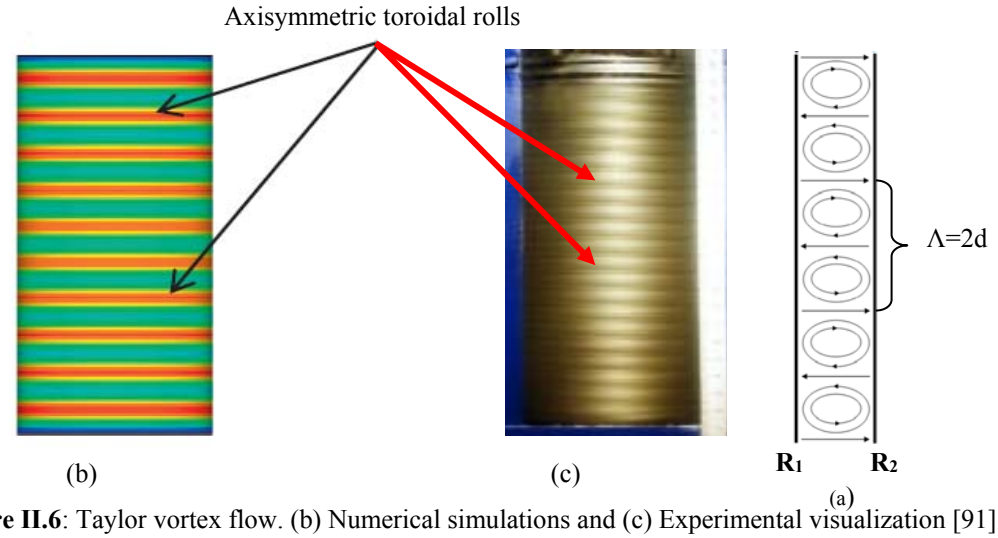

Figure II.6: Taylor vortex flow. (b) Numerical simulations and (c) Experimental visualization [91].

II.4.3 Wavy Vortex Flow (WVF)

At larger Taylor and Reynolds numbers, the axisymmetric time-independent Taylor vortex flow that is developed in the annular region of concentric cylinders changes to that of non-axisymmetric unsteady time-dependent wavy Taylor vortices. This wavy vortex flow is characterized by travelling azimuthal waves that are superimposed on the Taylor vortices. The azimuthal waves rotate around the inner cylinder at some wave speed as shown in Figure II.7. The wavy vortices have a defined azimuthal wavenumber and move with a finite wave velocity in the azimuthal direction. The waves travel around the annulus at a speed that is 30% to 50% of the surface speed of the inner cylinder, depending on the Taylor number and other conditions. Davey et al. [47] have shown that the Taylor number at which the onset of wavy vortex occurs is between 8% to 20% above the Taylor number at which the Taylor vortex flow first appears.

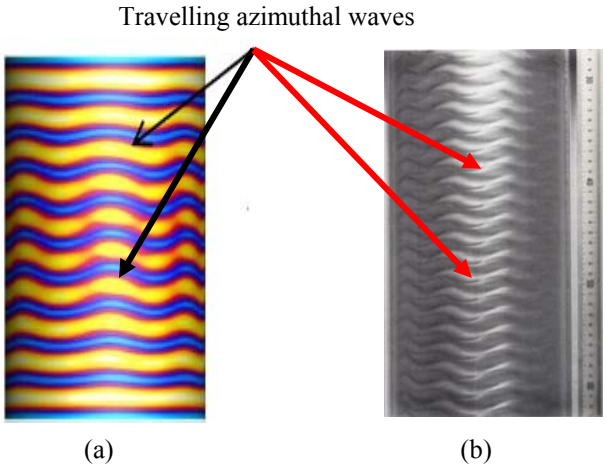

Figure II.7: Wavy vortex flow. (a) Numerical simulation and (b) Experimental visualization [1] .

II.4.4 Modulated Wavy Vortex Flow (MWVF)

At higher Taylor numbers, the wavy vortices transition to rotating waves that appear to be modulated, as shown in Figure II.8. This type of flow is termed quasi-periodic because it has

approximated but not exact recurrence [19]. As Re is increased still further, the amplitude of the azimuthal waves begins to vary with time, giving rise to quasi-periodic regimes known as modulated wavy vortex flow (MWVF) and chaotic wavy flow (CWF) [48]. The latter flow regimes are distinguished by the absence or presence, respectively, of a broad peak in the velocity power spectra. When the flow changes to MWVF, the flow pattern changes from the S-shape to a slight flattening of the wavy vortex outflow boundary. All the waves in the axial direction are modulated in phase, while, in the azimuthal direction, the wave modulation can have the same phase, or the modulation phase can vary with angle (Gorman and Swinney [49]). In MWVF, there are two rotating waves superimposed on the Taylor vortices with different frequencies and in general, different azimuthal wave-numbers.

(a) (b)

Figure II.8: Modulated wavy vortex flow (MWVF). (a) Experimental visualization and (b) Numerical simulations.

II.4.5 Turbulent Taylor Vortex Flow (TTVF)

Upon further increasing Taylor number, azimuthal waves disappear altogether, marking the onset of "weakly turbulent" or "soft turbulent" flow, although the axial periodicity associated with the Taylor vortices remains. This turbulent Taylor vortex flow (TTVF) becomes increasingly complex as the Taylor number ratio increases beyond 5 x 10^5 until the vortex structures themselves eventually become indiscernible. Koschmieder [1] stated that order emerges from chaotic flow that leads to turbulent flow when $Ta \approx 1000Ta_c$. In the case of the inner cylinder rotating and the outer cylinder fixed, increasing the Taylor number above the critical Taylor number results in higher instabilities than in the case of the outer cylinder rotating. In this flow, the vortical structure is retained, but the vortices are modified. Figure II.9 shows the turbulent Taylor flow pattern.

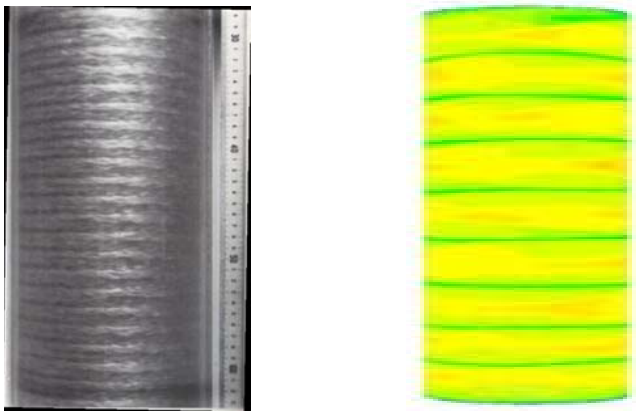

(a) (b)

Figure II.9: Turbulent Taylor Vortex Flow (TTVF). (a) Experimental visualization [1] and (b) Numerical simulations.

II.5 Factors influencing the Taylor-Couette flow

In this part, we propose to perform review and analysis of the influence of different parameters on the occurrence of instabilities in order to derive some physically interesting properties. Thus, we discuss the thermal, rheological, dynamic and geometric effects influencing the flow patterns and the laminar-turbulent transition in Taylor-Couette flow.

II.5.1 Thermal effect

The non-isothermal flow of a fluid within a rotating cylindrical device occurs in many industrial applications, including the cooling of rotating machines, such as turbines. Cylindrical and rotating heat exchangers have been introduced in the chemical, automotive and nuclear industries. This type of flow is also present in geophysical and astrophysical models explaining the circulation of fluids in the Earth's mantle, the formation of stars, and especially in electric motors. Indeed, different studies on the heat transfer of electric motors have demonstrated the importance of convective heat transfer within the cylindrical gap (area separating the rotor from the stator). In fact, the rotor is the locus for large-scale dissipations of electromagnetic origin, and its cooling is ensured principally by the air flow of the cylindrical gap. Two main families of rotating electric machines may be distinguished; closed machines (rotor rotation without axial air flow: Taylor-Couette flow), and open machines (axial flow combined with rotor rotation: Taylor-Couette-Poiseuille flow).

The study of the effect of a temperature gradient began with the work of Yih in 1961 [50] by imposing a negative temperature gradient (the inner cylinder being heated) this author showed that this has the effect of stabilizing the flow. On the other hand, a positive temperature gradient produces an opposite effect that can destabilize the flow. In 1964, Snyder et al. [51] experimentally studied the effect of a radial temperature gradient on the stability of the Taylor-Couette flow. In 1990, Chen et al. [52] considered the effect of a small radial

temperature gradient on the linear stability of the Taylor-Couette flow and observed that the critical Taylor number depends on the working fluid and the temperature difference. Ball et al. [53] studied the different flow transitions as a function of control parameters in a small aspect ratio system. Their experience has made it possible to measure the relative importance of rotation and thermal effects. Thus, they observed that these become predominant and vortices similar to those observed in natural convection, when the radial temperature gradient is increased. These results are confirmed in numerical simulations by Kuo and Ball [54]. Mutabazi et al [55] studied the influence of a radial temperature gradient on the stability of the Taylor-Couette flow. The authors made a particular effort to understand the mechanism of instability due to low temperature gradients ($\Delta T = 3°C$). They showed that the combination of the rotation of the inner cylinder and the temperature gradient leads to the transition to an oscillatory spiral flow in the axial direction. Ball et al. [56] classified the different flow regimes obtained by flow visualizations using the Richardson number $Ri = Gr/Re^2$ (Gr and Re are the Grashof and Reynolds numbers respectively), which is the ratio between the buoyancy and inertia forces. For $Ri < 0.01$, rotation is dominant over the buoyancy, whereas for $Ri \in [0.01; 10]$, both effects play an important role in the transition process. For $Ri > 10$, the flow is destabilized by the buoyancy only. Further, Ali and Weidman [57] performed a linear stability analysis for non-axisymmetric perturbations for a wide range of the global flow parameters. Liu et al. [58] investigated the stability of Taylor-Couette flows with radial temperature gradient by digital PIV for four different outer cylinders, smooth or with different number of slits ($\eta = 0.825$, $\Gamma = 48$). Moreover, Lepiller et al. [59] studied the influence of a radial temperature gradient on the stability of circular Couette flows in the non-rotating case. It is found to destabilize the flow leading to a pattern of traveling helicoidal vortices occurring only near the bottom of the system, and invade progressively the whole cavity by increasing the Taylor number Ta, as shown in Figure II.10. Recently, Yoshikawa et al. [60] performed a linear stability analysis for given values of *Pr* and η. A small stabilization zone is obtained near the isothermal situation. By studying the perturbation kinetic energy, they proposed different values of the Richardson number compared to Ball et al. [56] to distinguish the three flow regimes: $Ri < 0.002$ (rotation dominates), $Ri \in [0.01; 10]$ (both effects coexist) and $Ri > 3.75$ (buoyancy dominates).

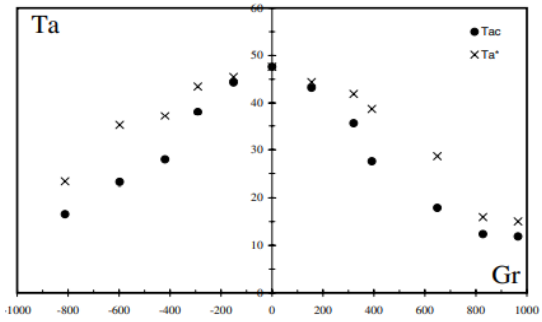

Figure II.10: Variation of the critical Taylor number vs. the Grashof number. The symbols • and × correspond respectively to the value of the Taylor number at the threshold and to that for which the spiral vortex flow fills the whole annulus. Adapted from ref. [59]

II.5.2 Rheological effect

The flows of non-Newtonian fluids, such as viscoelastic and viscoplastic, can behave in very different ways from the flows observed for Newtonian fluids. The study of the flow stability of the non-Newtonian fluids began in 1960s by Rubin and Elata [61] which used the Taylor - Couette flow system as a model hydrodynamic to investigate the behavior of liquids viscoelastic. After pioneering study in the sixties [61], there has been great interest in viscoelastic instabilities in the Taylor-Couette system [62-64]. Theoretical studies are nowadays complemented by numerical calculations using viscoelastic models, like the upper-convected-Maxwell fluid model [65] or the Oldroyd-B model [66] and also finite extensible nonlinear elastic (FENE) dumbbell models [67-69]. These studies were able to reproduce many flow properties observed in experiments, such as solitary steady states (diwhirls).

The study by Larson et al. [70] on Taylor- Couette flow for highly viscoelastic liquids (fluids of Böger) revealed purely elastic instabilities, which can destabilize a flow at relatively low velocities. These instabilities can lead to the elastic turbulence regime, where a viscoelastic flow exhibits turbulent behaviour under conditions for which a Newtonian fluid of comparable viscosity would flow in a laminar manner.

Halfway between the inertial instabilities, observed for Newtonian fluids, and the purely elastic instabilities are located the so-called inertio-elastic regimes, for which the observed modes of instabilities present a different nature from that observed for Newtonian fluids while being governed by inertial forces. Among the previous experimental results on the stability of Taylor-Couette flow in inertio-elastic regime include the observation by Groisman and Steinberg [71] of a mode of instability propagating both axially and radially, called Radial Waves (RW). In addition, Beavers and Joseph [72] used a viscoelastic solution for the Taylor-Couette system. They confirmed that the nature of the fluid does not influence the occurrence of the first instability, which occurs at a Taylor number almost identical to that observed for a Newtonian fluid. However, this influences the shape and behaviour of cells. They noticed that

as they increase Ta, the cells expand and decrease in number. More recently, Martinez-Arias and Peixinho [73] carried out an experimental study of Taylor-Couette flow using mixtures of water, PEG (Poly Ethylene Glycol), PEO (Poly Ethylene Oxyde) and IPA (IsoPropyl Alcohol) as working fluids. They reported that, for large concentrations, six different numbers of steady solitary pairs of vortices, called diwhirls, were observed, as shown in Figure II.11.

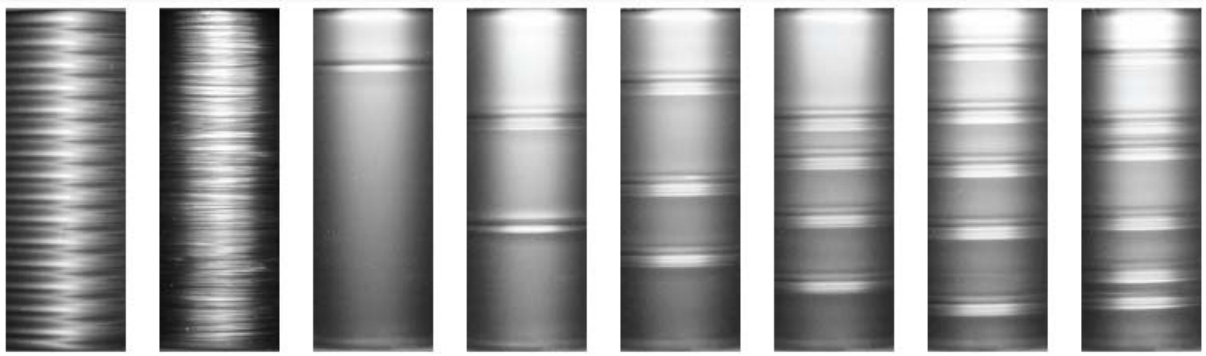

Figure II.11: Flow patterns for different working fluids (a) Newtonian fluid containing 30 Taylor vortices. The others are for mixtures containing 1000 ppm of PEO dissolved in 7% PEG aqueous solution and present: (b) inertio-elastically turbulent flow, (c-h) flows containing 1 to 6 diwhirls, from left to right, respectively. Adapted from Ref. [73]

II.5.3 Dynamic effect

II.5.3.a Axial flow effect

Taylor-Couette flow coupled with a Poiseuille flow in the axial direction, often called Taylor-Couette-Poiseuille flow (T.C.P.F), has a wide application in the field of cooling of turbomachines, chemical reactors and ultrafiltration devices. Several authors have investigated the coupling of Taylor-Couette flow with axial flow under a constant pressure gradient. This type of flow is generally governed by the ratio Ta / Re_z where Ta is the Taylor number and $Re_z = Re_{axial} = Ud/\nu$ is the Reynolds number related to the Poiseuille flow. In 1961, Chandrasekhar [31] studied flow stability using linear theory. He showed that for low Re_z values, the flow is dominated by rotation and after the first instability (TVF) occurs, the cells move in the axial direction. He showed that the distance between the position of appearance of the cells and the entry of the Poiseuille flow increases with Re_z and decreases with Ta. For intermediate Re_z values, the Taylor cell structure is transformed into a spiral flow. For high Re_z values, the flow becomes unstable due to the instability of the Poiseuille flow.

Stockert and Lueptow [74] investigated this flow problem with the PIV technique (Particle Image Velocimetry). Leuptow [75] also studied the stability of the Taylor-Couette flow under the simultaneous effects of axial and radial flow. Radial flow is achieved by using porous cylinders. He noted that the axial flow stabilizes the Taylor-Couette flow, however the radial

flow displaces the centers of the cells towards the porous cylinder. It seems to favor the stability of the Taylor-Couette motion which is subjected to the axial flow effect.

Di Prima [32] showed theoretically that the appearance of the first instability is delayed: from $Ta_c = 40$ for $Re_z = 0$, to $Ta_c = 80$ for $Re_z = 60$. Furthermore, Astill [76] observed that:

- The onset of instability is manifested by undulations of the fluid near the rotating inner cylinder, which transforms into Taylor rolls as the axial flow evolves towards the lower side of the cylinder.
- By keeping the axial flow constant and increasing Ta, the transition point moves up the axial flow (and vice versa).
- By keeping Ta constant and increasing Re_z, the transition point moves the axial current down the cylinder (and vice versa).
- The speed at which the transition point moves in the direction of the current increases with Re_z.

From a certain value Re_z, the rolls lose their horizontality to turn, in some cases, into spirals with a precise inclination. According to Piva et al. [77], these rings or spirals move at a speed of about 1.1U to 1.2U, U being the average axial velocity. Increasing Re_z results in overlapping rolls (unless $d/R_i<0.4$). Then, beyond a certain flow rate, there is disintegration of the rolls. Gu and Fahidy [78] concluded that the inclination of the rolls would be due to the struggle between two forces: the axial dynamic pressure force, due to the axial flow, moves the rolls away from their original position and the centrifugal force. As the flow rate increases, Gu and Fahidy [79], summarized the observed evolutions as follow:

- ✓ $Re_z = 30$: Tilt of the rolls (from 5 to 6°) that start to overlap,
- ✓ $Re_z = 35$: Increasingly important overlap area,
- ✓ $Re_z = 45$: Broken rolls to give disordered structures. There are vertical bands linking the adjacent rolls,
- ✓ $Re_z = 50$: Increasingly dominant bands and the rolls become difficult to distinguish,
- ✓ $Re_z = 75$: The bands are dominant within the flow which then becomes essentially parallel to the axial flow. There is complete disintegration of Taylor rolls.

Figure II.12 shows the evolution of the Taylor number as a function of the axial Reynolds number obtained by different authors.

Figure II.12: Evolution of the first critical Taylor number as a function of the axial Reynolds number.

More recently, Lancial et al. [80] investigated, both experimentally and numerically, the Taylor-Couette-Poiseuille flow in an annular channel of a slotted rotating inner cylinder, corresponding to a salient pole hydrogenerator. They noted four different flow regimes, summarized in Figure II.13.

- Regime I: Laminar ($0 \leq Re_z \leq 779$, $0 \leq Re_i \leq 972$),
- Regime II: Laminar with vortices ($0 \leq Re_z \leq 779$, $972 \leq Re_i$),
- Regime III: Turbulent ($3115 \leq Re_z \leq 6235$, $0 \leq Re_i \leq 1940$); ($6235 \leq Re_z$, $0 \leq Re_i \leq 9710$),
- Regime IV: Turbulent with vortices ($3115 \leq Re_z \leq 6235$, $1940 \leq Re_i$); ($6235 \leq Re_z$, $9710 \leq Re_i$).

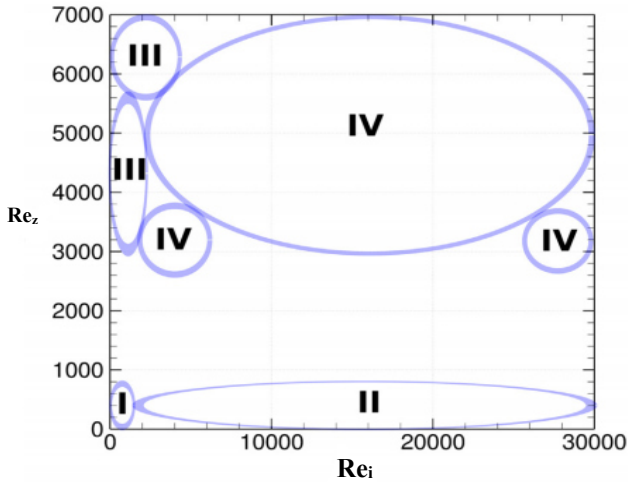

Figure II.13: Demarcation lines of the different flow regimes. Adapted from ref.[80].

II.5.3.b Magnetic effect

When studying the effect of magnetic field on the Ferro-fluidic Taylor-Couette Flow, as one example of magnetic flow dynamics, in terms of instability, bifurcation, and properties, one quickly finds out the additional challenges magnetic fluids introduce compared to the investigation of "classical", "ordinary" shear flows without any kind of particles. As a result, the classical Navier–Stokes equations become modified to the more complex ferro-hydrodynamical equation of motion, incorporating magnetic field and magnetization of the fluid itself, which typically makes numerical simulations expensive and challenging. Moreover, a rotating ferro-fluidic system, known as magneto-hydrodynamic (MHD) Taylor-Couette flows represent one example of magnetic particles with a variety of applications, ranging from liquid seals in rotating systems, their use in computer hard drives, as well as in laboratory experiments, to study geophysical flows. Indeed, in astrophysics and geophysics, the magneto-hydrodynamic (MHD) Taylor-Couette flow is usually considered as a prototypical flow to simulate the accretion disc and dynamo, namely, the study of magneto-rotational instability (MRI) and dynamo action [81-83].

Taylor-Couette flow under the influence of an applied magnetic field was first studied by Chandrasekhar in 1961 [31] and Donnelly and Ozima in 1962 [84]. Later in 1964, Roberts [85] developed calculations on the stability of non-axisymmetric perturbations. When the inner cylinder is the only one to rotate, it is noted that the critical value for the beginning of the non-axisymetric movement is just above the critical value in the hydrodynamic case.

Singh and Bajaj [86] studied numerically the instability of a viscous and incompressible ferro-fluid in Taylor-Couette flow with the presence of an axial magnetic field. The effects of the magnetic field can be summarized as an overall stabilization of the Taylor-Couette flow. Further, Kaneda et al. [87], studied numerically the MHD Taylor-Couette flow to determine the motor torque applied to the inner cylinder as a function of rotational speed and the axial magnetic field characterized by the Hartmann number (Ha). When the Reynolds number is less than its critical value (Re_c ~70), they found that the magnetic field increases the motor torque for the given value of Re. On the other hand, for values Re greater than the critical value, it is found that a moderate magnetic field lowers the motor torque. Beyond $Re > Re_c$ and for high values of Ha ($Ha \geq 50$), the cell mode decreases by 4 to 2 cells as shown in Figure II.14. This change in the meridian flow plane reduces the motor torque by almost 25% for Re=300. For $Re > Re_c$ and higher values of Ha , the two-cell mode is due to the fact that the Lorentz force tends to suppress azimuthal flow.

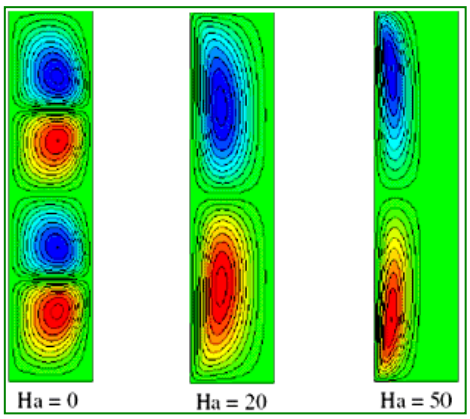

Figure II.14: Effect of the magnetic field on Taylor vortices. Adapted from ref. [87].

Moreover, Aberkane et al. [88] examined analytically and numerically the effects of an external axial magnetic field applied to the forced convection flow of an electrically conducting fluid between two horizontal concentric cylinders, considering the effects of viscous heat dissipation in the fluid. Recently, Kamış and Atalık [89] conducted a stability analysis for the non-isothermal Taylor-Couette flow of a non-conductive ferro-fluid under the action of an azimuthal magnetic field. They observed a significant stabilization under strong magnetic fields for all cases. More recently, Leng et al. [90] studied, by the direct numerical simulation, the effect of an axial homogeneous magnetic field on the turbulence in the Taylor-Couette flow confined between two infinitely long conducting cylinders. They employed two Reynolds numbers 4000 and 8000 with several Hartmann numbers varying from 0 to 120. Their results show that the mean radial induced electrical current, resulting from the interaction of axial magnetic field with the mean flow, leads to the transformation of the mean flow and the modification of the turbulent structure. The effect of turbulence suppression is dominating at a strong magnetic field, for which the flow becomes laminar (flow relaminarization), as illustrated in Figure II.15.

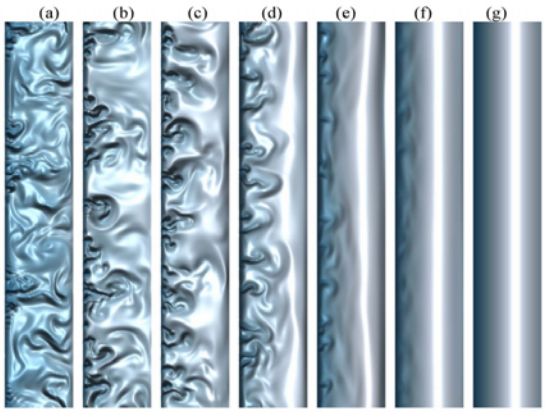

Figure II.15: Instantaneous contours of azimuthal velocity in the meridional plane at Re = 4000 with variation of the Hartmann number: (a) Ha = 0, (b) Ha = 10, (c) Ha = 20, (d) Ha = 40, (e) Ha = 60, (f) Ha = 80, and (g) Ha = 120. On the plot in this figure, the left side denotes the inner rotating cylinder and the right side denotes the outer cylinder at rest. Adapted from ref. [90].

II.5.3.c Inclination effect

Adnane et al. [91] conducted an experimental study of the Laminar-turbulent transition in a tilted Taylor-Couette system. The effect of the inclination angle was investigated on the different flow regimes occurring at fully and/ or partially filled space between two rotating cylinders. Their most significant result concerns the relaminarization of the flow when the aspect ratio is decreased and inclination angle is increased for a given value of Taylor number. They also noted that for a system partially filled, the experimental study showed up the coexistence of three flow modes in the Taylor-Couette system, as shown in Figure II.16.

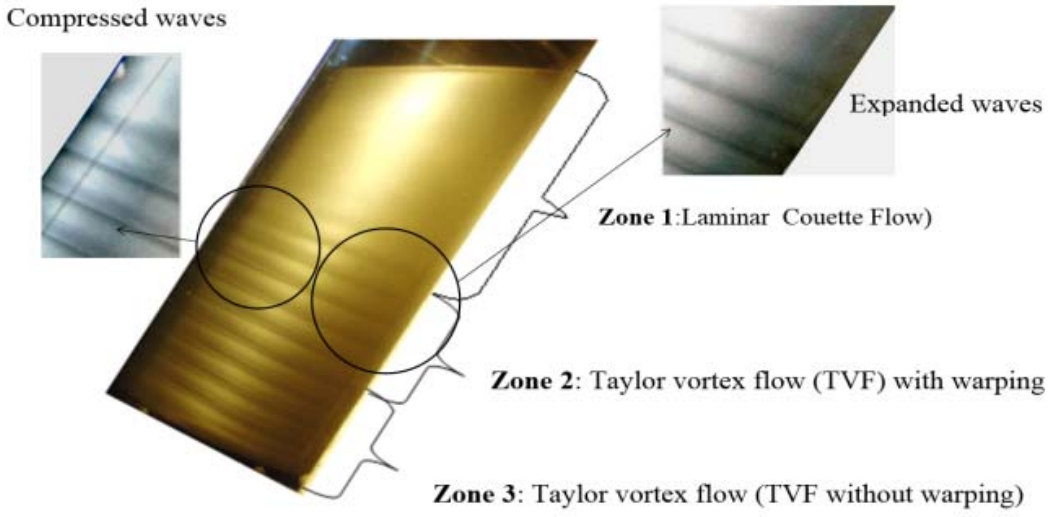

Figure II.16: Coexistence of three flow modes. Adapted from ref. [91].

II.5.3.d Acceleration effect

The transition from one flow state to another later state depends on the geometrical conditions and the speed-up protocol. Therefore, the flow may exhibit a character of non-uniqueness of solution for a given angular velocity of the inner cylinder. This behavior is first reported by Coles [18] who discovered the existence of 20 to 25 different flow states with distinct axial and/or azimuthal wavelengths for a given Reynolds number. He found that flow states depend not only on the initial conditions, but also on how the inner cylinder is accelerated. This phenomenon is confirmed by Snyder [92] and may result in the existence of several possible flow structures for the same Taylor number. The change from one state (k, n) to another depends strongly on the operating protocol and particularly on the value of dRe /dt (acceleration rate). Thus, Andereck et al. [5] found that the final states of Taylor-Couette flow are unique for an adiabatic protocol, i.e., for a quasi-static variation in velocity. Also, new types of spiral flows were observed by Lorenzen and Mulin [166] according to the different experimental protocols implemented, namely, the initial kinematic conditions and the

variation rate of the angular velocity. In an experimental study, Lim et al. [94] showed that rapid increases in velocity significantly modify the flow structure, in particular, the size of the cells and probably the number of azimuthal waves; in particular the wavy vortex flow (WVF) can switch to the first instability (TVF) but with a shorter axial wavelength. Further, Koschmieder [95] used two inner cylinder acceleration procedures (regular and abrupt acceleration) to examine the effect of acceleration on the axial wavelength. He found that, before the onset of the wavy mode, the axial wavelength obtained by the abrupt start is identical to that obtained by regular acceleration of the inner cylinder. However, when vortices begin to undulate, their axial wavelength is sensitive to changes in the initial conditions. Furthermore, Bielek et al. [96] experimentally examined the effect of the acceleration of the rotating inner cylinder on the onset of Taylor vortices in finite geometry. However, the authors could not find an explicit relationship between the appearance of the vortices and the acceleration rate imposed on the rotating inner cylinder. Furukuwa et al. [97] studied the effect of acceleration for a given aspect ratio Γ and Re.

II.5.3.e Free surface effect

The first study of Taylor-Couette flow with free surface is examined by Snyder [98] in 1969. This study determined a critical threshold of $\Gamma_c=H/d=10$ for the aspect ratio, beyond which negligible end effects can be considered. Mahamdia and Bouabdallah [99] examined Taylor-Couette flow subjected to free surface effect and the variation of filling ratio. Recently, Watanabe and Toya [100] and Watanabe et al. [101] have investigated, both numerically and experimentally, the effect of the free surface on the occurrence of the Taylor vortices in the annulus between to coaxial rotating cylinders. They showed that anomalous modes with outer flow near the bottom end wall or inner flow at the free surface appear in some conditions. They also determine transition diagrams between the normal three-cell mode (N3) and the normal one-cell mode (N1) and between the normal five-cell mode (N5) and the normal three-cell mode (N3), as shown in Figure II.17.

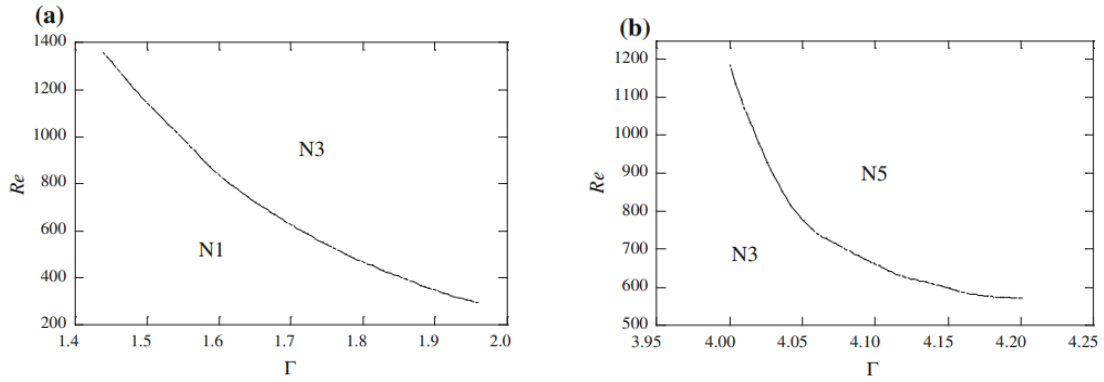

Figure II.17: Bifurcation diagrams found in the asymmetric system with the free surface at the top. (a) Bifurcation between N3 and N1. (b) Bifurcation between N5 and N3. Adapted from ref. [101].

II.5.4 Geometric effects

II.5.4.a Eccentricity effect

Flow between two eccentric cylinders found in the hydrodynamic bearing process, as illustrated in Figure II.18. When the bearing transmits a load, the shaft and bearing are no longer coaxial, the flow obeys a different evolution and a study of the flow stability between two eccentric cylinders is required in order to find a criterion marking the end of the laminar regime. Tests show that, in this type of flow, the coexistence of several types of movement for a given inner cylinder rotation speed. Moreover, stability problem of fluid between two eccentric cylinders or a journal bearing is receiving more and more attention. The reason is that there is a trend in modern technology toward increasingly higher operational speed of journal bearings and toward the use of low viscosity fluids for lubrication, which results in situations where the fluid in a bearing film becomes unstable.

Wilcock in 1950 [102] and Smith and Fuller in 1956 [103] were the pioneers to recognize that flow transition occurs between eccentric cylinders in journal bearings. Indeed, Di Prima in1963 [104] was the first one to establish a stability criterion of fluid between two eccentric cylinders, which is also called local theory of hydrodynamic stability. To account for the disagreement between the local theory and some experimental data, Di Prima and Stuart [105] established their nonlocal theory. Di Prima's local theory and Di Prima and Stuart's nonlocal theory define the threshold for the onset of fluid instability, which usually appears in the form of Taylor vortices in eccentric cylinders. With the further increase of inner cylinder speed, the flow becomes wavy vortices and eventually becomes fully developed turbulent. Constantinescu [106], Ng and Pan [107], and Hirs [108] established their own turbulence theories, which govern the fully developed "turbulence" in journal bearings.

In addition, Dris and Shaqfeh [109] examined, both theoretically and experimentally, the stability of a viscoelastic flow between two eccentric cylinders. In the relative analysis of their theoretical study of local linear stability, they used the Oldroyd-B fluid and suggested that the flow is unstable for all eccentric systems. Their experimental visualization of the flow showed the transition from circular Couette flow to Taylor vortex flow, as shown in Figure II.19.

Three-dimensional simulations of eccentric Taylor-Couette flow were presented by Shu et al. [110]. They conclude that the eccentricity stabilizes the onset of Taylor vortices. At a constant Taylor number the strength of the Taylor vortices decreases when eccentricity increases. The flow pattern of the Taylor vortex flow is distorted by the existence of separation at supercritical eccentricities. The recirculation area enlarges in axial, azimuthal and radial directions in the same time as eccentricity increases. On axial planes which are near the vortex center, the separation flow is closed, but on other axial planes, separation flow is opened with

a certain regulation. The strength of the Taylor vortices is different at different positions in azimuthal direction. The strongest Taylor vortex exists in the region between 45◦ and 90◦ downstream of the widest gap of cylinders, while the weakest one roughly appears at 45◦ downstream of the narrowest gap, as illustrated in Figure II.20.

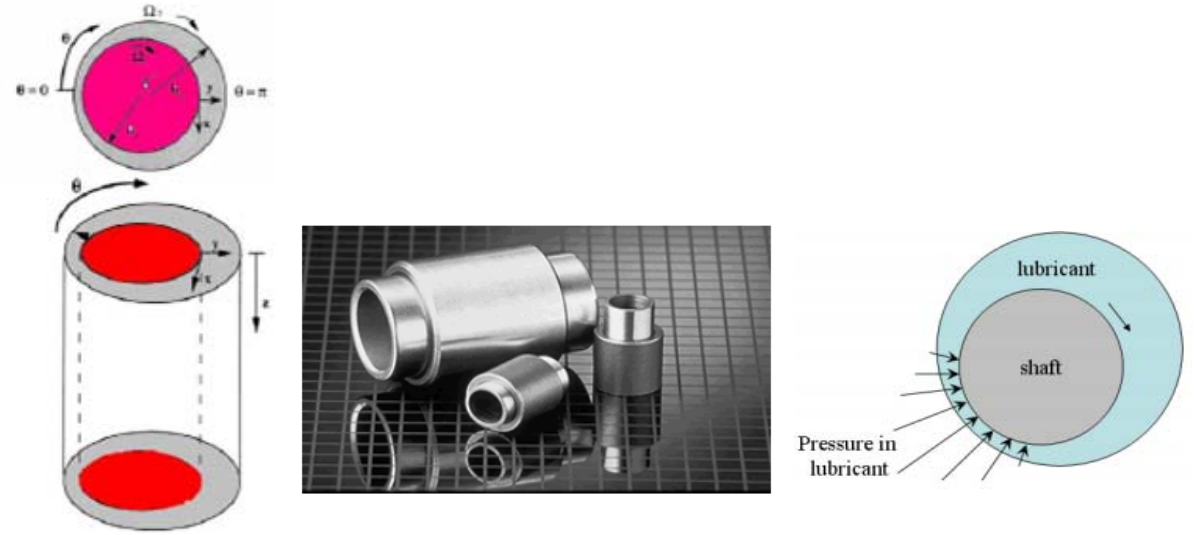

Figure II.18: Schematic of journal bearing.

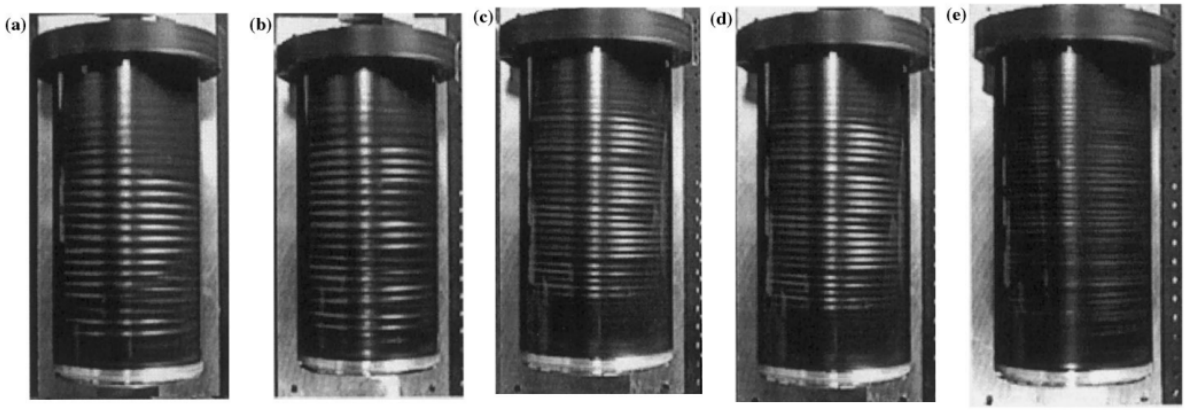

Figure II.19: Flow visualization of eccentric Taylor-Couette flow for the kerosene Boger fluid over various eccentricities (ε): (a) ε=0; (b) ε =0.1; (c) ε =0.2; (d) ε =0.3; (e) ε =0.5. Adapted from ref. [109].

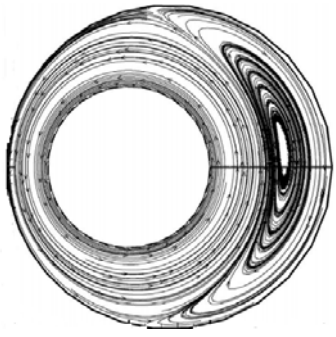

Figure II.20: Streamlines contour of an eccentric Taylor-Couette flow at Re = 50. Adapted from ref. [110].

II.5.4 b Surface roughness effect

The surface condition of the bearings is a very important factor influencing the effectiveness of lubrication. Therefore, the presence of roughness leads to changes the flow regime of lubricant film. Indeed, roughness in a Taylor-Couette geometry has been studied in various ways: Cadot et al. [111] and Van den Berg et al. [112] used obstacle roughness, in the form of axial riblets, to study the scaling of the angular momentum transport with the driving strength**.** Wang and Tsai [113] investigated the effect of roughness using two rough concentric cylinders separated by a viscous fluid. When the inner cylinder rotates, torque and unstable forces can occur. Torque and forces depend on the gap and radial ratio, the amplitude of the roughness, and particularly the numbers characterizing the roughness of the inner and outer cylinders n and m respectively. They conclude that to avoid any unstable torque, n must be different from m. The stable (regular) torque can be minimized by increasing n or decreasing m. Furthermore, Zhu et al. [114, 115] examined the influence of grooves for large Taylor number, and found that at the tips of the grooves, plumes are preferentially ejected. Very recently, Berghout et al. [116] studied the influence of sandgrain roughness in Taylor-Couette flow, and found similarity of the roughness function with the same type of roughness in pipe flow. In a more recent work, Bakhuis et al. [117] investigated, both experimentally and numerically, turbulent Taylor-Couette flow with spanwise-varying roughness, as illustrated in Figure II.21, to determine the effects of the spacing and spanwise width of the spanwise-varying roughness on the total drag and on the flow structures. They applied sandgrain roughness, in the form of alternating rough and smooth bands to the inner cylinder.

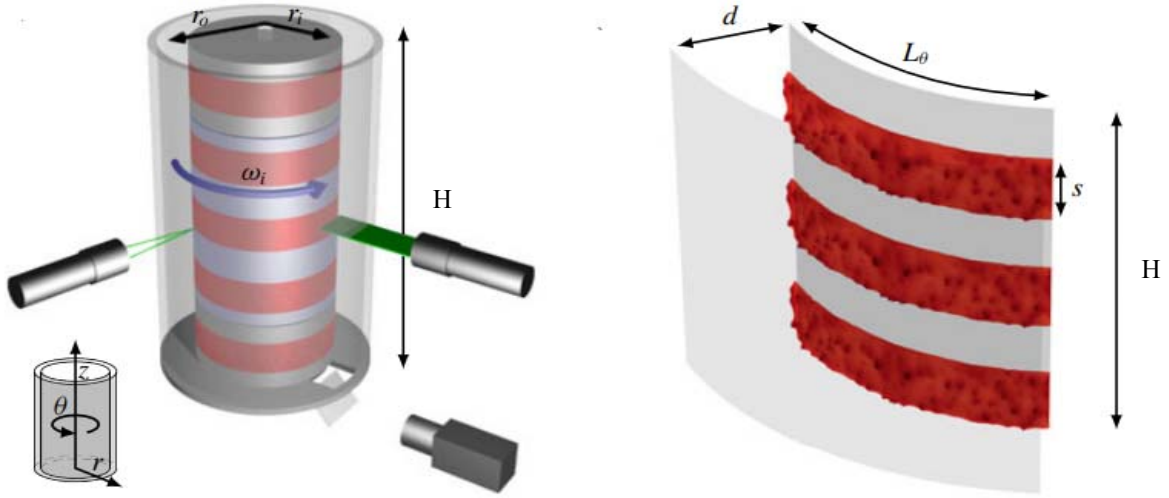

Figure II.21: Left: schematic of the Twente Turbulent Taylor–Couette (T^3C) facility showing the sandpaper roughness on the inner cylinder in red. Right: numerical domain (Computational is carried out using direct numerical simulations with an immersed boundary method).

II.5.4 c Endwalls effect

End-wall effects have been identified as one of the major factors affecting the type of flow regime in concentric rotating cylinders**.** The effects of the endwalls on the flow are avoided theoretically by assuming infinitely long cylinders, experimentally by using long cylinders (compared to the gap between the cylinders), and computationally by using periodic boundary conditions at the axial extrema of the computational domain.

Depending on the nature of the endwall boundary condition, the boundary-driven flow at the endwall can be considered either a Bödewadt flow, where the endwall is fixed and the fluid is rotating, or an Ekman flow, where the endwall and fluid are rotating at different angular velocities. Indeed, Taylor [14] in his original work recognized the important role end-walls play in his experiments. The presence of endwalls destroys the translation invariance characteristic of the infinite length H model. For short cylinders, the transition to non wavy vortical flow occurs at a slightly lower rotational speed, Cole [118] presumably because of the perturbation by the endwall vortices. Furthermore, the subsequent transition to wavy vortical flow occurs at a higher rotational speed than in the case of infinitely long cylinders, most likely because the endwall vortices related to the endwall boundary layers alter the vortical structure to minimize the tendency toward waviness.

In their paper on the anomalous modes in the Taylor experiment, Benjamin and Mullin [119] outlined the importance of endwall effects. The discontinuous nature of the boundary conditions, where the inner cylinder meets the endwalls, generates weak circulation cells adjacent to the endwalls. As the Reynolds number is increased, the cellular pattern propagates towards the centre of the apparatus until it fills the column. They concluded that the transition to Taylor vortex flow is not the result of a bifurcation but of a continuous process.

Furthermore, Czarny et al. [22] investigated the interaction between the endwall Ekman layers and the Taylor vortices near transition from non vortical to vortical flow via direct numerical simulation. To analyze the nature of the interaction between the vortices and the endwall layers, they considered three endwall boundary conditions: fixed endwalls, endwalls rotating with the inner cylinder, and stress-free endwalls. They found that, below the critical Taylor number, endwall vortices for rotating endwalls are more than twice the strength of the vortices for fixed endwalls. Stress-free endwalls result in endwall vortices that are similar in strength to those for rotating endwalls above the critical Taylor number. Kageyama et al. [120] considered both experimentally and numerically the flow in a small aspect ratio Taylor-Couette apparatus for $\eta = 0.256$ and $\Gamma = 0.45$. For such parameters, the vertical boundaries have a dynamical role on the secondary flow, that is why these authors proposed a novel approach to increase control over the velocity profile by increasing the number of endcap

boundary conditions. At lower Taylor numbers, Sobolik et al. [121] investigated the effect of a confining ring on the onset of Ekman vortices for $\Gamma = 4.93$ and $\eta = 0.91$ and showed that they appear below the critical rotation rate for the onset of Taylor vortices in an infinite system.

II.5.4 d Radius ratio effect

Studies on the influence of radius ratio $\eta = R_1/ R_2$ highlight the role of this parameter on the conditions of occurrence of the first two instabilities. Sparrow et al. [122] reported an experimental curve indicating the critical Taylor number Ta_{c1} as a function of the radius ratio, as illustrated in Figure II.22, in the case of a system where only the inner cylinder rotates and the outer one is kept fixed.

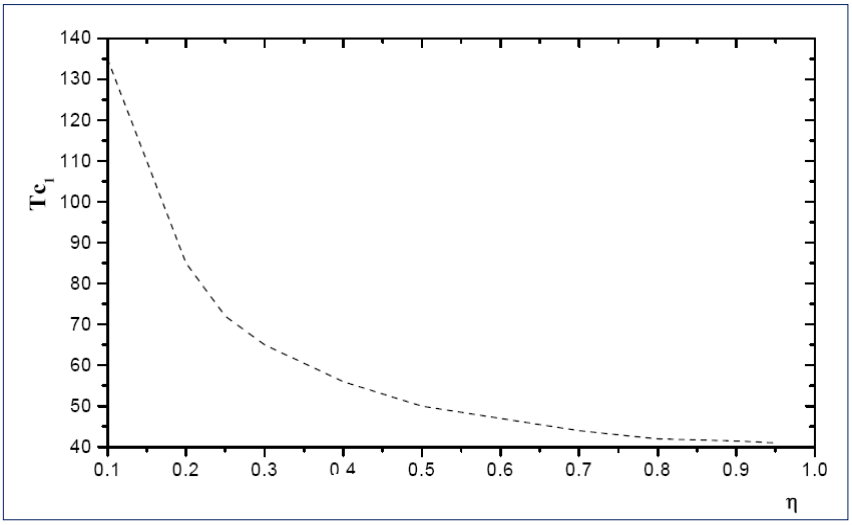

Figure II.22: Evolution of first critical Taylor number vs. radius ratio (Sparrow et al. [122]).

Chandrasekhar [16] obtained more general solution for instability for the entire range of rotational ratio of the cylinders for both narrow as well as wide gaps. The validity of Chandrasekhar's analysis was confirmed by Donnelly [44] by measuring torque for $\eta = 0.95$ and 0.5 with aspect ratio of 50 and 5, respectively. The case of wide gaps was also addressed by Roberts [33] and he found the critical Taylor number to vary with the gap according to the following relationship:

$$Ta_c = 4931\eta^2 - 10087\eta + 6895.2$$

Moreover, Xiao et al. [123] conducted an investigation on the effects of radius ratio on the "Second Taylor Vortex Flow" in concentric rotating cylinders when the inner cylinder is subject to some critical acceleration. They described their "Second Taylor Vortex Flow" as a special type of flow regime in which Taylor vortices are axisymmetric and do not display any wavy motion, even though the regime is located inside the wavy flow regime under quasi-steady condition. They concluded from their results that the "Second Taylor Vortex Flow" is sensitive to the gap size between the two cylinders and does not exist for some radius ratio.

Biage and Campos [124] proposed a classification of the systems depending on the value of their radius ratio η as follows:

- narrow-gap cavities for $\eta > 0.67$,
- middle-gap cavities for $0.33 < \eta < 0.67$,
- wide-gap cavities for $\eta < 0.33$.

II.5.4 e Aspect ratio effect

Multiplicity of Taylor- Couette flow is one of the most attractive features in studying the hydrodynamic stability of rotating fluids between two cylinders. Both analytically and experimentally, Benjamin [125, 126] examined the problem of bifurcation phenomena in steady flows of a viscous fluid between two rotating short cylinders. He concluded that the flow strongly depended on two parameters, one the Taylor number (Ta) and the aspect ratio (Γ=H/d). For a given value of Γ, a unique mode with an even number of Taylor cells emerges as the primary mode as the speed of the inner cylinder is gradually increased to a given value from rest. The other mode is also existed as the secondary mode, which appears with sudden increase of the inner cylinder's speed to the desired value. He also noted that for an aspect ratio Γ between 3.6 and 3.72 and when the Taylor number increases, the primary flow is destabilized in favour of another cellular mode.

The experiments of Cole [118] showed that the appearance of the wavy vortex flow regime is delayed as Γ decreases. In contrast, the critical value of the first Taylor number (Ta_{c1}) for the onset of Taylor vortex flow regime varies little with the aspect ratio Γ. In addition, Benjamin and Mullin [119] observed 15 different stable steady flows under the same geometrical and dynamical boundary conditions (η = 0.6, Γ = 12.61, and Re = 359). Furthermore, Blennerhassett and Hall [127] investigated the stability of Taylor-Couette flow in a finite-length cylindrical annulus by using linear theory. Their results showed that the instability changed from a two-cell to a four-cell primary flow at $\Gamma \approx 1.3$. This analytical work is close to Benjamin's [126] experimental observation that the primary flow changed from a two-cell to a four-cell mode when $\Gamma \approx 1.85$. Ohmura et al. [128] concluded that vorticity played an important role on the transition between steady solutions. For the case of $\eta = 0.615$, $\Gamma = 3.0$ and end wall boundaries, they. found that higher acceleration rates of inner cylinder speed produce such strong vorticity for the Taylor cells on the end walls that a pair of cells is induced toward the center and four cells are formed, while lower acceleration rates promote diffusion of vorticity into the center of the annulus and two cells are formed. Douaya [129], experimentally studied the effect of the aspect ratio Γ on the conditions of appearance of wavy vortex flow regime. Walgraef et al. [130] investigated the effects of finite geometry on the selection of flow structures. They showed that the transition between the first and second

instability is described by an amplitude equation. They also showed that the second critical Taylor number Ta_{c2}, characterizing the second instability (WVF), increases as the aspect ratio decreases. Bontoux et al. [131] studied, in the case of rigid axial limitations, the effect of the aspect ratio on Taylor-Couette flow stability. For large aspect ratios, two complex regimes (azimuthal waves and spiral shapes) appear within the flow. They found that axial limitations appear to dampen and stabilize flow as the aspect ratio decreases.

II.5.4 f Cylinders oscillations effect

The stability of the flow between two coaxial cylinders subjected to periodic oscillation over time has been the subject of much research. Donnelly [132] was the first who investigated, experimentally, the modulation of inner cylinder rotation in the Taylor–Couette system. He reported that the appearance of instability in Taylor-Couette flow can be inhibited by the modulate rotating of the inner cylinder. Hall [133], examined the case where the outer cylinder is at rest and the inner one rotates with a modulated angular velocity of the type: $\Omega(1+ \varepsilon \cos\omega t)$. Further, Marques and Lopez [134] used a sinusoidal axial movement of the inner cylinder in the Taylor-Couette flow system to delay the transition from stable laminar flow to disturbed laminar flow by using a visualizing fluid. Using Floquet theory, Lopez and Marques [135, 136] studied the outer cylinder angular velocity effect, varying harmonically, on the onset of spiral modes. Aouidef et al. [137] investigated the pulsed flow effect on Taylor vortices structures with both cylinders rotating at the same angular velocity $\Omega(t) = \Omega_0 \cos(\omega t)$. Furthermore, Barenghi and Jones [138] studied the temporally modulated angular velocity effect of Taylor–Couette flow on the onset of different instabilities. By comparing their results to experiment previous works of Walsh and Donnelly and Walsh [139, 140], they argued that the transient vortices, at low frequency, are the source of the large flow destabilization. Feugaing et al. [141] characterized the sinusoidal modulate inner cylinder rotating effect on the flow behaviour. From the spectral analysis, they showed that the modulating frequency pattern is independent of the Taylor number. Sinha [142] studied the effect of harmonic axial oscillations of the inner cylinder and noticed that this axial force causes asymmetry of the system and leads to an increase in axial waves with the number of azimuthal waves unchanged. Recently, Oualli et al. [143] investigated the flow behavior, affected by the cross section oscillation of the inner or outer cylinder. They reported that the onset of the first instability can be delayed or advanced by applying this radial oscillation strategy. More recently, Lalaoua and Bouabdallah [144] studied the Taylor vortices structures with the inner rotating cylinder when the outer cylinder is held stationary and oscillating radially. They found that the first instability mode of transition is retarded from $Ta_{c1} = 41.33$, corresponding

to the first critical Taylor number value, to $Ta_{c1} = 70$ when the deforming amplitude is equal to 12.5% the external cylinder diameter value.

II.6 Modified Taylor-Couette Flow

The existence of instabilities is not limited to the flow between straight rotating circular cylinders. They may also occur for other geometries, different from the cylindrical Taylor-Couette system. Instabilities and various flow modes can be detected for instance between rotating spheres, between rotating conical cylinders and between rotating ellipsoids. The flows and the instabilities occurring between rotating bodies can be regarded as part of the large domain of the flows in rotating systems. Hence, a rich variety of flow patterns and structures can be observed for unstable flows between these rotating bodies. In this section, literature which discusses the flow between different rotating bodies and the effects that they have will be reviewed.

II.6.1 Flow between rotating spheres: Spherical Couette flow

Spherical Couette flow (SCF) is the flow induced in a fluid-filled spherical shell by the rotation of either one or both spheres. SCF can generate an enormous variety of flow patterns and transitions. Generally, a SCF can be considered as a combination of parallel disks in the pole region and a cylindrical annulus near the equator, hence SCF resembles cylindrical Taylor-Couette flow near the equator and the flow between two rotating disks in the vicinity of the poles. Moreover, in SCF the basic flows are fully three dimensional. The centrifugal forces are a function of the latitude, so that different flow patterns can be expected at different latitudes. However, we have the advantage that no awkward boundary effects exist like those caused by the finite length of the cylinders.

Khlebutin [145] was the first to experimentally discover Taylor vortices in the gap between coaxial rotating spheres. Nakabayashi et al. [146] divided the gap width into four regimes, namely, narrow ($\beta < 0.13$), intermediate ($0.13 < \beta < 0.17$), medium ($0.17 < \beta < 0.3$), and wide ($\beta > 0.3$). For the narrow-gap regime, the cylinder-type disturbances such as spiral Taylor-Görtler vortices and traveling waves on Taylor-Görtler vortices play an important role. For the intermediate-gap regime, the velocity fluctuations caused by the cylinder-type disturbances disappear with increasing Reynolds number (reverse Hopf bifurcation or relaminarization). For the medium-gap regime, relaminarization does not occur, i.e., spiral Taylor-Görtler vortices and traveling waves on Taylor-Görtler vortices continue to exist. In addition, disk-type disturbances such as Stuart vortices and shear waves occur at high Reynolds numbers. For the wide-gap regime, the first instability is spiral vortices or waves rather than Taylor vortices. This flow problem has been extensively studied and has charmed many researchers to determine a general map of the laminar-turbulent transition. So far, an

abundance of theoretical, experimental and numerical results on the spherical Taylor-Couette flow is available in the literature. Among these are Refs. [147–153].

II.6.2 Flow between two rotating cones: Conical Taylor-Couette flow

Modifying classical Taylor-Couette flow by replacing right cylinders by conical cylinders, which may be known as Conical Taylor-Couette flow (CTCF), produces a complex flow pattern. In general, the structure of Conical Taylor-Couette flow is a lot more complicated than classical Taylor-Couette flow, being dependent on gap width, cylinder height, rate of rotation, angle of conic, and rate of acceleration, with many different flows possible at the same angular velocities, as reported by many authors [154-158].

Since the radius changes linearly with the length of the cylinder, a linear distribution of the centrifugal forces in the gap is obtained. The imbalance of the centrifugal forces causes the three-dimensional flow field even in the subcritical state. The fluid is centrifuged at the largest radius, moves in spirals towards the smaller radius in the vicinity of the stationary cone and flows back to the larger radius near the rotating cone, still in spirals. They join and form a closed flow, as it is illustrated in Figure. II.23.

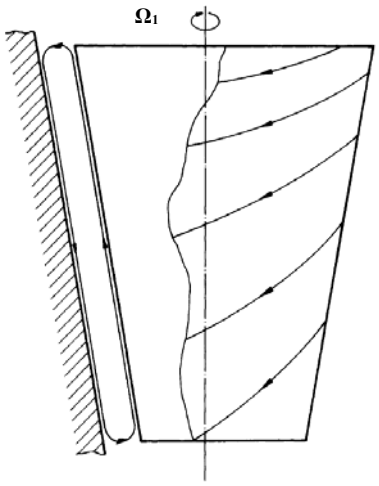

Figure II.23: Three-dimensional basic flow

The three-dimensional basic flow and especially the meridional component of the flow has a crucial influence on the Taylor vortices. Taylor vortices appear first at the largest radius in the upper part, whilst in the lower part - at the smaller radius - the undisturbed basic flow is still preserved. Hence, regions with subcritical and supercritical flows in the gap can be obtained, similar to the situation between rotating spheres. The still weak vortices at the beginning are most influenced by the three-dimensional flow and are floating upwards with the meridional flows, as shown in Figure. II.24.

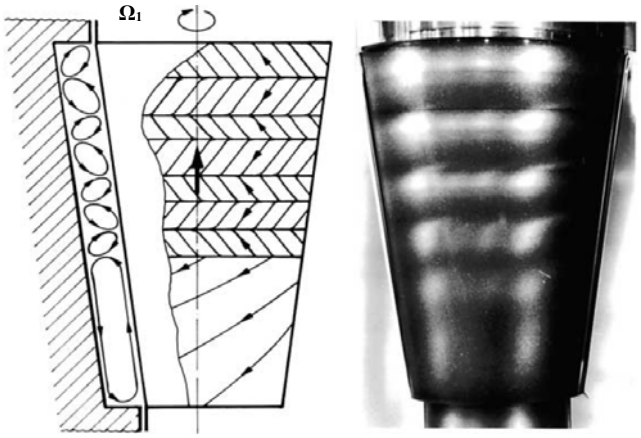

Figure II.24: Sketch and photo of sub- and supercritical regions. Toroidal vortices travel upwards. Adapted from Wimmer [157].

The occurrence of travelling closed toroidal vortex cells is astonishing. The travelling can only happen, if the upper cells are compressed to such an extent that one of them vanishes, while the two neighboring vortices join together, forming one large cell. The adjacent vortex pair follows up. At the same time, in the lower part a new pair is generated and the periodic process starts again. It is worthy to note that Taylor vortices appear as pairs of counter-rotating cells with alternately big and small vortex cells in the gap between conical cylinders, as displayed in Figure. 25.

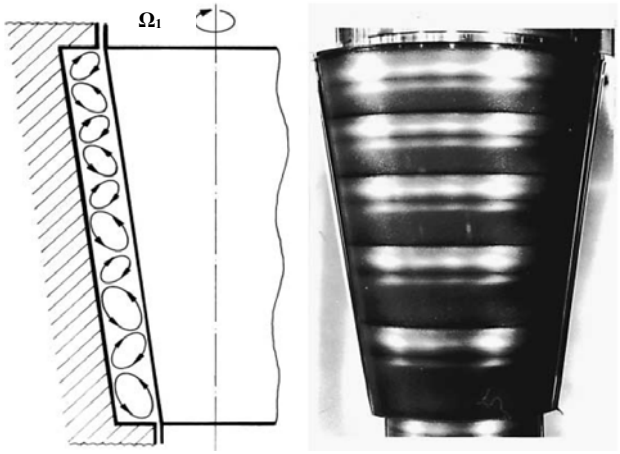

Figure II.25: Sketch and photo of the steady state with five vortex pairs. Adapted from Wimmer [157].

II.6.3 Flow between two rotating ellipsoids

Another variation of the classical Taylor-Couette geometry is the flow between rotating coaxial ellipsoids. This variant geometry is represented by two ellipsoids rotating about their shorter or longer axes to give oblate or prolate rotating ellipsoids, respectively. Indeed, the basic flow field between rotating ellipsoids is fully three-dimensional. However, it is more

complex than that between concentric rotating spheres because of the different curvature of the ellipsoids in circumferential and meridional direction.

The transition regimes present in the case of oblate ellipsoids resemble those existing in spherical geometry and inter-disc flows, hence the coexistence of two or more types of instabilities (Taylor vortex and spiral waves), as illustrated in Figure II.26.

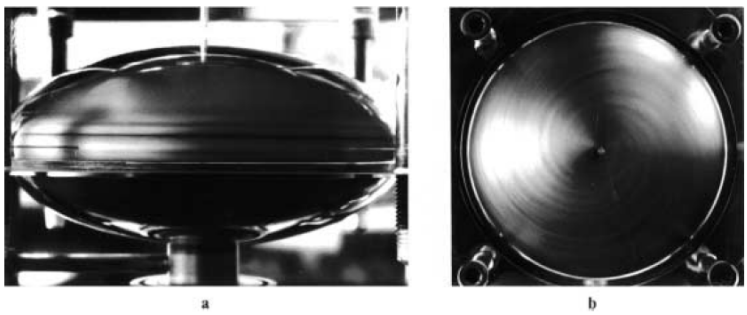

Figure II.26: Flow between oblate ellipsoids with rotating inner element and outer one at rest. a) Two Taylor vortices on each hemisphere, b) spiral instability around the pole. Adapted from Wimmer [157].

On the other hand, the prolate ellipsoids represent the transition from the spheres to the cylinders [157]. For small gap sizes between the prolate ellipsoids the analogy to the coaxial cylinders matches nearly ideally. For larger gap sizes the wavelength of the vortices becomes larger. The angle of inclination of the axes of the vortices grows with the gap size, and the occurrence of the Taylor vortices resembles more those between spheres rather than those between cylinders. For even larger gap widths the number of vortices diminishes and they are limited to a region near the equator. For these gap sizes and high Reynolds numbers a spiral instability around the poles appears, like for the rotating spheres, as shown in Figure II.27.

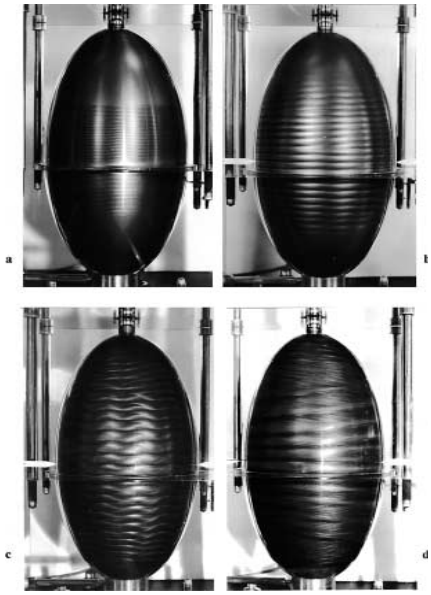

Figure II.27: Flow between prolate ellipsoids with rotating inner element and outer one at rest. From left to right and top to bottom: a) Taylor vortices for narrow gap sizes, b) broader Taylor vortices for broader gap sizes, c) wavy Taylor vortices, d) Taylor vortices near the equator and spirals around the poles; inbetween both systems overlap each other. Adapted from Wimmer [157].

II.7 Conclusion

After reviewing and analyzing the literature specific to the study of Taylor-Couette flow, it appears that despite the existence of numerous theoretical, numerical and experimental studies, they raise more questions than they provide answers on the fundamental phenomena governing the conditions under which instabilities occur, and the onset of various flow regimes. Moreover, literature reviewed in this section has shown that in this relatively simple setting, there are many interesting Flow phenomena. It has been established that classical Taylor-Couette flow is relatively sensitive to geometric, kinematic, dynamic and rheological effect. The main effect is to delay or advance the onset of different instabilities, which can cause a major disadvantage in terms of heat and mass transfer processes in the flow system under consideration.

In addition, by a variation of the cylindrical geometry to spherical, conical and ellipsoid configuration we can study the influence of geometric parameters very clearly. The effect of the three-dimensional basic flow on the instabilities depends on the ratio of the strength between the basic flow and the vortices. The varying centrifugal forces in the gap produce sub- and supercritical regions existing side by side. This fact allows to study the gradual spatial transition from sub- to supercritical flows. For certain geometries it is possible to have simultaneously two different types of instability in the gap, e.g. counter-rotating Taylor vortices and unidirectional-rotating cross-flow vortices. They are either separated or they influence and overlap each other, forming this way own, not clearly defined flow patterns. It has also been shown that a change from one instability system into another is possible by gradually changing the geometry. Therefore, by varying the geometry one can learn a lot about the onset of instabilities and the further development of vortex configurations and pattern forming systems.

CHAPTER III

Computational Fluid Dynamic Technique

« Whenever a theory appears to you as the only possible one, take this as a sign that you have neither understood the theory, nor the problem which it was intended to solve. »

Karl Popper

CHAPTER III: COMPUTATIONAL FLUID DYNAMIC TECHNIQUE

III.1 Introduction

Numerical computation, known as Computational Fluid Dynamics (CFD), is a tool that allows the numerical resolution of conservation equations written in a local form. These are, generally, partial differential equations (PDE) whose solution depends on two to four variables: the time variable with one to three spatial coordinates. This system of equations rarely has an analytical solution. Therefore, it is necessary to resolve them by a numerical method.

Numerical simulation software of flows can be considered true "numerical experiments" when done carefully. The advantage of "numerical methods" is that all the physical quantities related to the flow (velocity field, pressure field, stresses, etc.), are immediately available at any point in the flow. In an experiment, obtaining these physical quantities at any point in the field is often impossible or very difficult to put into practice.

III.2 Basic principles of CFD

There are three main elements in a CFD simulation. These are: (1) pre-processing (geometry and meshing), (2) processing (solver), and (3) post-processing (treatment of results).

The pre-processing comprises of the definition and discretization of the geometry to be analyzed. Specifically, the geometry or flow domain is divided up into a number of discrete elements by a grid or mesh. The geometry describes the shape of the problem to be analyzed. There are various ways of creating the geometry, depending on the complexity of the flow domain. In this thesis we have used **ANSYS Workbench**, which is a mesh generator that is part of the **ANSYS Fluent** software package.

The design and construction of a good quality grid is crucial to the success of the CFD analysis. The computational cells within the flow domain define an assembly of unit control volumes. The flow problem is solved in each cell. The cell shape and size have a significant impact on the rate of convergence, solution accuracy, and the CPU time required. Many different cell elements and grid types are available. A mesh can be coarse, medium, or fine. The appropriate choice of the mesh depends on complexity of the geometry on flow field, and on the cell types that are supported by the solver. Triangular and quadrilateral cells are commonly used for two-dimensional (2D) problems, in which the flow depends only on two spatial coordinates. Tetrahedral, prismatic or pyramidal cells are used in three-dimensional (3D). It is noteworthy that the pre-processing aspect is important, as over 50% of the time

spent in industry on a CFD project is devoted to the definition of the domain geometry and grid generation.

In our case, the generation of the mesh is an important phase as the precision and accuracy of the numerical results depends on it. Greater detail of the individual meshes used will be given in each chapter. Under ANSYS Workbench, the following three types of mesh can be chosen:

III.2.1. Structured mesh (Quadra/Hexa)

It is easy to generate using multi-block geometry and has the following advantages:

- Economical in terms of number of elements with a lower number of meshes compared to an equivalent unstructured mesh.
- Reduces the numerical error rate because the flow is aligned with the mesh.

Disadvantages:

- Difficult to generate in the case of complex geometry.
- Mesh quality not always satisfactory for complex geometries.

III.2.2. Unstructured mesh (Tri/Tetra)

The elements of this type of mesh are generated arbitrarily without any constraint as to their layout.

Advantage:

- Can be generated on complex geometry while maintaining good element quality.
- The algorithms for generating this type of mesh (sorting/tetra) are highly automated.

Disadvantages:

- Very greedy in number of meshes compared to the structured mesh.
- Generally, generates greater numerical errors (false diffusion) compared to structured meshes.

III.2.3. Hybrid mesh

It is a mesh generated by a mixture of elements of different types, triangular or quadrilateral in 2D, tetrahedral, prismatic or pyramidal in 3D. This mesh is characterized by the combination of the advantages of structured and unstructured mesh (Figure III.1).

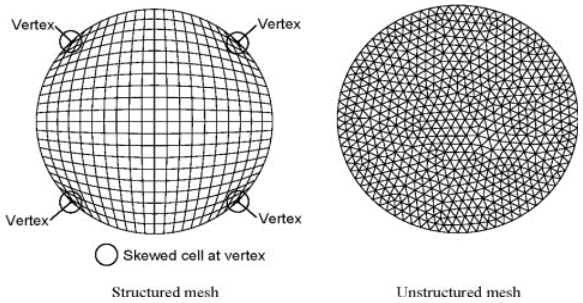

Figure III.1: Structured and unstructured meshes.

III.2.4. Mesh generation techniques

The generation of a very good mesh quality is essential for obtaining an accurate and meaningful calculation result. In practice, there is no standard rule for the creation of a valid mesh, however, different approaches can be used to obtain an acceptable mesh grid. We can summarize these rules as follows:

- Maintain a good **Quality** of the elements,
- Ensure good **Resolution** in areas with high gradients,
- Ensure a good **Smoothing** in the transition areas between fine and coarse mesh parts,
- Minimize the number of **Total** Elements (reasonable calculation time).

These rules can be remembered by using the mnemonic formulation **QRST.**

The processing stage (solver) involves the selection of an appropriate physical model for the flow that needs to be modeled, the specification of the fluid properties inside the domain, the definition of appropriate boundary and operating conditions as well as of thermodynamic properties of the flow. This stage involves the discretization of the governing equation (Navier-Stokes equations) of the system so that they can be solved iteratively. There are four major numerical solution techniques commonly used for discretized problems in commercial CFD. These solution techniques are: (1) the finite difference method, (2) the finite element method, (3) the finite volume method, and (4) the spectral method. In this work, the finite volume approach is followed. The advantages of finite volume method over all other techniques as outlined in ANSYS Fluent user's guide include:

- Flexibility in terms of its usage on either a structured or unstructured mesh.
- Its economical use of computer memory and speed for very large problems, higher speed flows, turbulent flows, and source term dominated flows.
- Easy programming in terms of CFD code development.

Post-processing is the process of displaying and visualizing the CFD results through the manipulation of the numerical output. In ANSYS Fluent, some post-processing tools are incorporated into the academic license package to visualize the flow, extract, and manipulate CFD data. Flow properties such as the dynamic pressure, velocity magnitude, wall shear stress, and velocity vectors are computed and plotted from the flow state output of the flow solver. An adequate analysis of the variation of the flow properties at any point in the medium can be performed using ANSYS Fluent's graphical interface. Several other features like 2D and 3D surface plots, streamlines, Power Spectral Density (PSD), particle tracking, view manipulations (translation, rotation and scaling) and color postscript output can be displayed. A key functionality of the post-processing software is the ability to visualize complex flows. In the ANSYS Fluent software, it is possible to export the geometry and the flow data to other

post-processing software, such as CFD Post and Tecplot. Tecplot offers a greater level of sophistication in the geometry and flow rendering tool, aiding the visualization and the interpretation of the predicted flow pattern.

III.3 Numerical modeling

There are three fundamental principles that govern physical aspects of any continuous flow, including turbulent ones. These three fundamental principles are:

- The conservation of mass.
- Newton's second law for the conservation of momentum.
- The first law of thermodynamics for the conservation of energy.

III.3.1 The governing equations

The above three fundamental principles can be expressed in terms of basic mathematical equations, the continuity equation, the momentum equations, and the energy equation which, in their most general form, are either integral or partial differential equations. These governing equations are solved subject to boundary conditions describing the physical state of the flow at the computational domain boundaries. The behaviour of the fluid properties is generally described in terms of macroscopic intensive properties such as velocity, pressure, density, temperature, and specific energy. We note that there are three important principles that are helpful for obtaining the basic equations of fluid motion as:

- Choosing of appropriate set from any of the law of physics described earlier.
- Application of this set to a suitable model of the flow.
- Obtaining an equation which represents the set.

In this study, all the CFD simulations assume an isothermal, viscous, and incompressible fluid condition. For an incompressible flow, the density is constant. As such the energy equation becomes uncoupled from the continuity and momentum equations. Therefore, all the discussions in this study will only focus on the continuity and momentum (Navier-Stokes) equations. The summary of these equations is presented in this thesis, while the detailed derivations of these equations can be found in Ansys Fluent and in other fluid mechanics text books.

III.3.1.a The continuity equation

The law of conservation of mass can be applied to any fluid flow in a control volume, so that the change of mass in the control volume is equal to the mass that enters through its faces minus the total mass leaving its faces. The unsteady, three-dimensional continuity equation can be written in conservative form as:

$$\frac{\partial(\rho)}{\partial t} + \nabla(\rho v) = 0 \qquad (III.1)$$

The first term on the left-hand side of equation III.1 is the rate of change in time of the density (mass per unit volume). The second term describes the net mass flux across the boundaries of an element control volume and it is called the convective term.

For an incompressible flow, the density, ρ is constant, hence the continuity equation III.1 simplifies to:

$$\nabla . v = 0 \qquad (III.2)$$

III.3.1.b The momentum or Navier-Stokes equations

When Newton's second law of motion is applied to the fluid flow in a moving control volume, the rate of change of momentum of a fluid particle equals to the sum of the forces acting on the particle (F = ma). There are two types of forces acting on a fluid particle, namely, surface forces and body forces. Surface forces act directly on the surface of the fluid element. They are due to only two forces: (a) the thermodynamic pressure distribution acting on the surface, imposed by the outside fluid surrounding the fluid element, and (b) the shear and normal viscous stresses acting on the surface, also imposed by the outside fluid "tugging" or "pushing" on the surface by means of friction. The body forces act directly on the volumetric mass of the fluid element. These forces "act at a distance". Examples are gravitational, centrifugal, Coriolis, and electromagnetic forces.

The Navier-Stokes equations applied to a fixed control volume are represented in vector form by:

$$\rho \frac{\partial v}{\partial t} + \rho(v.\nabla)v = -\nabla p + \mu \Delta v \qquad (III.3)$$

Where (U, V, W) are the physical components of the velocity v. P, ρ, t, and μ denote pressure, density, time and dynamic viscosity of the fluid, respectively.

This vector equation involves four basic quantities: Local acceleration, convective acceleration, the pressure gradient and viscous forces. The viscous forces are the normal and shear stress distributions acting on the surface. These are modeled in equation III.3 assuming a Newtonian fluid. In the momentum equation, it is a common practice to highlight the contribution due to the surface forces as separate terms and to include the effects of the body forces as source terms. Therefore, the conservative form of the linear vector momentum equation III.3 expressed in terms of surface (pressure and viscous stresses) and including the body forces is given as:

$$\rho \frac{\partial v}{\partial t} + \rho(v.\nabla)v = -\nabla p + \nabla \tau + S \qquad (III.4)$$

Neglecting the effects of the body forces as source terms, equation III.4 becomes

$$\rho\frac{\partial v}{\partial t}+\nabla.\rho vv=-\nabla p+\nabla\tau \qquad (III.5)$$

The continuity equation III.2 and momentum equation III.3 can be re-cast into an integral form by integrating them over an arbitrary volume **V** bounded by a close surface **S**. This gives:

$$\int_V \nabla.v dV = 0 \qquad (III.6)$$

$$\rho\int_V \frac{dv}{dt}dV+\rho\int_V v.\nabla v\,dV=-\int_V \nabla p\,dV+\mu\int_V \Delta v\,dV \qquad (III.7)$$

By the application of the Gauss divergence theorem, these become:

$$\int_S v.dS = 0 \qquad (III.8)$$

$$\rho\frac{d}{dt}\int_V v\,dV+\rho\int_S vv.dS=-\int_S pI.dS+\mu\int_S \nabla v.dS \qquad (III.9)$$

where **I** is the identity unit diagonal matrix.

In flows of simple geometry, the continuity and Navier-Stokes equations can be solved analytically, while more complex flows can be tackled numerically with CFD techniques, such as the finite volume method, without additional approximations at low and moderate Reynolds numbers. The ease with which solutions can be obtained and the complexity of the resulting flows often depend on which quantities are important for a given flow.

III.3.2 Numerical scheme

The CFD software package ANSYS Fluent used in this research work is a finite volume code. The computational domain is divided into unit control volumes. To solve the flow governing equations numerically in each control volume, they have to be transformed into algebraic expressions. The process of transforming these equations into solvable algebraic expressions is known as discretization. The finite volume approach in ANSYS Fluent involves the integration of the flow governing differential equations over all the control volumes of the solution domain to yield a volume averaged estimate of the flow state at each cell. The discretization using the finite volume method involves the substitution of piece-wise constant approximations for the terms in the integral equation representing flow processes such as convection, diffusion, and sources terms. This converts the integral equations into a system of linear algebraic equations. These linear algebraic equations are solved iteratively over the control volumes to compute the flow state until convergence. The accuracy of a converged solution is dependent on the physical models, on the grid resolution, as well as on the problem setup.

There are two numerical solution techniques provided by ANSYS Fluent. These are:

- A pressure-based solver (segregated and coupled algorithms).
- A density-based solver.

In both methods, the velocity field is obtained from the momentum equations. The integral form of the governing equations for the conservation of mass and momentum are solved using either method. Both methods use a control-volume-based technique and the discretization process for the two numerical methods is the finite-volume one. The two methods differ in the approach used to linearize and solve the discretized equations.

The pressure-based solver is formulated either as a segregated or a coupled algorithm. In this thesis, the pressure based segregated solver has been used. In this solver, each discrete governing equation is linearized implicitly with respect to the conservative variable of that equation. That is, the conservative variables in the governing flow equations are solved implicitly by considering all cells one after another in a sequential manner. This results in a system of linear equations with one equation for each cell in the domain. The reason for selecting the pressure based segregated solver is that this is computer memory efficient, since the discretized equations need only be stored in the memory one at a time. The pressure based segregated solver requires about 1.5 to 2.0 times less computer memory than the pressure based coupled solver. The general solution procedure for the pressure based segregated and coupled algorithms as well as the density-based solvers is fully described in ANSYS Fluent.

III.3.2.a Spatial discretization

In all CFD simulations involving finite volume method, the computational domain is divided into a finite number of elements or cells. The cell is the control volume into which the physical domain is broken down by the regular and irregular arrangement of nodes to construct the mesh. The flow problem is solved in the cell that is defined around grid points or nodes. The cell averaged flow state is determined at these nodes, so that the flow can be described mathematically by specifying the cell averaged flow state at all grid points in space and time. The accuracy and stability of the numerical computation is dependent on the quality of the mesh. The attributes associated with mesh quality outlined in ANSYS Fluent are the node point distribution, the smoothers, the cell skewness and the cell aspect ratio.

- **The node point distribution** determines the degree to which shear layers, separated regions, shock waves, and boundary layers are resolved. Poor node density and node distribution in critical regions leads to poor resolution, which adversely affects the flow predictions. To achieve a good resolution of the boundary layer for a laminar flow, the grid adjacent to the wall should satisfy the condition

$$y_p \sqrt{\frac{\rho u_\infty}{\mu x}} \leq 1 \qquad (III.10)$$

where y_p is the distance to the wall from the adjacent cell centroid, u_∞ is the free stream velocity, ρ is density of the fluid, μ is the dynamic viscosity of the fluid, and x is the distance along the wall from the starting point of the boundary layer. Equation III.10 places the first grid point within the lower quarter of the boundary layer thickness. The resolution of the laminar boundary layer plays a significant role in the accuracy of the computed wall shear stress.

The numerical results for the turbulent flows tend to be more susceptible to grid dependency than those for a laminar flow, due to the interaction of the mean flow and turbulence. The mesh resolution required at the near-wall region depends on the turbulence closure model being used.

- **Smoothness** in the computational mesh reduces the truncation error of the numerical solution. The smoothness of the mesh can be improved by refining the mesh based on the change in cell volume or the gradient of the cell volumes along computational mesh lines.
- **The cell skewness** is the difference between the shape of the cell and the shape of an equilateral cell of equivalent volume. Highly skewed cells can decrease the solution accuracy and de-stabilize the solution procedure. For a good unstructured mesh, the skewness should always be below 0.98.
- **The cell aspect ratio** is a measure of the stretching of the cell. It is defined as the ratio of the maximum distance between the cell centroid and face centroid to the minimum distance between the nodes of the cell. A general rule of thumb is to avoid aspect ratios in excess of 5:1.

The three major types of mesh that are generally used in CFD simulation are the single-block structured, single-block unstructured, and multi-block structured meshes. The choice of the type of mesh depends on the problem and the solver capabilities.

A structured mesh is typically restricted to topologically rectangular computational domains and is hexahedral in shape. This type of mesh is preferred for analysis of rectangular shapes and of simple cuboid geometries. An unstructured mesh, on the other hand, is typically a mesh with irregular spacing between grid points that are joined to form a tetrahedral mesh. This type of mesh is designed for more complex geometries as nodes can be placed within the computational domain depending on the shape of the body. In other word, the grid can acquire a shape more closely matching a body surface.

Multi-block structured meshes combine the lower computing cost associated with a structured mesh and the flexibility associated with an unstructured mesh. In this type of mesh,

the computational domain is subdivided into different blocks that can be structured meshed. Note that, a structured mesh has been used for all flow configurations presented in this study.

III.3.2.b Equation discretization

There is the need to solve the integral form of the governing partial differential equations III.6 and III.7 by the CFD solver. The flow governing equations are solved for each control volume iteratively in discrete form. The discretization process results in a set of algebraic equations that resolve the variables using a pseudo-time integration method at a specified finite number of points within the control volumes. The flow field within the whole domain is then obtained. The semi-discrete form of the governing equations is given by:

$$\sum_{i=1}^{N} v \,.\, \Delta S = 0 \qquad (III.11)$$

$$\rho \frac{\partial}{\partial t}\langle v \rangle + \rho \sum_{i=1}^{N} vv \,.\, \Delta S = -\sum_{i=1}^{N} p \Delta S + \mu \sum_{i=1}^{N} \nabla v . \Delta S \qquad (III.12)$$

Where

$$\langle \mathrm{v} \rangle = \int_{\mathrm{V}} \mathrm{v} d\mathrm{V}$$

and $\Delta \mathbf{S}$ is the i^{th} facet of each control volume V, which is fully enclosed by N facets. The equations solved by ANSYS Fluent are defined at the control volumes generated by the unstructured computational grid. The discrete variable values such as pressure, velocities and specific turbulent kinetic energy are calculated and stored at the cell centers by ANSYS Fluent. Using the finite volume method, the integral conservation laws are approximately satisfied over the control volume. That is, the net flux through the control volume boundary is the sum of integrals over the different control volume faces as the control volumes do not overlap. At the control volume faces, the values of the integrand are required for the convection terms of the turbulence closure model. This can only be determined by interpolation from the cell-averaged flow state. This is accomplished by using an upwind scheme to determine the values at the faces. The up-winding is the process of deriving the cell face values of the state variables from quantities in the cell upstream, relative to the direction of the mean velocity.

*** First-order upwind scheme**

This is the simplest numerical scheme available in ANSYS Fluent. In this scheme, quantities at the cell faces are determined by assuming that, for any variable throughout the entire cell, the face values are identical to the cell average. Hence, when the first-order upwind scheme is selected, the face value of a variable is set equal to the cell average value of the variable in the upstream cell.

The main advantages of this scheme are:

- Easy to implement resulting in very stable calculations.
- Can yield better convergence.
- Can be applied without any significant loss of accuracy when the flow is aligned with the grid, especially for a quadrilateral or hexahedral grid, so that numerical diffusion is naturally low.
- Can be used as a starter to perform first a few iterations for any numerical simulation that involves complex flows.

The disadvantage is that this scheme is prone to numerical discretization errors (numerical diffusion) in a tetrahedral mesh and it will yield less accurate results than on a hexahedral mesh.

*** Second-order upwind scheme**

This scheme is more appropriate than a first order scheme for triangular and tetrahedral grids where the flow is never aligned with the grid. The scheme is more accurate than the first-upwind scheme because it applies a reconstruction of the state variable gradient inside each cell. In this scheme, quantities at cell faces are computed using a multidimensional linear reconstruction approach, whereby higher-order accuracy is achieved at cell faces through a Taylor series expansion of the cell-centred solution about the cell centroid. Hence the face value of a variable is computed by averaging the cell values in the two cells adjacent to the face using a gradient method. The main disadvantage of this scheme is that it can result in face values that are outside of the range of cell values in regions with strong gradients. In such case, it is then necessary to apply limiters to the predicted face values to achieve accuracy and stability. The Green-Gauss node-based method is applied as the limiter for the computation of the gradients in the cell centers. The Green-Gauss node-based method computes the arithmetic average of the nodal values on the face. The nodal values are computed from the weighted average of the cell values surrounding the nodes of the face.

There are, also, other discretization schemes such as:

*** QUICK (Quadratic Upwind Interpolation for Convective Kinetics) scheme**

This scheme provides better accuracy than the second-order scheme for rotational and swirling flows with a regular mesh size. However, it is not recommended for a triangular mesh.

*** Power Law scheme**

It is more precise than the "First Order Upwind Scheme" for very low Reynolds number flows (<5).

*** Third-Order MUSCL scheme (Monotone Upstream-Centered Schemes for Conservation Laws):** Unlike the QUICK scheme, which is applicable to structured hex meshes only, the MUSCL scheme is applicable to arbitrary meshes. Compared to the second-order upwind scheme, the third-order MUSCL has a potential to improve spatial accuracy for all types of meshes by reducing numerical diffusion, most significantly for complex three-dimensional flows, and it is available for all transport equations. In addition, it gives more precision than the other schemes.

The different interpolation schemes for precision orders 1, 2 and 3 available in the ANSYS Fluent code are summarized in Figure III. 2:

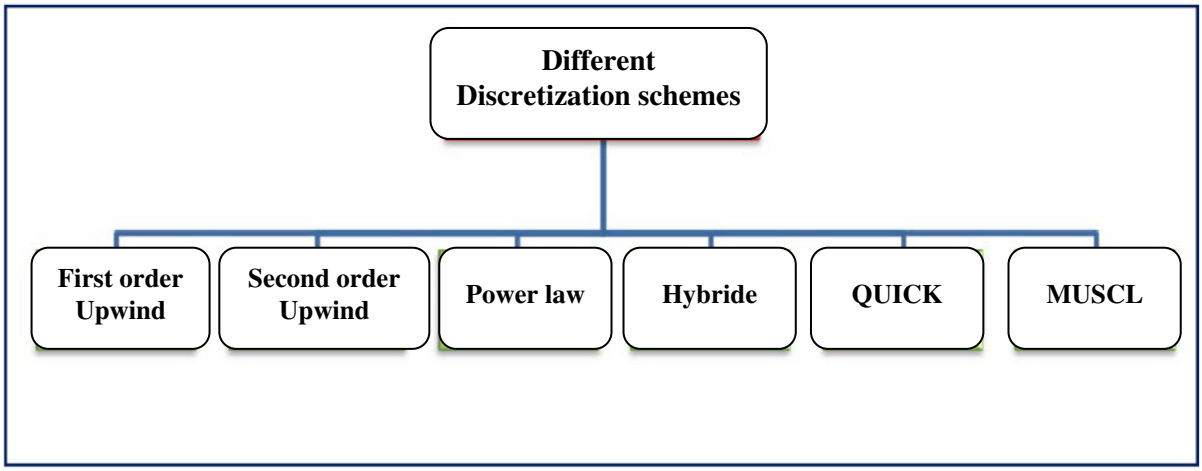

Figure III.2: Different discretization schemes.

III.3.2.c Numerical scheme for pressure

The conservative variables in the vector momentum equation are stated in the form of convection-diffusion terms, except for pressure. Pressure appears as a source term in the integral momentum equation III.7, thus, the pressure field needs to be calculated at the computational cell boundaries in order to solve these equations. Therefore, an interpolation scheme is required to compute the face values of pressure from the cell values.

ANSYS Fluent offers the following options for interpolating the pressure values at the faces. By default, the **Second Order** scheme is used except in the case of mixture or VOF (Volume Of Fluid) multiphase simulations in which case **PRESTO!** is the default.

- The **Linear** scheme computes the face pressure as the average of the pressure values in the adjacent cells.
- The **Standard** scheme interpolates the pressure values at the faces using momentum equation coefficients.
- The **Second Order** scheme reconstructs the face pressure using a central differencing scheme. The **Second Order** scheme is not applicable for the VOF or mixture model

for multiphase flow. This scheme may provide improved accuracy over the **Standard** and **Linear** schemes.

- The **Body Force Weighted** scheme computes the face pressure by assuming that the normal gradient of the difference between pressure and body forces is constant. This works well if the body forces are known a priori in the momentum equations (for example, buoyancy and axisymmetric swirl calculations).
- The **PRESTO!** (PREssure STaggering Option) scheme uses the discrete continuity balance for a "staggered" control volume about the face to compute the "staggered" (that is, face) pressure. This procedure is similar in spirit to the staggered-grid schemes used with structured meshes. Note that for triangular, tetrahedral, hybrid, and polyhedral meshes, comparable accuracy is obtained using a similar algorithm. The **PRESTO**! scheme is available for all meshes.

The various face pressure interpolation schemes available in the Ansys Fluent code are summarized in Figure III.3:

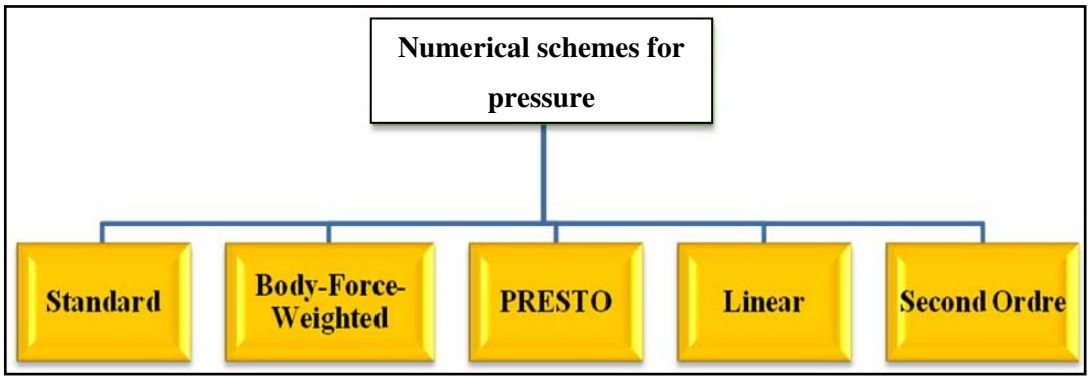

Figure III.3: Different numerical schemes for pressure.

III.3.2.d Pressure-velocity coupling

In an incompressible flow model, the density is constant and hence it is not linked to pressure. As there is no governing partial differential equation for pressure, a constraint is therefore introduced in the coupling between pressure and velocity on the solution of the flow field. The continuity equation can only be satisfied for the velocity field if the correct pressure field is applied to the momentum equations. To achieve this, a pressure-velocity coupling algorithm adds a correction factor to the face flux, so that the corrected face flux satisfies the continuity equation. ANSYS Fluent provides the option to choose among five pressure-velocity coupling algorithms: **SIMPLE**, **SIMPLEC**, **PISO**, **Coupled**, and (for unsteady flows using the Non-Iterative Time Advancement scheme (NITA)) Fractional Step (FSM). All the aforementioned schemes, except the "coupled" scheme, are based on the predictor-corrector approach.

- The **SIMPLE** algorithm (The Semi-Implicit Method for Pressure Linked Equations) uses a relationship between velocity and pressure corrections to enforce mass conservation and to obtain the pressure field. This algorithm substitutes the flux correction equations into the discrete continuity equation to obtain a discrete equation for the pressure correction in the cell. The **SIMPLE** algorithm is recommended for steady-state calculations.
- The **SIMPLEC** (SIMPLE-Consistent) procedure is similar to the SIMPLE procedure outlined above. The only difference lies in the expression used for the face flux correction.
- The Pressure-Implicit with Splitting of Operators (**PISO**) pressure-velocity coupling scheme, part of the **SIMPLE** family of algorithms, is based on the higher degree of the approximate relation between the corrections for pressure and velocity. One of the limitations of the **SIMPLE** and **SIMPLEC** algorithms is that new velocities and corresponding fluxes do not satisfy the momentum balance after the pressure-correction equation is solved. As a result, the calculation must be repeated until the balance is satisfied. To improve the efficiency of this calculation, the **PISO** algorithm performs two additional corrections: neighbor correction and skewness correction. Furthermore, the main idea of the **PISO** algorithm is to move the repeated calculations required by **SIMPLE** and **SIMPLEC** inside the solution stage of the pressure-correction equation. After one or more additional **PISO** loops, the corrected velocities satisfy the continuity and momentum equations more closely. This iterative process is called a momentum correction or "neighbor correction". The **PISO** algorithm takes a little more CPU time per solver iteration, but it can dramatically decrease the number of iterations required for convergence, especially for transient problems.

III.3.3 Interpolation methods of gradients

The gradients are needed to evaluate diffusive flows, velocity derivatives and for high-order discretization schemes. The gradients of the variables at the centres of the mesh faces are computed in ANSYS Fluent according to the following methods:

- **Green-Gauss Cell-Based:** Default method and the solution can lead to false diffusion.
- **Green-Gauss Node-Based:** More accurate method and minimizes the value of false diffusion. It is recommended for tri- and tetradimensional meshes.
- **Least-Squares Cell-Based:** This method is recommended for polyhedral meshes.

The gradients of the variables on the faces of the meshes are calculated using a Multidimensional Taylor series.

III.3.4 Convergence criteria

In all CFD simulations, the governing equations must be transformed to algebraic expressions that are solved iteratively. To obtain a solution, there is the need to specify the information that is required to control the numerical solution algorithm. During the process of CFD simulation, there are integration errors in the discretized equations, summed over all control volumes, which may lead to inaccuracy in the flow solution. The solution to the numerical equations can be used to evaluate such errors. These measures of error, which are generally known as residual errors or residuals, can be used as a guide to see if a solution process is converging or not. The residual is the imbalance of the conservation equation for either mass or momentum summed over all the computational cells. The residual of the solutions can also be used to monitor the performance of a simulation. Progress towards a converged solution can be greatly assisted by the careful selection of the settings of various under-relaxation factors. Each Under-Relaxation Factor (URF) is adjusted *ad hoc* for its respective conservative variable in order to improve the convergence rate. As the solution process progresses from iteration to iteration, the residual errors from each equation should reduce. Low residuals suggest a solution that converges and the simulation can be considered stable if the residuals keep decreasing in magnitude monotonically with further iterations. That is, solutions of CFD problems are considered to converge when the flow field and the scalar fields are no longer changing.

In many applications, the momentum and continuity residuals are monitored to measure the error in the solution. When the value of each residual is between three to four orders of magnitude below its initial value, the solution is said to achieve convergence to an acceptable level, depending on the level of accuracy required. At the completion of every flow solver iteration, the sum of the residual squared of each conserved variable is computed and stored to a data file or displayed on terminal screen, where the convergence history is visualized. This enables a quick check on the progress of the solution to be made. Low residuals do not however guarantee that the converged solution is correct. Additional reports of integrated quantities at surfaces and boundaries are often used to judge convergence. A physical variable of the solution flow field therefore needs to be monitored to ensure the convergence of the computation to a physically correct solution. This convergence is reached when the physical variable remains constant for a sufficient number of iterations and the residuals have reached a pre-determined reduction. Mass imbalance is also often used to monitor convergence. This is a report of the mass flow rates at the inlet and outlet flow boundaries, which should add to zero for a converged solution.

CHAPTER IV

Numerical investigation of the onset of axisymmetric and wavy Taylor-Couette flows between combinations of cylinders and spherocylinders

« Everything should be made as simple as possible, but not simpler »

Albert Einstein

Results and discussion

Chapter IV: Numerical investigation of the onset of axisymmetric and wavy Taylor-Couette flows between combinations of cylinders and spherocylinders

IV.1 Introduction

The Taylor-Couette flow system consisting of fluid in an annular gap between two concentric rotating bodies has been a paradigm for the study of the pattern-formation phenomena and the transition to turbulence following a progression of instabilities. Moreover, fluid motion in cylindrical or spherical annulus is among the most fundamental problems in fluid dynamics, and presents a great interest in hydrodynamic stability theory. Furthermore, these canonical flow geometries generate an enormous variety of flow regimes and bifurcations. Such flow systems appear over a range of scales in technology and nature. For example, on a small scale in filtration systems, the fabrication of Nano-sensors, emulsion polymerization devices, centrifuges used in the chemical and pharmaceutical industries, the cultivation of cells, blood detoxification, reaction vessels viscometry, cooling of rotating electrical machinery, and particularly on a large scale in the fields of geophysics, astrophysics, oceanography, meteorology, and dynamics of planetary atmospheres.

In cylindrical Taylor-Couette configuration there exists a large variety of flow regimes, as the flow evolves from laminar flow to fully turbulent. Over one hundred years ago, Mallock [10] and Couette [11] conducted independent experiments using concentric rotating cylinders. Their experiment results started the academic research on the flow instability in concentric rotating cylinders, however, neither Couette nor Mallock established a criterion for the hydrodynamic stability of the flow problem. Later, Rayleigh [12] was the first to publish a criterion for the hydrodynamic stability of inviscid fluid between two concentric rotating cylinders. Taylor [14] examined viscous incompressible flow in a cylindrical annulus, and found that if the angular velocity of the inner cylinder is greater than a critical value, the laminar Couette flow (LCF) becomes unstable to axisymmetric perturbations (TVF). Taylor's work is considered as the first case of a stability calculation quantitatively matching experimental values. Coles [14] observed experimentally 26 states with differing azimuthal and axial wave numbers, known as wavy vortex flow (WVF). Since the pioneering work of Taylor [14], and with the interplay between experimental, numerical, and analytical works, a wide range of flow regimes has been observed by

numerous researchers for different boundary conditions (Chandrasekhar [17], Fenstermacher et al. [20], Diprima and Swinney [4], Donnelly [8], Marcus [159], Koschmieder [1], Czarny et al. [22], Avila et al. [160], Martinez-Arias et al. [73], Adnane et al.[91], Griffini et al. [161], Froitzheim et al. [162], Brauckmann et al. [163], Chouippe et al. [164], Grossmann et al. [165], Lalaoua and Bouabdallah [144], Mullin et al. [166]). These authors and other concluded that depending on the radius ratio, the aspect ratio, acceleration rate and Reynolds number, the cylindrical Taylor-Couette flow can produce a large number of flow patterns and instabilities.

Whereas the majority of the pioneering works were focused on the flow between two coaxial rotating cylinders, later researches were extended to the flow between two concentric spheres where the Taylor vortices could appear. This flow problem has been studied extensively and has charmed many researchers to determine a general map of the laminar-turbulent transition. So far, an abundance of theoretical, experimental and numerical results on the spherical Taylor Couette flow is available in the literature. Among these are Khlebutin [145], Yavorskaya et al. [167], Nakabayashi [168], Marcus and Tuckerman [169, 147], Bühler [149], Egbers and Rath [150], Hollerbach [170], Peralta et al. [171], Bühler [172], Yuan [151], Tigrine et al. [152], lalaoua and Bouabdallah [153].

On the other hand, many modifications can be made to Taylor-Couette flow, which can result in much more complex flow structures, by either geometrical changes, or by combining different system (Wimmer [148, 173, 174], Abboud [175], Ning et al. [176], Denne and Wimmer [177], Sprague et al. [178]. Furthermore, Wimmer [157] conducted an extensive experimental study of the occurrence of different instabilities in the gap between differently shaped rotating bodies, prolate and oblate rotating ellipsoids. He found that a change from one instability system into another is possible by combining different geometries.

While the appearance of various flow modes in cylindrical and spherical annuli is deeply investigated in the past and substantial experimental and numerical works have been published for the regime transitions and the flow behavior in rotating bodies with a shape between cylinder and sphere have not yet been investigated; and to our knowledge, this computational investigation is the first for these flow configurations. The present numerical study focuses on the occurrence of different hydrodynamic instabilities in combined Taylor-Couette geometries. Three flow geometries are considered in which three flow regimes are studied, namely laminar Couette flow (LCF), Taylor vortex flow (TVF) or Taylor vortices, and wavy vortex flow (WVF).

IV.2 Flow configurations and CFD modelling

In this work, we consider the motion of a viscous incompressible Newtonian fluid contained in an annulus between two concentric bodies. Three types of flow configurations were numerically

simulated, namely flow between two concentric cylinders with fixed end-caps (Type 1), flow between two concentric cylinders with hemispheres on the lower end wall (Type 2), and flow between two spherocylinders, i.e, cylinders with hemispheres on the upper and lower end surfaces (Type 3). The outer element is stationary while the inner one rotates freely about a vertical axis through its center, which is taken to be the origin of the coordinate system. The plate end-caps in Type 1 and Type 2 configurations are kept fixed. All the flow geometries investigated in this study, are bodies of revolutions with symmetry about the axis of rotation, as shown in Figure IV.1. The flow fields are characterized by the Reynolds number $Re= (\Omega_1 R_1 d)/ \nu$, which is used to describe the ratio of inertial to viscous forces, where R_1 and R_2 are the radii of the inner and outer elements, respectively, d is the gap width, Ω_1 is the angular velocity of the inner element and ν is the kinematic viscosity. The working fluid used in this study is water. The flow features are described by the following dimensionless parameters:

- The aspect ratio: $\Gamma_1=H_1/d=20$, $\Gamma_2=H_2/d=30$ and $\Gamma_3=H_3/d=40$ for the flow configurations type 1, type 2 and type 3 respectively.
- Radius ratio: $\eta= R_1/R_2=0.909$
- Gap width: $\beta=(R_2-R_1)/R_1=0.1$

The Reynolds number was increased stepwise by a quasi-static increase of the angular velocity of the inner element with a rate of increase $\Delta\Omega_1/\Omega_1 \leq 5\%$ ($\Delta\Omega_1$ is the velocity increasing), and the final flow field of the last step was used as the initial condition for obtaining the flow at the next step.

The continuity and momentum equations for an incompressible viscous flow are written as follows:

$$\mathrm{div}\,\mathbf{v} = 0 \qquad (IV.1)$$

$$\rho\frac{\partial \mathbf{v}}{\partial t} + \rho(\mathbf{v}.\nabla)\mathbf{v} = -\nabla \mathbf{p} + \mu\Delta\mathbf{v} \qquad (IV.2)$$

With (U, V, W) are the physical components of the velocity **v**. Time and pressure are denoted by t and **p**, respectively.

The 3D geometries were meshed with structured hexahedral cells. Grid resolution studies for the different flow modes showed that 450000, 760000 and 1200000 cells were needed for each type of flow configuration, respectively. The grid spacing was refined in both the axial and radial directions to improve resolution near the walls where there are a high shear (due to steep gradients near these boundaries), and more complex flow features are expected. The grid resolution was increased until further increases in resolution did not improve the solutions (mesh dependence).

The numerical results are obtained using the simulation code Ansys Fluent based on the finite volume method for the discretization of the equations of the problem. The discretization scheme chosen for the pressure is the second order model. The second order upwind scheme was used for the moment equations. The velocity-pressure coupling is solved using the PISO algorithm.

Gradients were evaluated using a node cell-based method. Convergence of the solution was monitored by checking the absolute residuals of the continuity equation and three velocity components until they all fell below 10^{-4}. No-slip boundary conditions for the velocity are applied at all surfaces. In addition, all the variables are set to zero at the walls except for the tangential velocity W, which is set to $\Omega_1 R_1$ on the inner rotating element and zero on the outer stationary element.

Note that the flow was assumed to be steady state and isothermal for LCF and TVF, therefore for the calculations steady-state solver was used, while for WVF, which is time-dependent, the flow was assumed to be unsteady and isothermal, hence a transient solver was employed.

As there is no experimental works available for the flow geometries type 2 and 3, our computational results are compared and validated against experimental works of Adnane et al. [91] and Parker and Merati [179] for a similar flow geometry (type 1). A good agreement is found between the two approaches, within 3%.

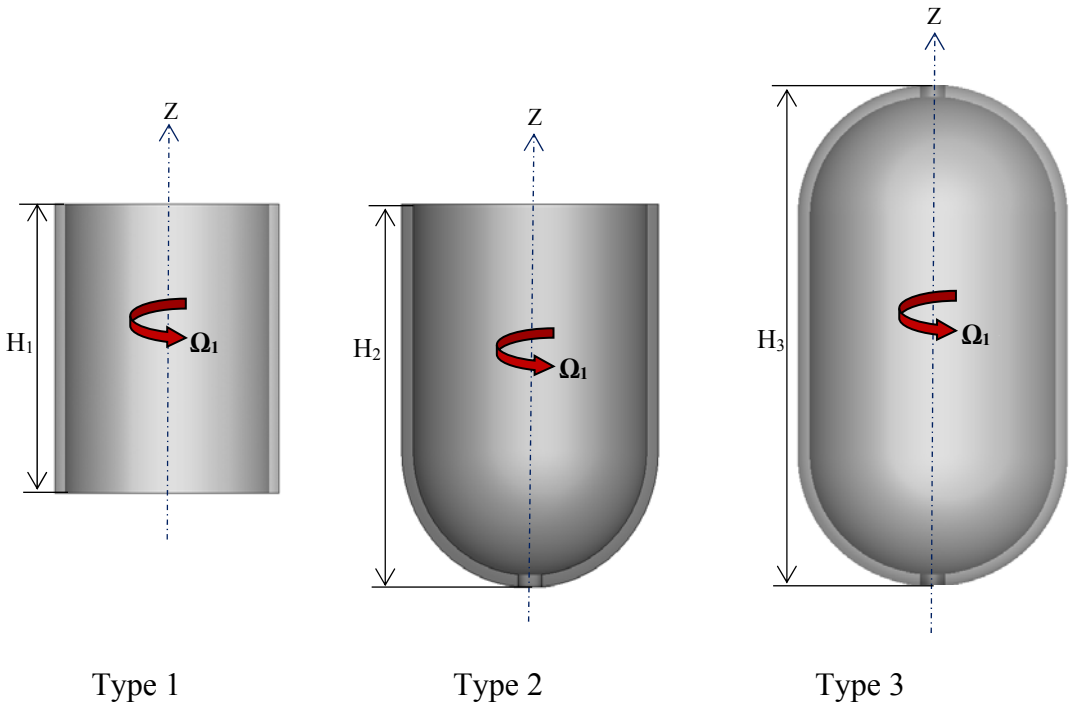

Figure IV.1: Sketch of the Taylor-Couette flow system at different geometries/ Possible combinations of cylinders and spheres.

IV.3 Main numerical results

The flow behaviors of a viscous incompressible Newtonian fluid confined in the annular gap between two concentric bodies (type1, type2 and type 3) are presented in terms of wall shear stress and skin friction coefficient for three flow regimes defined as laminar Couette flow, Taylor vortex flow and Wavy vortex flow, respectively, as shown in Figure IV.2 and Figure IV.3. As the angular velocity of the inner element is increased, the flow systems exhibit a series of instabilities. For very low Reynolds number the flow is laminar with the absence of any disturbance. As we gradually

increased the Reynolds number, two vortices appeared for flow configuration type 1, one on each side of the endplates, known as Ekman vortices. It is worth mentioning that the presence of Ekman effects is restricted to the two cells closest to the end-caps. For the flow configuration type 2, only one cell occurs at the top endplate, whereas no Ekman cells are observed for the flow configuration type 3, as illustrated in Figure IV.2(a) and Figure IV.3(a).

When the angular velocity of the inner element is increased, the flow undergoes centrifugal-driven instability from laminar Couette flow, in which the only non-zero velocity component is in the azimuthal direction, to Taylor vortex flow, which consists of pairs of toroidal vortices wrapped around the inner element and filling the annular gap, as shown in Figure IV.2(b) and Figure IV.3 (b). This first transition from LCF to TVF is a continuous process and not an instability.

For the flow configuration type 1, the fluid is confined radially between the cylinders, and axially by endplates. The Ekman cells induce Taylor vortices, that build up gradually from the top and bottom end plates. The angular momentum decreases outwards from $r^2\Omega_1$ to 0 due to the no-slip boundary conditions. It is noteworthy that, for the flow configuration type 2 and 3, no appearance of Ekman's vortices is observed when we replace the end plates of the cylinders by hemispheres.

For all three flow configurations investigated here, it is seen that TVF is periodic in the axial direction and has full rotational symmetry in the azimuthal direction.

Unlike the flow between two concentric cylinders, which is one-dimensional, the flow between two concentric spherocylinders is fully three dimensional, where the centrifugal force is a function of the latitude, but no end walls effects exist like those caused by the end-walls of the cylinders.

As the Reynolds number is further increased, TVF becomes unstable to non-axisymmetric perturbations, and azimuthal waves are formed which rotate around the inner element.

Wavy vortex flow is characterized by azimuthally wavy deformation of the vortices both axially and radially, i.e., the axial motion of the vortex centers decreases monotonically, while the radial motion of the vortex centers has a maximum. Furthermore, elongated vortices at the ends (upper and bottom endplates) and compressed vortices at the centre can be observed clearly for flow geometry type 1, as shown in Figure IV.2(c) and Figure IV.3(c).

The values of the Reynolds number for the different flow configurations at which appeared the various flow modes are presented in table 1. The transition from LCF to TVF and then to WVF in the combined flow systems (type 2 and 3) is substantially delayed with respect to the classical Taylor-Couette flow system (type1), therefore the combination of cylinders and spheres has a stabilizing effect on this flow problem.

Table IV.1: Reynolds number values for different flow configurations

Flow configurations / Flow regimes	Type 1 $\Gamma_1=20$	Type 2 $\Gamma_2=30$	Type 3 $\Gamma_3=40$
LCF	Re=15	Re=37	Re=70
TVF	$Re_{c1}=133$	$Re_{c1}=142$	$Re_{c1}=158$
WVF	$Re_{c2}=164$	$Re_{c2}=177$	$Re_{c2}=210$

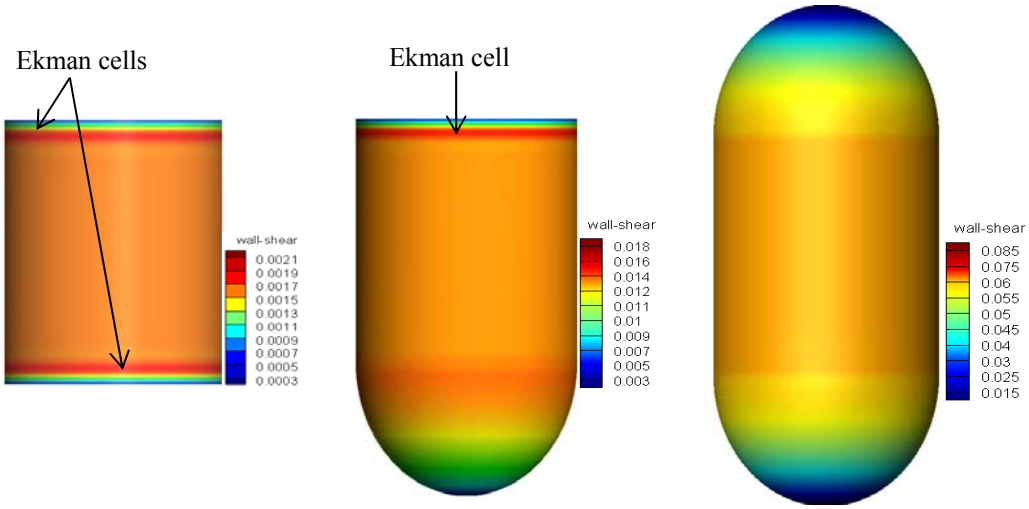

a) Laminar Couette flow

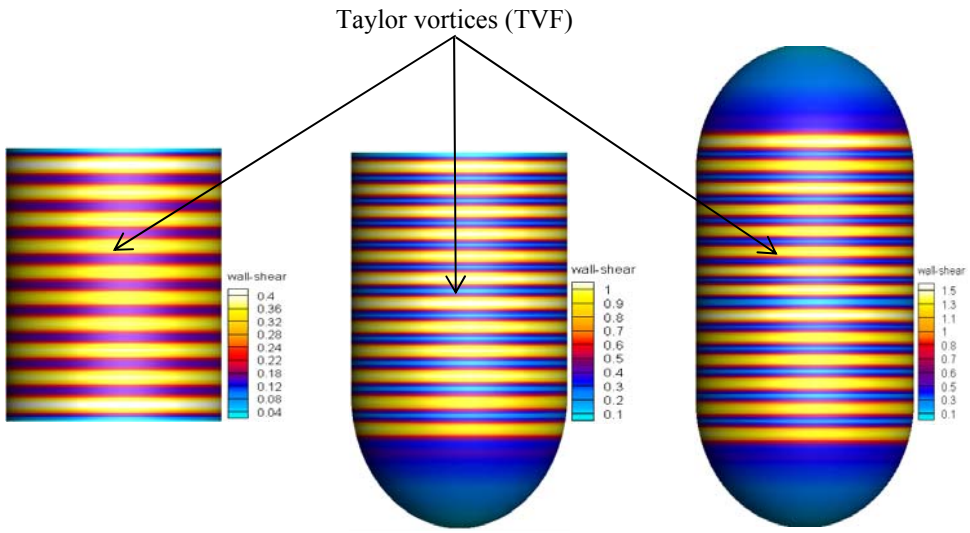

b) Taylor vortex flow

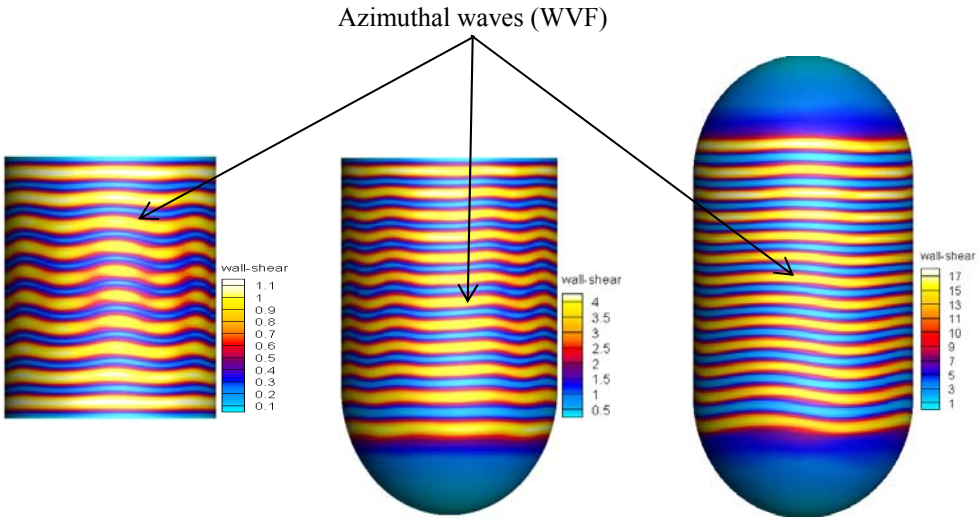

c) Wavy vortex flow

Figure IV.2: Various flow regimes in different geometries/ Wall shear stress on the outer element.

Figure IV.3 shows the Evolution of the skin friction coefficient (C_f) as a function of the axial position for various flow regimes and at different flow configuration. The C_f is the ratio of the shear stress at the outer wall and the dynamic pressure.

From Figure IV.3 (a), it can be seen that two weak peaks are formed on the curve at the end surfaces of the cylinders. The appearance of these double weak peaks is due to the creation of Ekman's cells. For the flow configuration type 2, only one peak is observed at the top end surface. Whereas, no peaks are observed on the curve of the flow configuration type 3; criterion of the absence of Ekman's cells. In addition, a noticeable increase of the skin friction coefficient values can be observed in Figure IV. 3 (b) and (c). The C_f, for TVF and WVF, is intensified by a factor of nearly 258 and 2400 for the flow configuration type 3, compared to the flow configuration type 1.

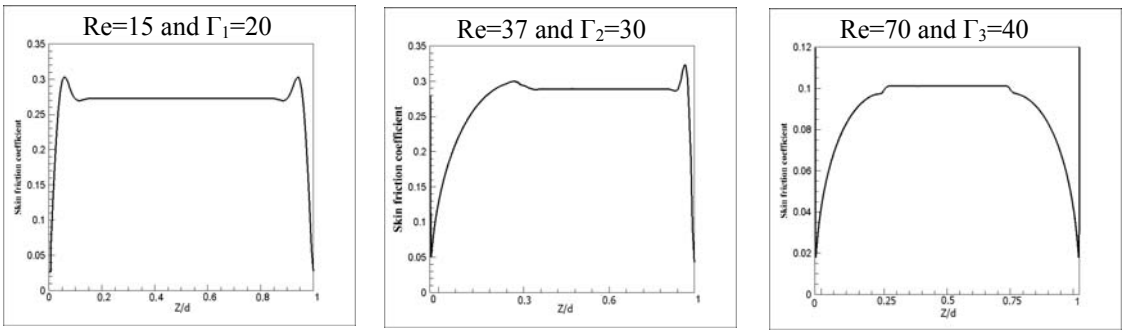

a) Laminar Couette flow

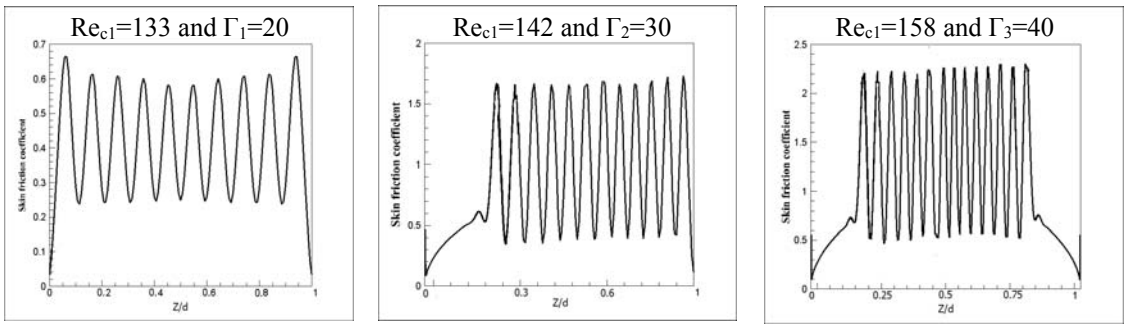

b) Taylor vortex flow

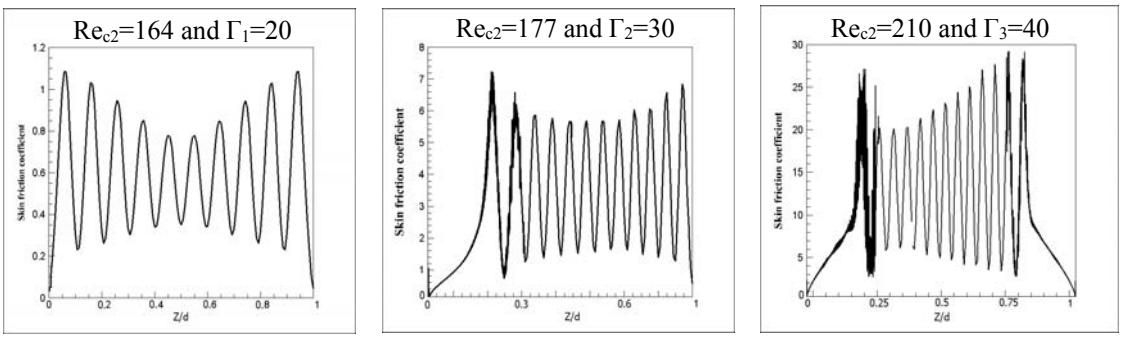

c) Wavy vortex flow

Figure IV.3: Evolution of the skin friction coefficient for various flow regimes.

IV.4 Conclusion

In this study, the transition from purely circumferential flow (LCF) to Taylor vortex flow (TVF) and wavy vortex flow (WVF) has been successfully predicted by CFD simulations for different flow configurations. Three flow configurations are investigated when only the inner element rotates and the outer one is held at rest. The Reynolds number values at which axisymmetric Taylor vortex flow and wavy vortex flow appear have been determined for the different flow geometries. By combining different geometries one can learn a lot about the onset of various hydrodynamics instabilities and the pattern forming systems.

The study of these instabilities has led to a better understanding of the regime transitions in different combined flow systems. Low angular velocity of the inner element generates laminar Couette flow. As Reynolds number is increased a new flow pattern (Taylor vortex flow) develops, which is characterized by a system of axisymmetric vortices superimposed on the basic laminar Couette flow along the column of fluid. As Reynolds number is further increased, TVF gives way to wavy vortex flow (WVF), which is characterized by travelling azimuthal waves superimposed on the inflow and outflow boundaries of the Taylor vortices. The transition from LCF to TVF and then to WVF in the combined flow systems (type 2 and 3) is substantially retarded compared to the cylindrical Taylor Couette flow system (type1), therefore the combination of cylinders and spheres has a stabilizing effect on this flow problem.

CHAPTER V

Numerical investigation of the effect of different working fluids on the pattern formation in a narrow rotating annulus

« Whereof one cannot speak, thereof one must be silent»

Ludwig Wittgenstein

Results and discussion

CHAPTER V: Numerical investigation of the effect of different working fluids on the pattern formation in a narrow rotating annulus

V.1 Introduction

Nowadays, the global energy consumption is rapidly increasing, while the primarily energy sources, fossil fuels, are rapidly depleting. Moreover, the climate change and pollution represent undesirable side effects and major challenges for international community. For this reason, it is appropriate to look for other sources of clean energy such as hydrogen, helium, lithium, biofuels, etc., which are currently being explored worldwide. These liquids are widely recognized as alternative energy carriers, which can be used in many applications. For example, liquid hydrogen (LH2) is a common liquid rocket fuel, and it is also used as a propellant for nuclear powered rockets, and as the fuel for internal combustion chamber or fuel cell. Liquid helium is known as an excellent cooler when it is in contact with another body. Some applications of liquid helium in engineering are: cooling samples in solid state physics, cooling infrared detectors in astrophysics, cooling superconducting magnets in hospitals and particle physics accelerators. The physical and chemical features of liquid lithium: low melting point, high boiling point, low vapour pressure, low density, high heat capacity, high thermal conductivity and low viscosity, allow it to be used as a primary coolant for nuclear fusion reactors (Tokomak-type devices) and space power systems. Hence, what happens if the liquid contained in the annular gap between two concentric cylinders is hydrogen, helium or lithium instead of an ordinary conventional liquid such as water?

Little is known on the flow behaviour and pattern formation of these liquids in Taylor-Couette system compared to the vast literature existing on other conventional liquids.

On the other hand, the flow evolving in the cylindrical annulus has been studied extensively for more than a century, and has long been regarded as one of the fundamental problems in fluid mechanics. This flow problem is useful in many research areas, and is also a subject of widespread practical interest owing to its direct connection with engineering applications including, the drilling of oil wells, turbo machinery, combustion, electric motors, chemical mixing filtration, bearing chambers, pumps for the oil and water industries, rotating tube heat exchangers, emulsion polymerization, flocculation reactors, desalination, rheology, liquid-liquid extraction, and biomedical. Mallock [10] and Couette [11] were the first who measured experimentally the torque

on the inner cylinder to determine the viscosity of water in an annular gap between two concentric cylinders. Later, Taylor [14] used a linear stability theory and built an experiment to predict a stability threshold for flow between two rotating concentric cylinders. He obtained an excellent quantitative agreement between analytical and experimental results. This flow system has been used as a benchmark for fluid mechanics since Taylor's [14] pioneering work to investigate the transition from laminar to turbulent flow. Moreover, a large number of flow regimes existing in this system has been widely investigated by numerous researchers focusing on different aspects of the flow, and a sizable literature now exists dealing with this flow system (Chandrasekhar [31], Fenstermacher et al. [20], Diprima et al. [180], Donnelly [8], Marcus [159], Cole [118], Andereck et al. [5], Avila et al. [160], Martinez-Arias et al. [73], Adnane et al. [91], Tokgoz et al. [181], Froitzheim et al. [162], Brauckmann et al. [163], Viazzo and Poncet [182], Grossmann et al. [165], Lalaoua and Bouabdallah [144], Mullin et al. [166], Avgousti and Beris [183], Batra and Das [184], Baumert and Muller [185], Groisman, and Steinberg [186], Khayat [187]). These researchers and other concluded that the fluid dynamics behaviour and the transition between different flow states strongly depend of different flow control parameters such as the radius ratio, rate of acceleration, the aspect ratio and the Taylor number. In addition, the Taylor-Couette system has been used to understand the behavior of non-classical fluids such as liquid helium. Kaptiza [188] was the first who performed experiments on helium between concentric cylinders. The first attempt to calculate the hydrodynamic stability of the flow of liquid helium in the Taylor Couette system was made by Chandrasekhar & Donnelly [189]. Subsequently, some experimental and theoretical studies have been conducted on helium Taylor-Couette flow to examine various aspects of the flow from the first appearance of quantized vortices to turbulent flow (Donnelly [190], Donnelly and Lamar [191], Barenghi and Jones [192], Swanson and Donnelly [193], Barenghi [194], Henderson and Barenghi [195], Henderson et al. [196], Henderson and Barenghi [197], Donnelly and Barenghi [198], Henderson and Barenghi [199], Henderson and Barenghi [200], Henderson and Barenghi [201]). It is interesting to mention that the physical properties of helium liquid vary dramatically with temperature. Helium is a gas at ordinary room temperatures. To transform helium into a liquid it is necessary to cool it to about - 269.15 °C. If the temperature T is reduced further, at the critical value $T_\lambda \approx$ -271.15 °C (Lambda point transition or critical triple points), a phase transition takes place, quantum effects become important and liquid helium acquires the remarkable property of superfluidity. Helium II is considered to be made up of two completely mixed components: the normal fluid and the superfluid (Barenghi and Jones [192], Henderson and Barenghi [200]). The former is similar to a classical Navier–Stokes viscous fluid, whereas the latter is similar to a classical Euler inviscid fluid. In this numerical study, we only concerned with higher temperature liquid phase, which occurs for $T > T_\lambda$ (known as helium I), and neglect the lower temperature liquid

phase (known as helium II), which exists in the range -273.15 °C < T < T_λ. It is worthy emphasizing that progress in the non-classical fluids problem has been slower than for classical fluids, which may be due to flow visualisation problems at such low or high temperatures, hence, we have much less information available than in the vast classical Taylor-Couette literature.

Moreover, the appearance threshold of the Taylor vortex flow in the cylindrical annulus has been, and still is, widely studied whether from a numerical or experimental point of view. Indeed, the triggering threshold of this instability, as well as the cellular patterns formation, are strongly dependent on the geometry of problem, but also on the nature of the fluid used. While a large number of studies are focused on the influence of geometric or dynamic parameters on the flow behaviour between two coaxial cylinders, our interest focuses on the effect of the working fluids on the onset of Taylor vortices, when the inner cylinder rotates and the outer one is stationary. The working fluids used for numerical calculations are water, hydrogen, helium, and lithium, which are taken in their liquid states. To our knowledge this numerical investigation provides some new results on behaviour of liquids (in particular hydrogen and lithium) and the formation of patterns in a narrow rotating annulus that are not so extensively studied in the open literature. A proper understanding of Taylor-Couette flow using different working fluids strengthens our understanding of the appearance of different instabilities as well as the laminar-turbulent flow transition.

V.2 CFD modelling

V.2.1 Fluid proprieties, flow configuration and control parameters

The flow system sketched in Figure V.1 is composed of two coaxial cylinders. The inner cylinder rotates at constant angular velocity Ω_1 and the outer cylinder and the top and bottom plates are stationary. The fluid motion is mainly governed by three flow control parameters: The radius ratio $\eta = R_1/R_2=0.909$, its aspect ratio $\Gamma = H/d=30$, and the Taylor number which is used to describe the ratio of inertial to viscous forces and this is commonly defined as $Ta = (\Omega_1 R_1 d/ \nu) (d/R_1)^{1/2}$, where H, d, R_1, R_2 and ν are the height of the of the fluid column, the gap width, the inner and outer radii, and the kinematic viscosity, respectively. Noteworthy that the rotation rate of the inner cylinder was increased quasi-steadily, from rest up to the onset of Taylor vortex flow. The physical properties of the working fluids used in this study are given in table V.1.

Table V.1: Properties of the working fluids (taken in liquid state)

Proprieties / Liquids	ρ (kg/m^3)	ν (m^2/s)	T (°C)	Pressure (atm)
Water	998.2	10^{-6}	25°C	1
Hydrogene [202, 203]	70.85	$0.188\ 10^{-5}$	-253°C	1
Helium [204, 205]	124.74	$0.0253\ 10^{-6}$	-269.5 °C	1
Lithium [206, 207, 208]	516	$1.25\ 10^{-6}$	180.54°C	1

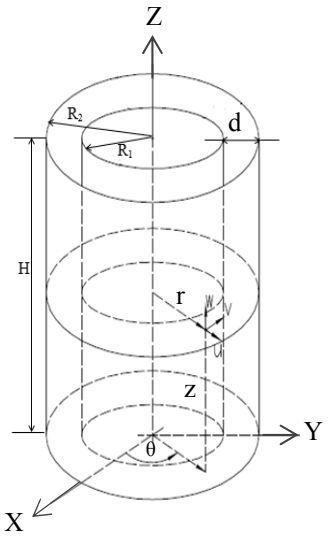

Figure V.1: Sketch of the Taylor-Couette system.

V.2.2 Governing equations, meshing and numerical schemes

The equations of the continuity and momentum for an incompressible viscous flow are written as:

$$\operatorname{div}\mathbf{v} = 0 \qquad (V.1)$$

$$\rho\frac{\partial \mathbf{v}}{\partial t} + \rho(\mathbf{v}.\nabla)\mathbf{v} = -\nabla\mathbf{p} + \mu\Delta\mathbf{v} \qquad (V.2)$$

Where (U, V, W) are the physical components of the velocity **v** in cylindrical coordinates (r, θ, z). P, ρ, t, and ν denote pressure, density, time and kinematic viscosity of the fluid, respectively. For the flow system, all the variables are set to zero at the walls except for the tangential velocity V, which is set to $\Omega_1 R_1$ on the inner rotating cylinder and zero on the outer stationary cylinder. A linear profile for the mean tangential velocity component is imposed at the inlet as the aspect ratio of the cavity is quite weak. Therefore, V varies linearly from $\Omega_1 R_1$ on the inner wall up to zero on the outer wall. In addition, no-slip boundary conditions for the velocity are applied at all surfaces.

The boundary conditions used in this study are summarized as follow:

- For the cylinders (inner and outer):

  1. $V = R_1 \Omega_1$ and $U = W = 0$ at $r = R_1$
  2. $V = U = W = 0$ at $r = R_2$,

- For the end-caps (top and bottom plates): $U = V = W = 0$ at $Z = 0, Z = H$

The cylindrical annulus is divided into equally spaced intervals in the azimuthal (N_θ = 252) and axial (N_z = 252) directions respectively, while the mesh is clustred in the radial direction with a number of cells N_r = 32. It is important to note that the grid sizes near the inner and outer cylinder walls have been refined because there is a high shear. Furthermore, several calculations have been carried out to verify the influence of the grid density on the numerical results, i.e, increasing the grid resolution until further increases in resolution did not improve the solutions (mesh dependence). The converged solution from the coarse mesh was employed as an initial solution for the medium mesh, and likewise the converged solution of the medium mesh was used as an initial solution for the finer mesh.

The numerical simulations were performed using the CFD code Ansys Fluent based on the finite volume method. The pressure has been discretized with the second order scheme. The second order upwind scheme was applied for the momentum equations. The velocity-pressure coupling was linked via the PISO algorithm (Pressure Implicit with Splitting of Operator). In addition, the relaxation factors have been carefully adjusted to ensure the convergence criteria which are based on the residual values. The solution is assumed converged when all standardized residuals are less than 10^{-4}. Note that the obtained numerical results, concerning the onset of Taylor vortices for an ordinary fluid, are carefully validated and compared against experimental work of Adnane et al. [91] for the same flow control settings. A good agreement was found between CFD results and the experimental data, as shown in Figure V.2. The computed critical Taylor number in the current study, for an ordinary liquid, agrees quite well with experimental work of Ref. [91].

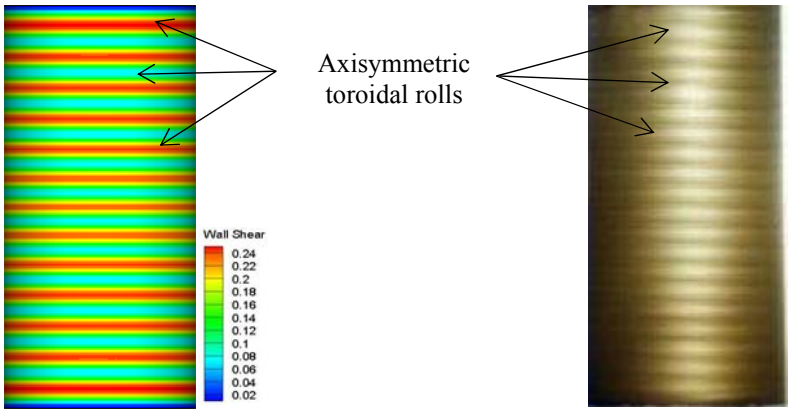

Present numerical simulation (Ta_{c1}=42.4) Experimental work of Ref. [91] (Ta_{c1}=42)

Figure V.2: Comparison between our computational result and the experimental work of Adnane et al. [91] for the onset of Taylor vortices for a classical fluid.

V.3 Results and discussion

The fluid dynamic behaviour between two concentric cylinders, for different working fluids, is presented in terms of distributions of wall shear stress and skin friction coefficient, as illustrated in Figure V.3 and V.4. The shear stress τ_w at the wall of the outer cylinder is defined as:

$$\tau_w = \mu \left. \frac{\partial V}{\partial r} \right|_{r = R_2} \qquad (V.3)$$

When the angular velocity of the inner cylinder is increased quasi-statically from the rest, the flow system makes a transition from laminar Couette flow to Taylor vortex flow. For low Taylor number the flow is laminar, the viscous force dissipates the centrifugal force induced by the rotation of the inner cylinder. With increasing further, the angular velocity of the inner cylinder, the driving force overcomes the viscous force resulting the onset of the first instability, which is known as Taylor vortex flow. More accurately, it is the no-slip condition at the walls of the cylinder that provides the driving force by producing a shear stress on the fluid between the cylinders. The Taylor vortex flow is a steady axisymmetric flow and has full rotational symmetry in the azimuthal direction, in which periodic toroidal rolls are piled in the axial direction along the outer cylinder. It is worth noticing that for water and helium, 13 axisymmetric toroidal rolls are appeared in the Taylor Couette system, whereas 12 and 14 axisymmetric toroidal rolls are observed for hydrogen and lithium, respectively, as shown in Figure V.3.

On the other hand, the flow behaviors for different working fluids are characterized by the skin friction coefficient which is a dimensionless parameter defined as a ratio of shear stress at the wall of the outer cylinder and the dynamic pressure according to the following relationship:

$$C_f = \frac{wall\ \ shear\ \ stress}{dynamic\ \ pressure} = \frac{2\tau_w}{\rho V^2} \qquad (V.4)$$

For all working fluids treated here, the C_f has an axial symmetrical distribution with respect to the center of cylinder. Furthermore, for hydrogen, helium and water the maximum of C_f occurs in the vicinity of the end-walls and in the central region of the outer cylinder, while it is minimum (close to 0) at the end-walls. However, the bahaviour of lithium is completely different, i.e., the maximum of C_f is observed at the end-caps, and the minimum is in central zone of the outer cylinder. In addition, the magnitude of skin friction coefficient increases drastically for the case of lithium compared to the other working fluids. The amplitude of C_f for lithium is doubled with respect to water. The C_f for lithium is also intensified by factors of nearly 112 and 36 compared to hydrogen and helium, respectively, as shown in figure V.4. It is important to note that the flow control parameters were the same for all simulation. In addition, we found that the critical Taylor number is the same for the four cases (Ta_{c1}=42.4), however, the critical angular velocity of the inner cylinder

varies from one fluid to another, which is due to the variation of the kinematic viscosity and density.

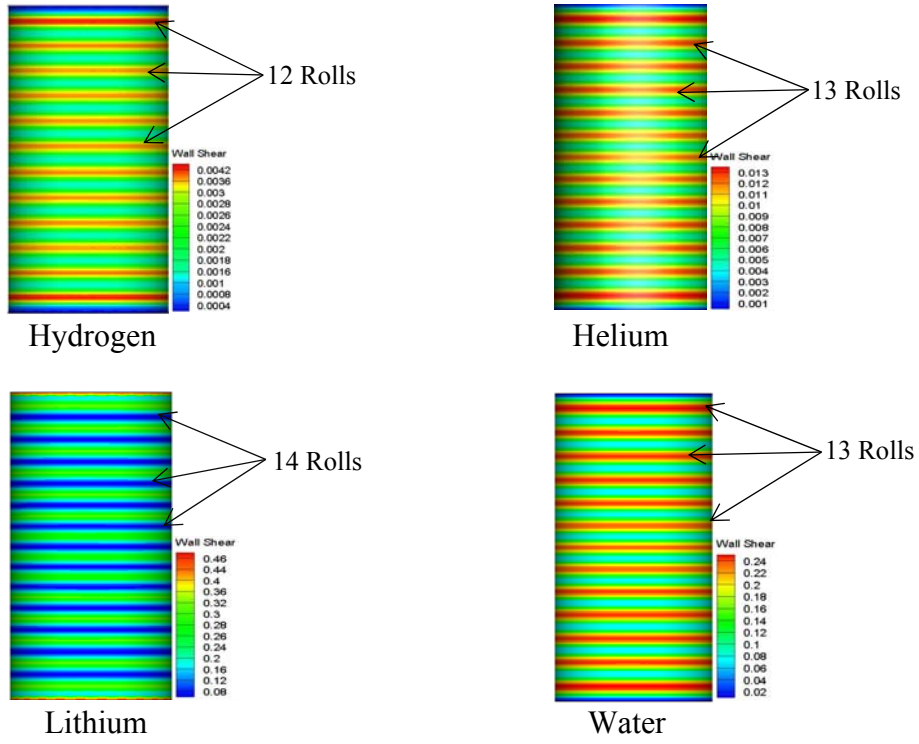

Figure V.3: Axisymmetric Taylor vortex flow in a cylindrical annulus for different working fluids/ wall shear stress on the outer cylinder for Ta_{c1}=42.4.

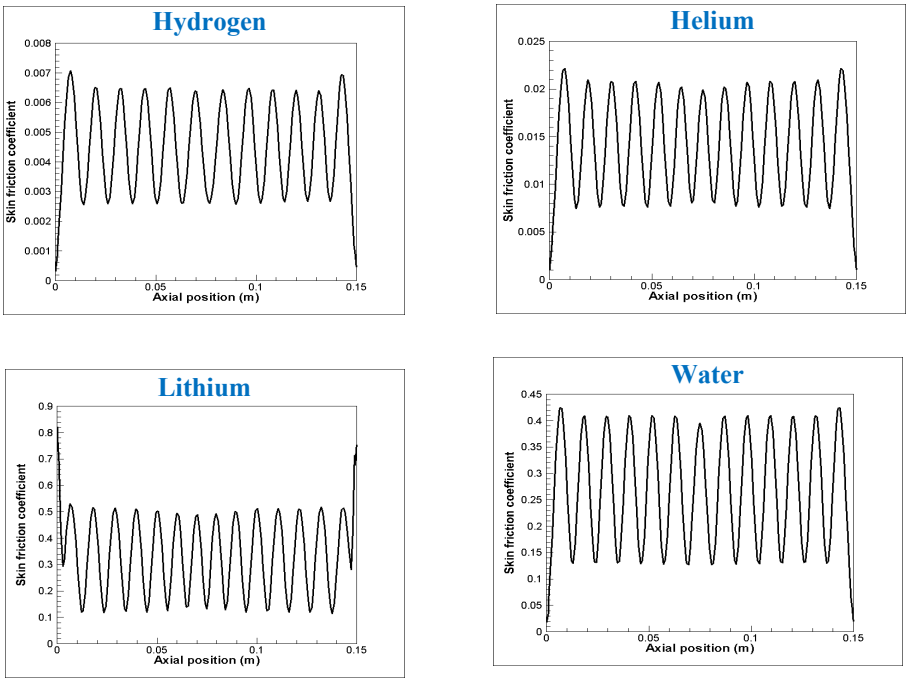

Figure V.4: Evolution of the skin friction coefficient for different working fluids at Ta_{c1}=42.4.

Figure V.5 shows the flow pattern in the annular gap between two coaxial cylinders represented by the streamlines in (r, z) plane for different working fluids. In order to understand the formation mechanism of the cellular patterns in the Taylor-Couette flow for different working fluids, our calculations begin with a low rotation rate of the inner cylinder until the appearance of the first instability. The flow system is terminated axially by two rigid, non-rotating plates forming a large cell at each end of the flow system, termed as Ekman's cell. The presence of fixed end walls induces an Ekman circulation in which the fluid moves radially inward near the upper and lower ends of the flow system and moves radially outward in the middle. This effect is caused by the no-slip boundary conditions; the centrifugal force pushes the fluid outwards at the centreline, where the braking effect of the end plates is least, hence, the fluid near the end plates moves inwards to conserve mass. By increasing further the Taylor number, the Ekman's cells induce Taylor vortices that build up gradually from the end plates and piled axially in the fluid column. Due to the effects of the fixed endplates, the Ekman's cells at the top and bottom of the flow system are elongated more than the Taylor vortices in the central region. Note that the formation mechanism of Taylor vortices for hydrogen, helium and lithium is the same as that of ordinary fluid such as water.

Moreover, the cellular patterns in the central region are flat and perpendicular to the cylinder axis, and each pair of counter-rotating vortices forms a wave. For water and helium, there are 24 Taylor vortices (12 waves), while for hydrogen the number of vortices decreases to 22 (11 waves), and for lithium the number of vortices increases to 26 (13 waves).

In addition, the numerical results obtained here show significant topological changes on the shape of the Ekman cell. For hydrogen liquid, the Ekman vortices are substantially elongated to about 1.6d and the Taylor vortices are also elongated, so that their height is 1.2d (λ=2.4d) where λ is the wavelength of the vortex cell pair in units of the gap width d, which is substantially superior to the height of 1.001d (λ =2d) for the case of water and helium. However, for lithium liquid, the Ekman cells are compressed to about 1.1d thereby compressing the Taylor vortices, their wavelength decreases up to λ = 1.6d.

In the axial direction the pattern is characterized by the dimensionless wave number $k = 2\pi d/\lambda$, and the dimensional $k = 2\pi/\lambda$. In the case of water, the critical value of the dimensionless axial wavenumber is $k_c \approx \pi$, hence, each individual Taylor cell is approximately square, i.e. the extension in the axial direction is equal to the size of the gap. In the case of helium liquid, we found that $k_c \rightarrow \pi$, as in water, which it is in good agreement with the study of Barenghi and Jones [275]. However, for hydrogen and lithium the dimensionless axial wavenumber changes significantly, with $k_c \approx 2.66$ for hydrogen and $k_c \approx 3.92$ for lithium.

A noticeable feature of the streamlines in Figure V.5 is the mixing and exchange of momentum at the meeting point of two adjacent vortices. It is can be seen from Figure V.5 that there is significant

flow mixing between adjacent vortices, with each vortex adding to the mixing region at the centre of a vortex pair, close to the inner cylinder and then receiving fluid from this mixing region, close to the outer cylinder. A similar mixing process occurs at the inflow region, between neighbouring vortex pairs.

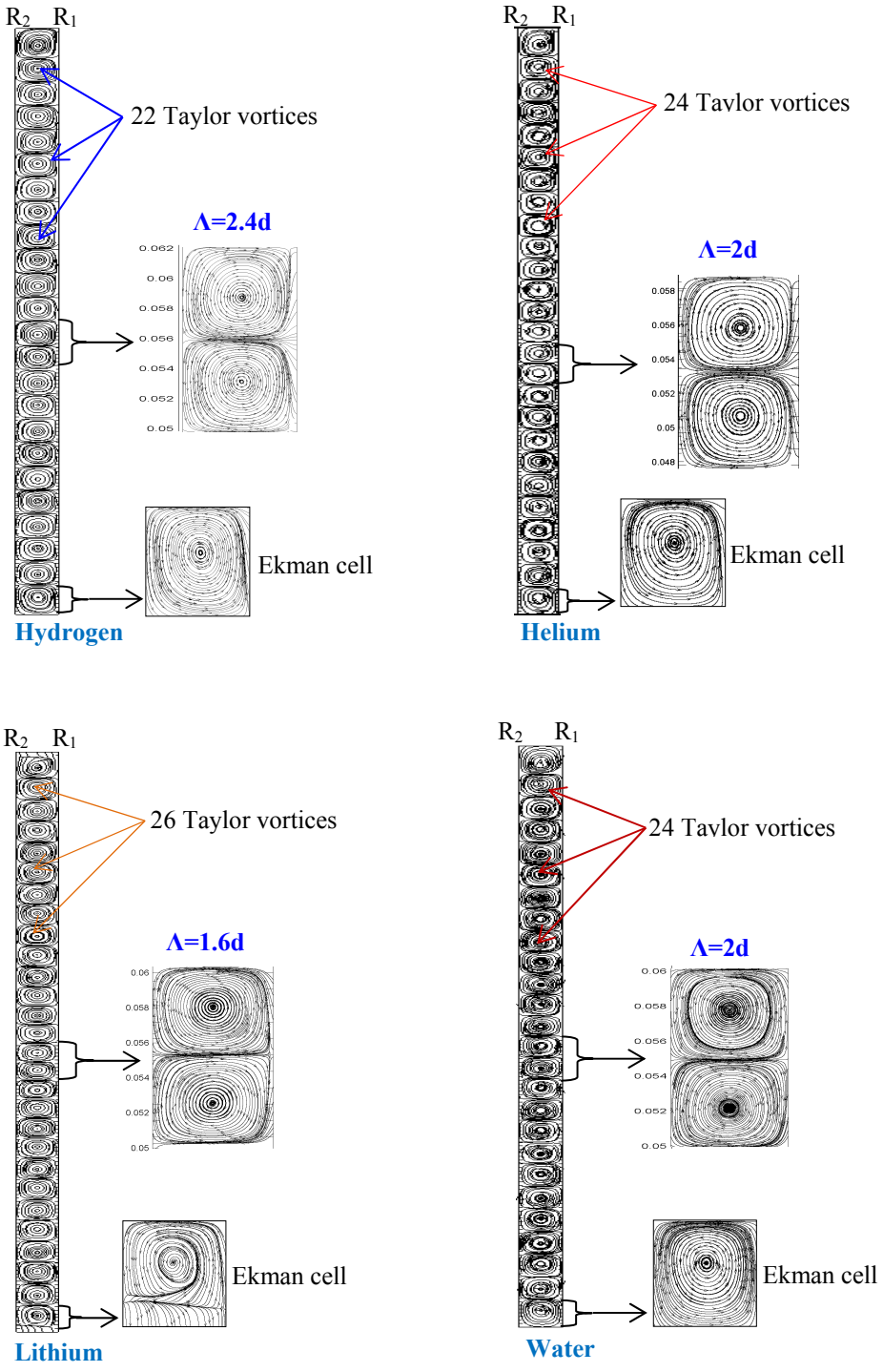

Figure V.5: contour plots of streamlines in (r, z) plane for different working fluids (Ta_{c1}=42.4)

Figure V.6 shows the flow patterns in an enclosed annulus represented by the contour plots of axial velocity, radial velocity and tangential velocity in the meridional plane (r, z) for different working fluids.

The rotation of the inner cylinder induces a centrifugal force that moves the fluid radially outward. This motion is resisted by the radial pressure gradient due to the stationary outer cylinder. When the Taylor number reached its critical value, the centrifugal force overpowers the radial pressure gradient and the system makes a transition from the laminar Couette flow regime to Taylor vortices regime. The first instability develops into axisymmetric cells of alternating positive and negative circulation, stacked axially in the fluid column, well known as a Taylor vortex flow state.

The minima and maxima of the radial velocity (U) appear in the radial inward and outward flow regions, respectively. The radial velocity minima near the bottom end-surface at Z=0 is lower than the corresponding values in the central region which may be due to the non-slip boundary conditions. The tangential velocity (V) is maximum near the inner cylinder in agreement with the direction of rotation of the inner cylinder that drives the flow by rotating at constant angular speed $\Omega_1 R_1$, while the tangential velocity is minimum near the wall of the stationary outer cylinder. The angular momentum fluid is transported by the Taylor vortices from near the inner rotating cylinder outwardly toward the stationary outer cylinder, i.e., from $\Omega_1 R_1^2$ to 0. The contour of axial velocity (W) shows the formation of an alternating pattern of maxima and minima in the annulus along the axial direction.

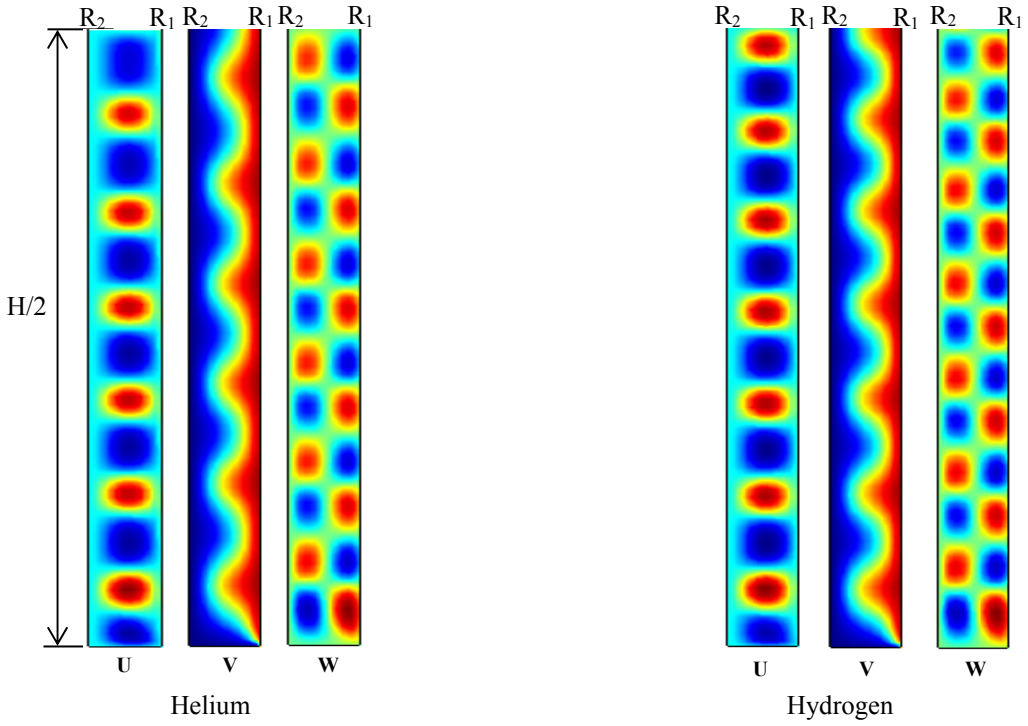

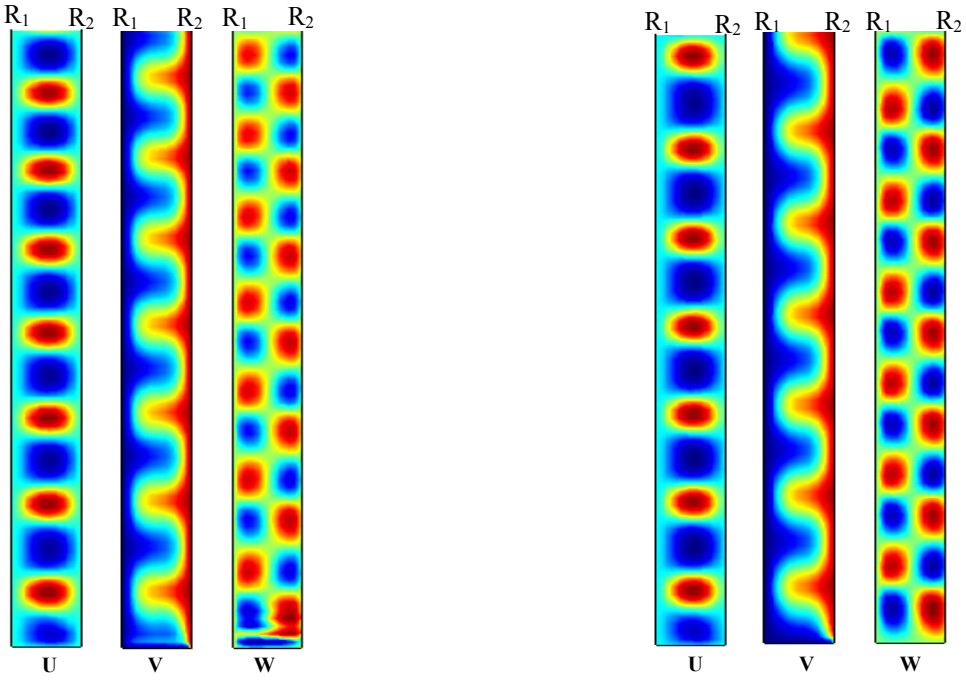

Figure V.6: Contours of the velocity components in (r, z) plane for the axisymmetric Taylor vortices obtained at Ta_{c1}=42.4 for different working fluids. U (radial), V (azimuthal), and W (axial) where the red (blue) colours represent high (low) values of the fields.

V.4 Conclusion

This study is especially devoted to investigate the effect of working fluid on the flow behavior and instabilities that occur in an annular gap between two rotating concentric cylinders. The fluid motion was simulated using a three-dimensional CFD for incompressible viscous flow. Four fluids were used in the computations namely water, hydrogen, helium, and lithium. For all working fluid, when Taylor number increases from laminar Couette flow, Eckman's vortices develop at the end plates of the cylinders. These end-walls have a local effect and strongly elongate the two cells close to the ends. It is also found that the critical Taylor number, characterizing the onset of Taylor vortex flow, for the four working fluids is the same, Ta_{c1}=42.4. Furthermore, the number of toroidal rolls and the number of vortices for water and helium are the same, however for hydrogen and lithium are completely different to water and helium, which may be caused by the kinematic viscosity and the density of different working fluids. Therefore, we concluded that the physical properties of fluids play an important role on the stability of flow. The number of vortices occurring in the annulus and their wavelength are varied from one fluid to another. Water and helium have the same behaviour, while for hydrogen and lithium show significant changes on the number and shape of cellular patterns. For hydrogen liquid, the Ekman cells and the Taylor vortices are substantially elongated. However, for lithium liquid, the Ekman cells and the Taylor vortices are compressed. Since there are no studies, in the previous literature, on the stability of Taylor-Couette flow using

lithium or hydrogen as a working fluid, this numerical study requires a deep experimental investigation to examine in detail the behavior of lithium and hydrogen in an annulus between two concentric cylinders. Thus, much more research effort is needed to broaden and deepen the knowledge on the flow behavior and the onset of different instabilities in the Taylor-Couette system using non classical fluids such as hydrogen, helium and lithium. Taylor-Couette flow will be an important test bed for studying the dynamics of lithium and hydrogen in much the same way as it has served in the study of classical fluid dynamics.

CHAPTER VI

Transition to Taylor vortex flow between combinations of circular and conical cylinders

« Scientists work from models acquired through education and through subsequent exposure to the literature often without quite knowing or needing to know what characteristics have given these models the status of community paradigms».

Thomas Kuhn

Results and discussion

Chapter VI: Transition to Taylor vortex flow between combinations of circular and conical cylinders

VI.1 Introduction

The instability and transition of fluid flows in an annulus between two coaxial rotating bodies such as cylinders, spheres and cones, which is known as Taylor-Couette flow (TCF), presents a paradigm for experimental, theoretical and numerical studies of hydrodynamic stability as well as for the transition to turbulence. Further, this seeming simplicity of the Taylor-Couette system has tremendous interests for various applications. It is used in many area of technology such as filtration, tribology, wastewater treatment, biomedical, mixing processes, liquid- liquid extraction, rheology and bio-reaction.

Many researchers have extensively investigated the various flow regimes existing between the laminar and turbulent flow and the bifurcations in the circular Couette flow (CCF) for more than a century. Ever since the earliest work of Couette [11], Mallock [10] and Taylor [14], the formation of Taylor vortices between two rotating cylinders, with either or both of them rotating, has been the subject of numerous investigations, which several studies have been presented with different geometric parameters (aspect ratio and radii ratio) in order to understand the flow behavior and determine a general map of the laminar-turbulent transition (Chandrasekhar [31], Coles [18], DiPrima et al. [180], Donnelly [8], Marcus [159], Koschmieder [1], Avila et al. [160], Lalaoua and Bouabdallah [144], Adnane et al. [91]). These authors and others have concluded that, when the inner cylinder rotates and the outer one is stationary, the onset of Taylor vortices depends on the radii ratio and aspect ratio of the flow system.

In contrast, if the gap width is no longer constant, as fluid flow in the annulus between combinations of circular and conical cylinders, a rich variety of interesting flow modes can be obtained. This type of flow has the advantage that the Taylor number changes when the radii vary axially which may therefore produce more complex flow structures and profoundly affect the flow patterns. So far, the behavior of flow and the selection of the wave number for a variety of inner/outer non-circular cylinder arrangements have been previously explored by many authors (Ahlers et al. [209], Dominguez-Lerma et al.[210], Abboud [175], Paap and Riecke [211], Wimmer [148], Wimmer [157]). Furthermore, Cannel et al. [212] and Ning et al. [176] have presented experimental results on the wave number selection in a Taylor-Couette system where a section of

the gap was tapered from a supercritical Reynolds number to a subcritical Reynolds number. They found that a sufficiently slow ramp connecting the supercritical region to the subcritical region resulted in the selection of a unique wavelength. They also shown that even very small opening angle of the outer cylinder wall could lead to a multiplicity of state selections.

In addition, Noui-Mehidi et al. [213] presented numerical results of the effect of miss-alignment of the outer cylinder wall on the flow instability in a finite Taylor-Couette geometry. This study revealed that the bifurcation from a particular mode to another one occurs in a range of specific values of the opening angle of outer cylinder.

In two relatively recent articles, Sprague et al. [178, 214] have used numerical and physical experiments to investigate the stability of circular Couette flow when only the geometry of the inner cylinder is modified or else the inner and outer radii varied axially. They have shown that the onset of Taylor vortices of different wavelengths can be produced simultaneously. Hence, a steady and unsteady vortex flows also may occur for different modifications of the circular Couette geometry. Savin and Kornaeva [215] have presented a mathematical model of the fluid flow in the annular space between inner rotating cylinder and outer stationary cone.

More recently, Raju [216] has presented a numerical computation of the occurrence of Taylor vortices in a stepped cylinder configuration. He has shown that if one of the cylinders has a step change in radius, there can be even or odd number of vortices in the wide and narrow gap regions.

While the flows between two rotating cylinders are examined and detailed very well both numerically and experimentally, the issue of the existence and nature of Taylor vortices as well as the wave number selection processes in the flow between combinations of circular and conical cylinders remain still unexplored. The main objective of the present study is to investigate, using CFD simulations, the effect of cylinder wall alignment on the flow behavior by opening the outer fixed cylinder with different angles with respect to the vertical axis. Special attention has been paid to the onset of Taylor vortices and the structures shape as well as the impact of the geometrical modification on the process of the wave number selection in order to reveal the mechanism at the origin of the observed structures.

VI.2 Flow configuration and parameters

We consider a viscous incompressible flow between cylinder–cone combinations. The inner cylinder rotates with a constant angular velocity Ω_1 around the vertical z-axis while the outer element is held stationary. The bottom and the upper surfaces are kept fixed, as illustrated in Figure VI.1. The opening angles of the outer cylinder are increased stepwise such that the configuration changed from two rotating coaxial circular cylinders toward a rotating cylinder in a stationary cone. The outer fixed cylinder is opened with different angles ranging from 0 until 12°, resulting in a gap width not perfectly parallel.

We note that the annular gap increases from the upper base downward when the apex angle is non-zero. Therefore, the definition of the geometrical parameters for all cases studied above is related to the gap defined at the upper base, z=H, which is the same for all configurations with $d_0 = R_2 - R_1 = 5$ mm. The flow features are described by the following dimensionless parameters:

- Aspect ratio: $\Gamma = H/d_0 = 20$;
- Radius ratio: $\eta = R_1/R_2 = 0.909$;
- Ratio of the gap to the radius of the inner cylinder: $\delta = d_0/R_1 = 0.1$;
- Apex angle: $0 \leq \alpha \leq 12°$;
- The Taylor number is defined at the upper base of the flow system by: $Ta = \frac{\Omega_1 R_1 d_0}{\nu} \sqrt{\frac{d_0}{R_1}}$

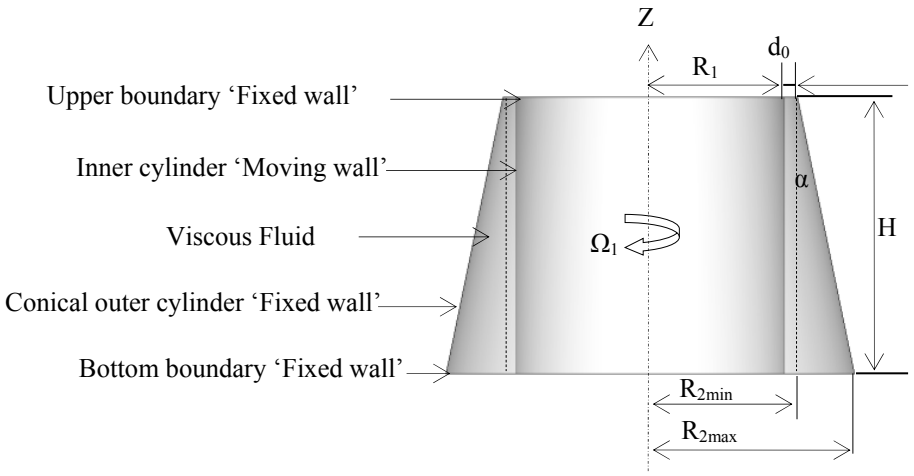

Figure VI.1: Schematic of the combined Taylor-Couette geometry.

The flow field is presented in an axisymmetric concentric annulus configuration. The equations of the continuity and momentum for an incompressible viscous flow are the following:

$$\nabla . \boldsymbol{u} = 0 \qquad (VI.1)$$

$$\frac{\partial \boldsymbol{u}}{\partial t} + (\boldsymbol{u}.\nabla)\boldsymbol{u} = -\frac{1}{\rho}\nabla \boldsymbol{p} + \nu \Delta \boldsymbol{u} \qquad (VI.2)$$

Let (U, V, W) the physical components of the velocity $\boldsymbol{u}$ in cylindrical coordinates (r,θ, z). Time and pressure are denoted by **t** and $\boldsymbol{p}$, respectively. The boundary conditions used in this study are:

- For the cylinders:
  - $V = R_1 \Omega_1$ and $U = W = 0$ if $r = R_1$;
  - $U = V = W = 0$ if $r = R_2$;
- For the bottom and upper surfaces:
  - $U = V = W = 0$ if $Z = 0$ and H

The working fluid used during the numerical calculations is water, which has a density of 998.2 kg/m3 and viscosity of 100.3×10^{-5} kg/m.s at temperature of 25 °C. The angular velocity of the inner cylinder

is increased quasi-steadily, from rest up to the occurrence of the Taylor vortices. The boundary condition on the solid wall is no slip condition.

VI.3 Numerical modeling

The 3D geometries are meshed with hexahedral cells (structured mesh). The mesh size is uniform in the axial and azimuthal directions. The grid is stretched near both walls in the radial direction where there is a high shear.

The Navier-Stokes equations have been solved using the CFD code, Ansys Fluent, based on the finite volume formulation. The discretization scheme chosen for the pressure is the second order model and the momentum equations have been discretized with Third order MUSCL scheme, while the Pressure-Implicit with Splitting of Operators, PISO algorithm, pressure-velocity coupling scheme has been used for the calculations. The convergence criteria used to terminate the simulations was 10^{-6} for continuity and three velocity components.

In order to validate our numerical calculations as well as verifying the correctness of CFD code, we have firstly examined the classical Taylor Couette flow (α=0). The critical Taylor number computed for this study is 41.6, which is close to the value of 41.2 reported by Fenstermacher et al.[20] for the same geometrical parameters, as illustrated in Figure VI.2. Therefore, the obtained numerical results agree very well, both qualitatively and quantitatively, with the experimental result within 1%.

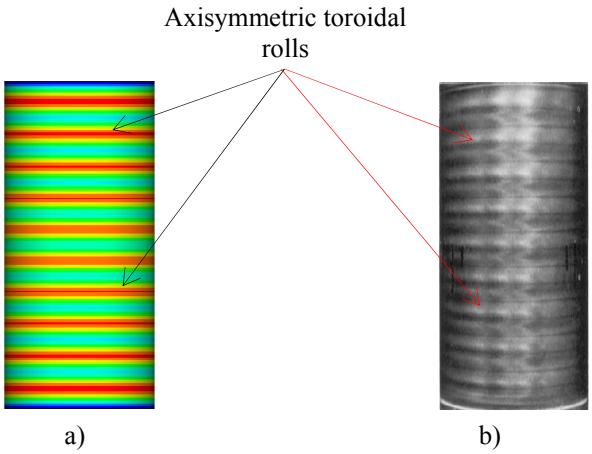

Figure VI.2. Time-Independent Taylor vortex flow/ Classical case (α=0) with: (a) Our computed result (Γ=20 and η=0.9) and (b) Experimental result of Fenstermacher et al. [20] (Γ=20 and η=0.877).

VI.4 Main numerical results

VI.4.1 Evolution of the critical Taylor number

Figure VI.3 shows the variation of the Taylor number versus the opening angle of the outer cylinder. It is noteworthy that the critical Taylor number, characterizing the occurrence of Taylor vortices, decreases when the apex angle increases. For the classical case, α=0, Tac1=41.6 and when the value of α reaches 12° the Tac1 decreases rapidly up to 20.3. Thus, the onset of Taylor vortex flow is substantially advanced with respect to nominal case. We note that the decreasing of Taylor

number is observed for the entire range of the α from 20' to 12°. Therefore, the opening angles of the outer cylinder have a destabilizing effect on the appearance of the first instability.

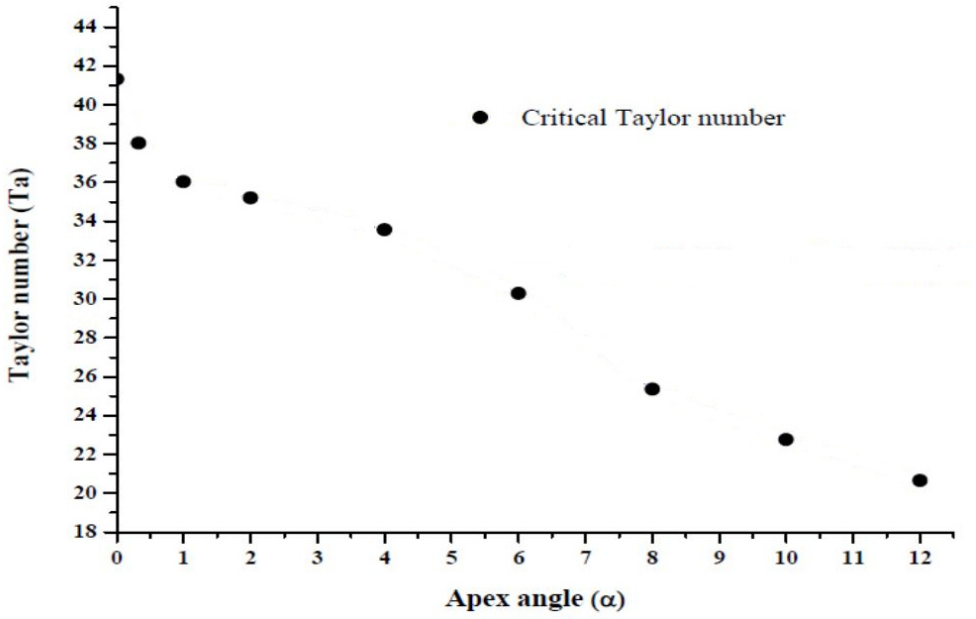

Figure VI.3: Critical Taylor number versus apex angle

VI.4.2 Flow patterns

Figure VI.4 shows the Taylor vortices structures represented by streamlines in (r, z) plane for several α.

At α= 0, when the Taylor number reaches the critical value, a series of periodic vortices are developed between the concentric cylinders and are stacked in the axial direction, known as Taylor vortices. For this case, there are 20 cells of equal size and intensity inside the annulus, each vortex rotating in the opposite direction with the adjacent vortices. Thus, the constant gap guarantees the same centrifugal forces at every point in the z-direction.

For α≠0, it is observed that, when the apex angle increases, the number of cells decreases from 20 up to 8 at α=12°. The number of vortices filling the entire gap is inversely proportional to the opening angle of the outer fixed cylinder. For α= 0 (CCF), 20 vortices are established, whereas 18, 16, 14, 12, 10 and 8 vortices are observed for α=20', 2, 4°, 6°, 8°, 10° and 12°, respectively.

Furthermore, the Taylor vortices are deformed, having larger differences in their axial extension. These vortices are distinct from those found in a classical Taylor-Couette system (CCF) in two respects. First, the vortices translate in the direction of increasing gap width. Second, neighboring clockwise and counterclockwise vortices are not reflectively symmetric: vortices in the wide gap, which have a large-scale circulation, are stronger and larger than those in the narrow gap. The variation of the vortices size may be due to the non-constant annular gap, i.e. the centrifugal force is stronger in the larger than in the smaller part of the gap, as can be seen Figure VI.5 showing the

variation of axial wavelength λ (distance between two cells) versus apex angles. The size of the bottom vortex is greater than the upper vortex. The effect of the growing bottom vortex could be seen clearer in the case of higher values of α. It should be mentioned that the wavelength and the number of the vortices between the inner rotating cylinder and the fixed outer conical cylinder can be changed by changing the angles of conic. Therefore, the development and the behavior of the Taylor vortex flow strongly depend on the opening angle of the outer cylinder. This result could provide useful guidance for the design and optimization of semi-batch Taylor-Couette devices.

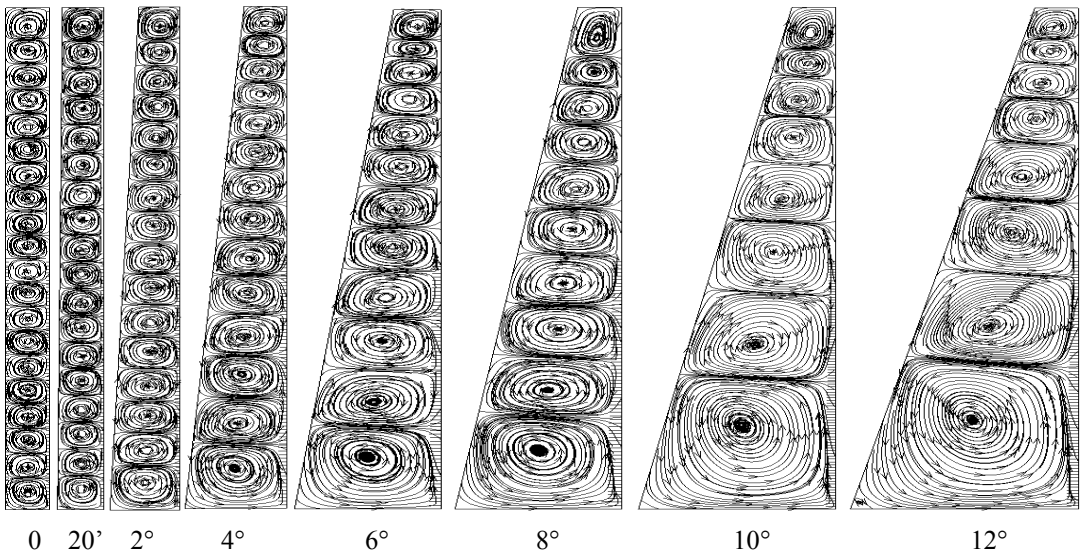

Figure VI.4. Taylor vortices for different apex angle / Streamlines in (r,z) plane.

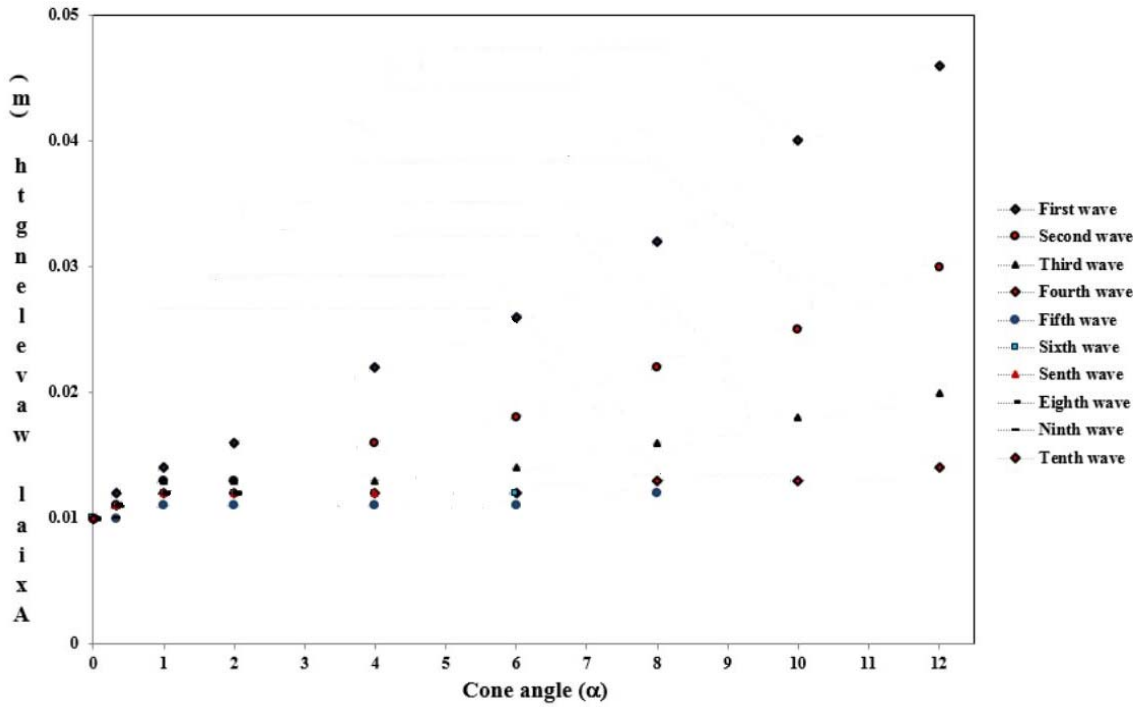

Figure VI.5: Variation of axial wavelength versus apex angle.

VI.4.3 Formation mechanism of Taylor vortices

For $\alpha=0$, the classical Taylor-Couette flow system, the formation mechanism of Taylor vortices was well known (Czarny et al. [22]). As Ta increases from the laminar Couette flow, Ekman's cells develop at the ends of the cylinders. A further increase in angular velocity leads to the beginning of the onset of Taylor vortices. Then these vortices rapidly join at the center of the cylinder at Ta_{c1} = 41.32. At steady state, there are 20 cells of equal size and intensity inside the annulus, each vortex rotating in the opposite direction with respect to the adjacent vortex (counter-rotating).

Modifying Taylor-Couette flow by replacing right outer cylinder by conical cylinder, $\alpha\neq0$, a large vortex near the bottom wall and one circulation cell are established within the gap for subcritical Taylor number at Ta=3.5. As the angular velocity is further increased, we observe the development of a pinch within the large vortex at Ta=7.6. The circulation in the closed streamlines of the pinch always has the same sign as that in the large basic vortex. Although the pinch has a strong radial flow, the closed streamlines in the pinch are not separated from the large basic vortex by a radial inflow or outflow boundary. Regions with and without vortices may be observed within a gap for Ta=13.4. With a further increase of the Taylor number more vortices, with variable sizes, will be added in the direction of the smaller gap. It is interestingly worth noticing that the Taylor vortices can only appear through the process of pinch-detachment, as it is demonstrated by figure VI.6 for $\alpha=12°$. This flow pattern is caused by the different centrifugal forces, which are at a constant radius stronger in the larger than in the smaller part of the gap. Therefore, it is found numerically that the size of the vortices is depending on the opening angle of the outer conical cylinder. The result of this is that the gap width varies in height, and the Taylor vortices then vary in size, being large where the gap is wide and small where the gap is narrow.

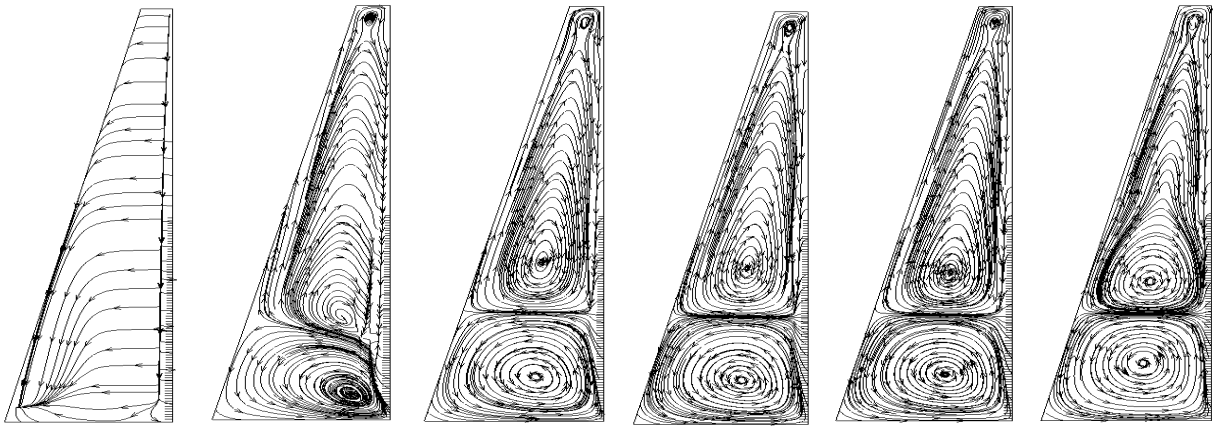

Ta= 0.1 Ta=1.2 Ta=3.5 Ta=4.3 Ta=5 Ta=7.6

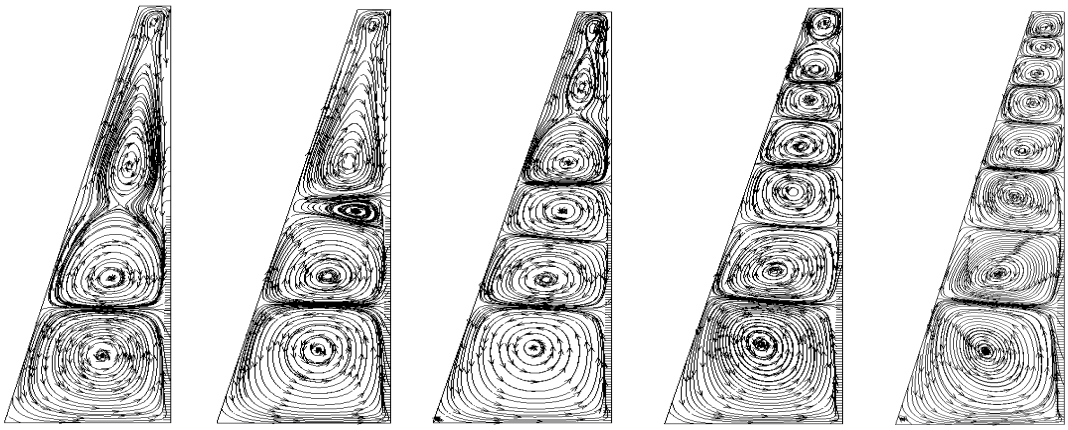

Figure VI.6: Formation mechanism of Taylor vortices for an apex angle α=12°.

VI.4.4 Tangential velocity distribution

Figure VI.7 shows the axial distribution of the tangential velocity plotted in dimensionless form for different apex angles. These quantities are calculated along a middle line from the midpoint of the bottom end cap to the midpoint of the top endplate in the (r, z) plane.

It is clearly shown that, when the apex angle increases, the magnitude of tangential velocity increases at the larger than at the smaller part of the gap. In the larger part of the gap the fluid moves outwards, then down along the conical shell and finally back towards the straight rotating cylinder. The constant radius of the inner cylinder guarantees the same tangential velocity at every point of its surface (α=0). However, the non-constant gap width leads to the variation of tangential velocity, which has a large radial extension at the wider than at the narrower part of the gap, as illustrates in, figure VI.7 for $\alpha \neq 0$. The size of the cells is not uniform over the whole axial length and increases with α from one angle to another.

These flow patterns may be due to the interaction between the boundary layer formed on the inner cylinder surface and the axisymmetric toroidal rolls; toroidal Taylor vortices. The vortices induced by the boundary layer will cause the stretching of toroidal Taylor vortices along the axial direction. Therefore, the toroidal Taylor vortices are elongated in the axial direction so that the number of vortices is reduced. The axial profile of the tangential velocity along the midline of the gap width decreases with increasing axial coordinate.

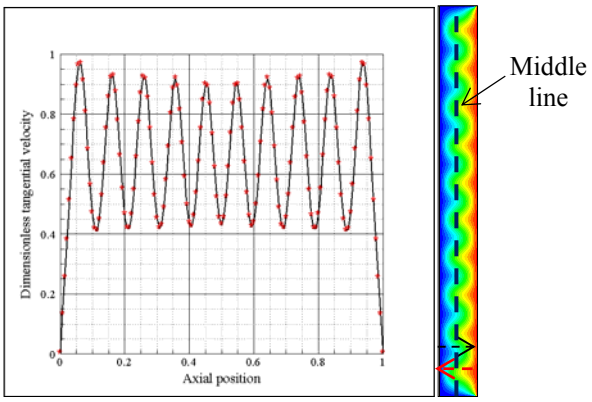

α=0

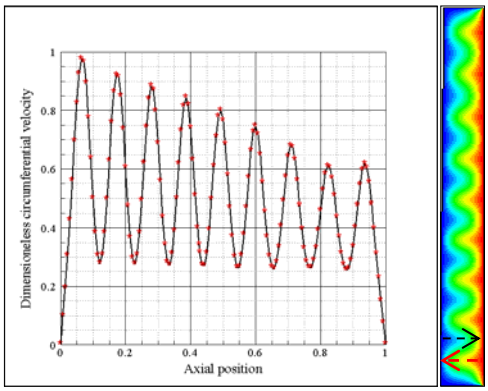

α=20'

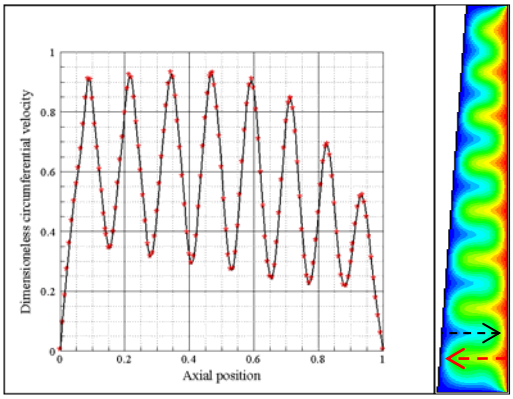

α=2°

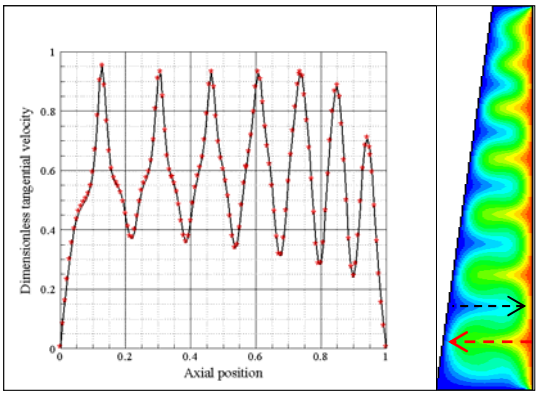

α=4°

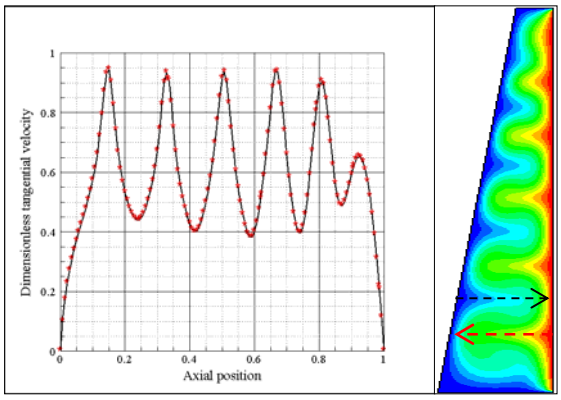

α=6°

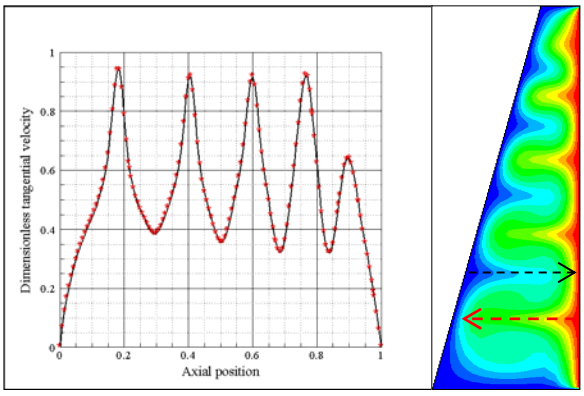

α=8°

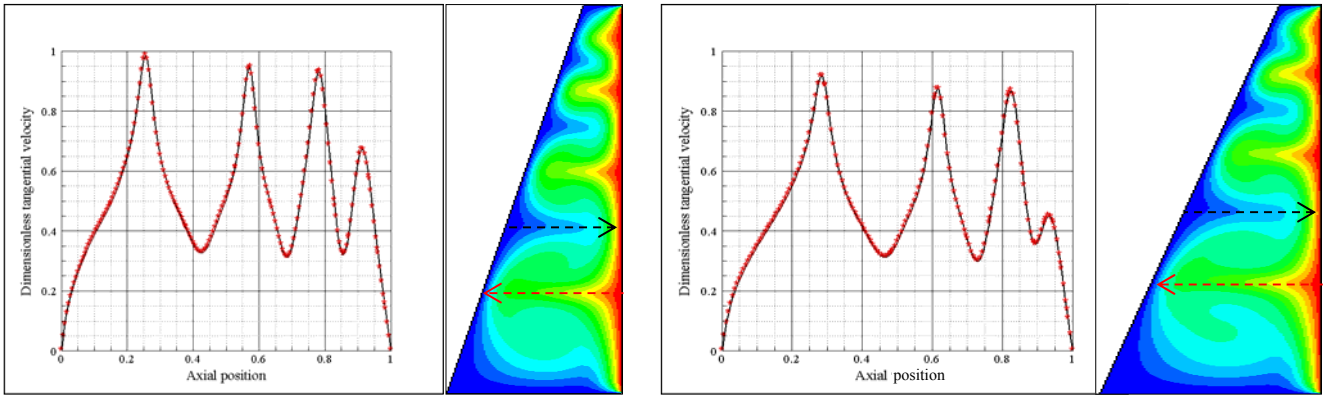

α=10° **α=12°**

Figure VI.7: Evolution of the tangential velocity for different apex angles. --> outflow and <-- inflow. In each figure, the left presents the dimensionless tangential velocity distribution, and the right illustrates its contour in (r,z) plane.

VI.5 Conclusion

In this paper, we have presented numerical calculations of Taylor-Couette flow where the inner cylinder is a regular straight cylinder, but the outer cylinder has a tilted, conical shape. The calculations are carried out with a CFD code, Ansys Fluent, when the inner cylinder rotates with a constant angular velocity while the conical outer cylinder is stationary. The apex angle between the inner cylinder and the outer cone is varied between 0 and 12 degrees. Computations for the onset of Taylor vortex flow in the classical configuration with straight cylinders show good agreement with experimental data. For the case of a conical outer cylinder, numerical results show a decrease in the critical Taylor number for the onset of the first instability along with the number of vortices with the apex angle. Measurements of the axial extension of the vortices show linear decrease with decreasing width of the gap for which the gap width varies in height, and the Taylor vortices then vary in size, being large where the gap is wide and small where the gap is narrow.

CHAPTER VII

Stability of a conducting fluid contained between two rotating spheres subjected to a dipolar magnetic field

«Half of science is asking the right questions»

Roger Bacon

Results and discussion

Chapter VII: Stability of a conducting fluid contained between two rotating spheres subjected to a dipolar magnetic field

VII.1 Introduction

The flow behaviour in an annulus between two concentric rotating spheres, termed spherical Couette flow (SFC), has a major interest in many branches of physics and technology where centrifugal force plays a dominant role. This flow configuration generates a various flow patterns during the transition to turbulence, the study of which is an important part of hydrodynamic stability theory. This flow geometry can be considered as a combination of a cylindrical Taylor Couette system near the equator and two parallel disks in the pole region. A rich variety of flow patterns and instability mechanisms occurred during the laminar-turbulent transition as the Reynolds number is increased quasi-statically. Numerous investigations, either numerically and/or experimentally, have been carried out on spherical Couette flow, for different ranges of Reynolds number and gap widths, in order to understand the flow behaviour and determine a general map of the laminar-turbulent transition. Thus, a large variety of interesting flow modes has been identified by several authors (Wimmer [217], Marcus and Tuckerman [169], Nakabayashi et al. [146], Bühler [172], Yuan [151], Lalaoua and Bouabdallah [153]).

On the other hand, applying a magnetic field on this flow problem, termed MHD spherical Couette flow, crucially affects the flow structures and the occurrence of instabilities, which can radically alter the flow patterns. Furthermore, the transitional phenomena encountered in magnetized spherical Couette flow are of fundamental relevance for the understanding of global processes in the planetary atmospheres, accretion discs and oceanic circulations as well as in astrophysical and geophysical motions.

The rotating spherical Couette flow under an imposed magnetic field has been studied, numerically, for the first time by Hollerbach [170]. He showed that the insulating surfaces give a shear layer, but conducting walls yield a super rotating jet, i.e., a zone of fluid rotating faster than either boundary. Later, many researchers have extensively studied this problem for a variety of imposed magnetic fields (axial and/or dipolar) and different boundary conditions, i.e., insulating or conducting walls.

Among these are Hollerbach [218], Hollerbach and Skinner [219], Schmitt et al. [220], Nataf et al. [221], Travnikov et al. [222], Gissinger et al. [223], Kaplan [224], Lalaoua and Bouabdallah [225]. Numerical studies of Dormy et al. [226] and Hollerbach et al. [227] highlight the nature and structure of the flow that appear when the magnetic field lines are not parallel to the rotation axis. In addition, the MHD spherical Couette system has also been proposed as a model to produce a dynamo (Cardin et al. [228], Kelley et al. [229], Sisan et al. [230]).

The main purpose of this paper is to investigate numerically the effect of an imposed dipolar magnetic field on the behaviour of spherical Couette flow, when the inner sphere rotates freely about a vertical axis passing through its centre and the outer one is kept stationary, and where liquid sodium is used as conducting fluid. The calculations are done with a CFD software package, Ansys Fluent, for a wide range of Hartmann number (Ha), and a fixed Reynolds number characterizing the first instability. This flow problem has relevant applications in geophysical and astrophysical, where configurations similar to MHD spherical Couette flow are often encountered.

VII.2 Numerical modeling

Here, we consider the flow of an electrically conducting fluid confined in an annular gap between two concentric spheres of inner radius R_1 and outer radius R_2, in a dipolar magnetic field. The inner sphere rotates while the outer one is at rest. Liquid sodium of kinematic viscosity $\upsilon=7.4\times10^{-7}$ m^2/s, density $\rho=927$ kg/m^3 and electrical conductivity $\sigma= (\eta\mu)^{-1} =10^7$ Ohm/s. m (where η and μ are, respectively, the magnetic diffusivity and magnetic permeability) was used as working fluid, as shown in figure VII.1(b). Hereafter we assume that ρ, ν, η and μ are constant. The geometry is fully determined by the gap width $\beta = (R_2-R_1)/R_1$ which has been kept constant and equal to 0.18 throughout this study. Both outer and inner spheres are considered insulating. There are two dimensionless numbers that completely determine the flow behaviour: the Reynolds number and Hartmann number defined as follow:

$$\mathrm{Re} = \frac{\Omega_1 R_1^2}{\nu} \qquad (VII.1)$$

$$Ha = \frac{B_0 R_1^2}{\sqrt{\mu\rho\nu\eta}} \qquad (VII.2)$$

Points in the domain are defined by the spherical coordinates (r, θ, φ) with:

- Radial position : $r \in [R_1, R_2]$ with $R_1 \le r \le R_2$
- Meridional Position : $\theta \in [0, \pi]$ with $0 \le \theta \le \pi$
- Circumferential position : $\varphi \in [0, 2\pi]$ with $0 \le \varphi \le 2\pi$

The equations governing incompressible hydromagnetic flow are given as follow

$$\begin{cases} \nabla . V = 0 & (VII.3) \\ \rho \dfrac{\partial V}{\partial t} + \rho (V.\nabla) V = -\nabla P + \rho \nu \nabla^2 V + \dfrac{1}{\mu_0} (\nabla \times B) \times B & (VII.4) \\ \dfrac{\partial B}{\partial t} = \nabla \times (V \times B) + \eta \nabla^2 B & (VII.5) \\ \nabla . B = 0 & (VII.6) \end{cases}$$

Let (*u, v, w*) the physical components of the velocity **V** in cylindrical coordinates (r,θ, z). Time and pressure are denoted by **t** and **P**, respectively. **B** is the magnetic field, which contains the imposed dipolar magnetic field B_d defined as:

$$B_d = B_0 \left(\frac{R_2}{r} \right)^3 \left(2\cos\theta \, e_r + \sin\theta \, e_\theta \right) \qquad (VII.7)$$

B_0 is the intensity of the field at the equator on the outer surface of the fluid ($r = R_2$).

The boundary conditions used in this study are:

* $r = R_1,\ u = v = w = 0$

* $r = R_2,\ u = v = 0 \ and \ w = \Omega_1 R_1 \sin\theta$

* $\theta = 0,\ \dfrac{\partial u}{\partial \theta} = v = \dfrac{\partial w}{\partial \theta}$

* $\theta = \pi,\ \dfrac{\partial u}{\partial \theta} = v = \dfrac{\partial w}{\partial \theta}$

No-slip boundary conditions for the velocity are applied at all surfaces, hence, $u = v = w = 0$ applied at the boundaries $r = R_1$ and $r = R_2$. Therefore, all the near-wall regions are explicitly computed.

The spherical annulus is divided into equally spaced intervals in the meridional (θ) and circumferential (φ) directions, and is clustered in the radial (r) direction in order to refine the grids near the walls of the spheres where there is a high shear, as shown in Figure VII.1(a). In this study, several calculations have been performed, to see the impact of the grid density on the numerical results (mesh dependence). The converged solution from the coarse mesh was interpolated for use as an initial solution for the medium mesh, and likewise the converged solution of the medium mesh was used as an initial solution for the finer mesh.

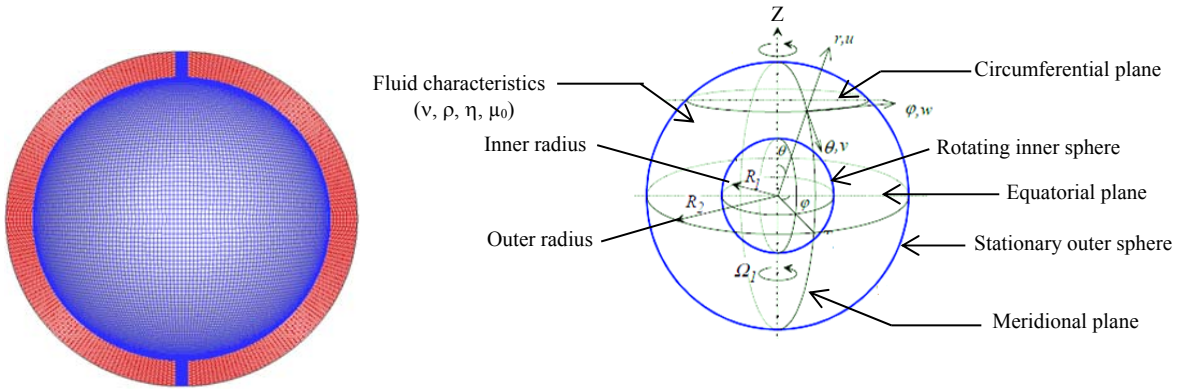

a) Grid discretizing the computational domain b) Spherical Couette geometry

FigureVII.1: Sketch of spherical Couette flow system.

The numerical results are obtained using the simulation code, Ansys Fluent, based on the finite volume method. The discretization scheme chosen for the pressure is the second order model. The third order MUSCL scheme was used for the moment equations. The velocity-pressure coupling was linked using the PISO algorithm (Pressure Implicit with Splitting of Operator). In addition, the time step, the maximum number of iterations per time step, and the relaxation factors need to be carefully adjusted to ensure the convergence criteria which are based on the residual values. The solution is assumed converged when all standardized residuals less than 10^{-4}.

The validation of our calculations for the onset of Taylor vortices, first instability, was made with the experimental and theoretical work of Bühler [149] for the same geometrical parameters. A good agreement between our numerical simulation and the study of Bühler [149]has been found, as illustrated in figure VII.2.

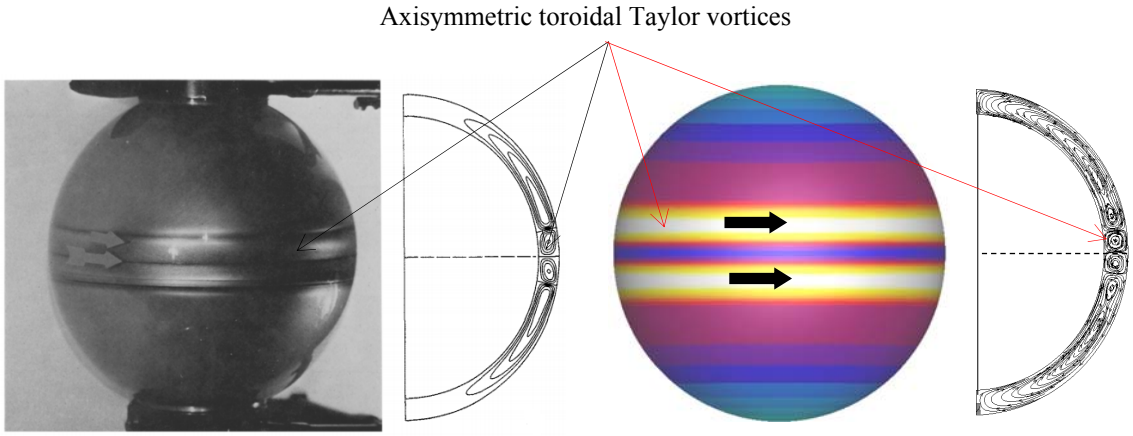

a) Experiment work of Bühler [149] b) Our numerical result

Figure VII.2: First instability in nonmagnetic spherical Couette flow/ Wall shear stress on the outer sphere.

VII.3 Main Results

VII.3.1 Flow patterns

Figure VII.3 shows the contours of the pressure field on the outer sphere for several Hartmann number and for a fixed critical Reynolds number, Re_{c1}=980. We have firstly simulated spherical Couette flow without an imposed magnetic field, Ha=0, in order to highlight the first instability. For this case, the Reynolds number was gradually increased, from rest until the appearance of Taylor vortices. At low Reynolds numbers, the laminar basic flow is a steady axisymmetric, unique and equatorially symmetric yielding a homogeneous movement throughout the fluid in the absence of any disturbance. As the angular velocity of the inner sphere is increased further, two steady rolls occur, one on each side of the equator representing the first stage of laminar-turbulent transition at Re_{c1}=980. However, when the rotational Reynolds number of the inner sphere is fixed and a magnetic field is applied to this hydrodynamical state, additional magnetohydrodynamic effects are generated. As illustrated in figure below, the inhibiting role of the magnetic field; the rolls at the equator move toward the pole when the Hartmann number is further increased. This flow mode is strongly damped by the applied field.

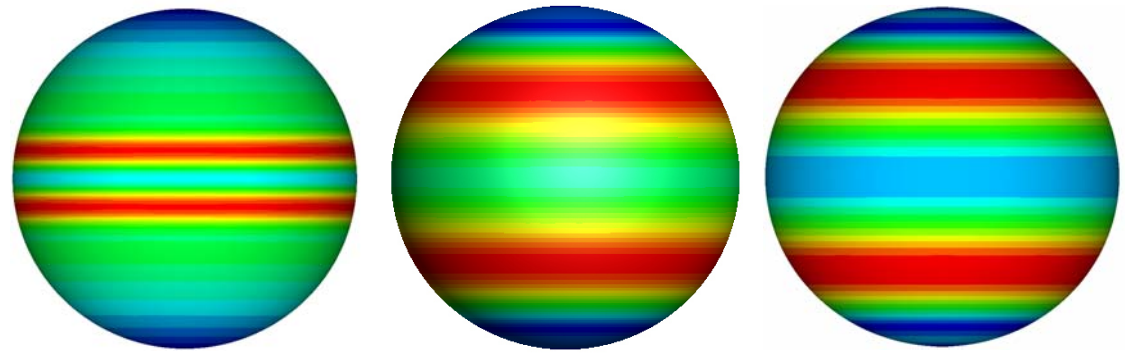

Ha=0 Ha =25 Ha= 60

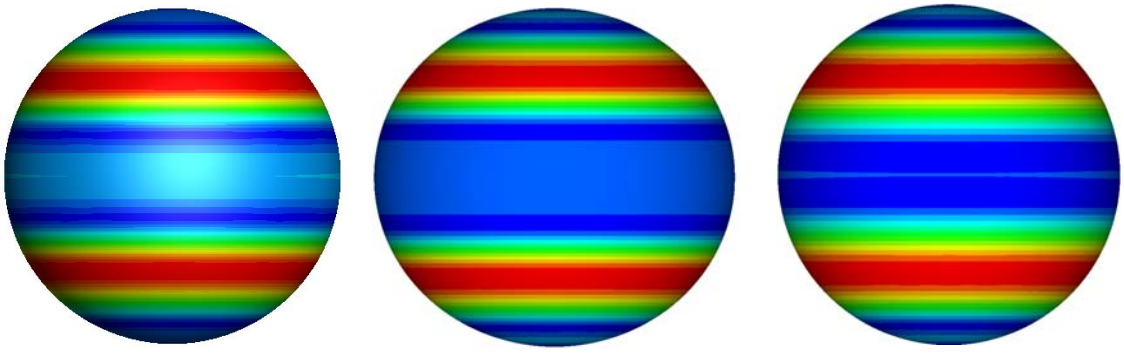

Ha=180 Ha= 410 Ha=600

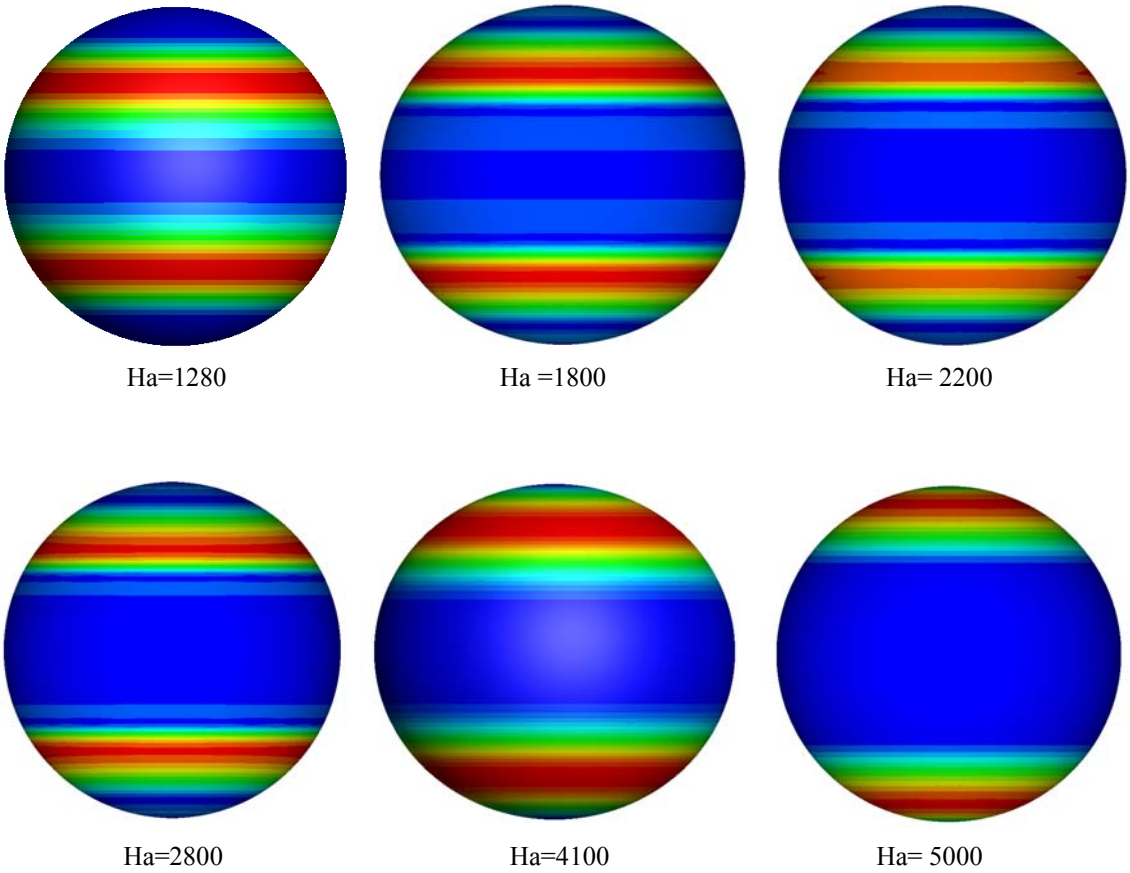

Figure VII.3: Flow patterns for different Hartmann number at fixed Reynolds number/ Pressure field.

VII.3.2 Tangential velocity distribution

Figure VII.4 shows the tangential velocity distribution at a fixed Reynolds number Re=980, and Hartmann number increasing from 0 up to 4600. The velocity profiles are plotted in dimensionless form in which the tangential velocity is divided by the surface speed, and the radial distance from the wall of the inner sphere is divided by the annular gap (gap width=$(r-R_1)/d$, where d is annular space between the coaxial spheres). The salient features of the numerical profiles are summarized as follow:

- For the case without imposed magnetic field, Ha =0 and Re=980, the profile is monotonically decreasing and it is analogous to the laminar profile in classical Taylor–Couette flow. The tangential velocity is stronger near the inner rotating sphere than at the outer sphere that is stationary.
- At low Hartmann number, Ha=25, the profile is still monotonic but slightly deformed near the outer sphere.
- As the intensity of the magnetic field is further increased, it is observed that the velocity profiles are completely deformed, having negative values in the whole annular gap. Note also that the tangential velocity becomes zero at the outer sphere.

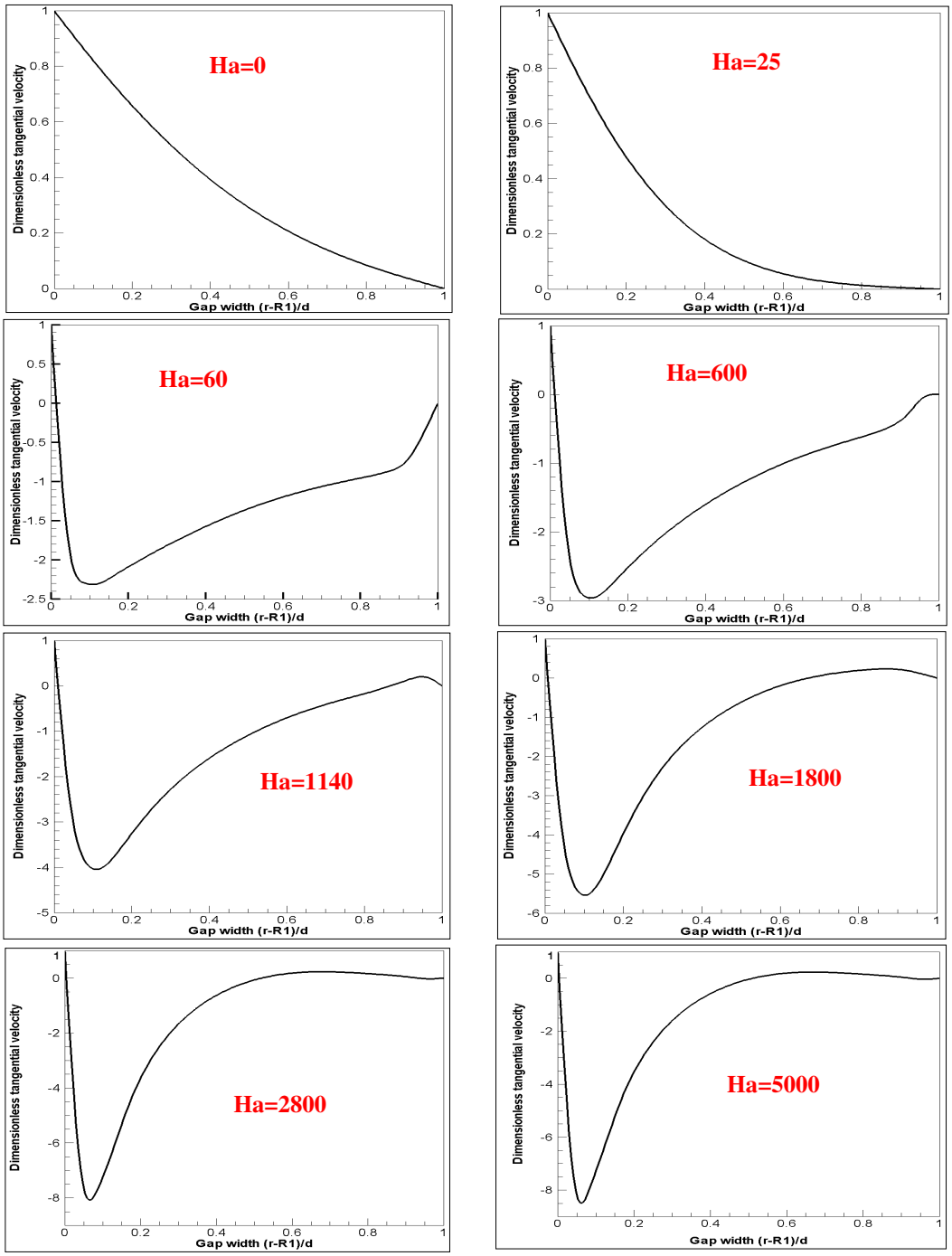

Figure VII.4: Dimensionless Tangential velocity distributions versus Hartmann number plotted at the equator (z=0, θ=0 and φ=90°.

VII.4 Conclusion

In this work, we have presented numerical calculations of the flow behavior of an electrically conducting fluid in an annular gap between two rotating concentric spheres subjected to a dipolar magnetic field. The calculations are carried out with a CFD code, Ansys Fluent, when the inner sphere rotates with a constant angular velocity while the outer one is stationary. The specific case considered is that with a medium gap width β = 0.18 and a wide range of Hartmann number, ranging from 0 up to 5000. Computations for the onset of Taylor vortices in the nonmagnetic

spherical Couette flow, without an imposed magnetic field, show good agreement with experimental data. In the case of magnetic spherical Couette flow, we have increased the Hartmann number for a fixed Reynolds number, and studied the resulting balance and competition between magnetic and inertial effects. We found that increasing the Hartmann number stabilizes the flow and delayed the occurrence of the Taylor vortices at the equator.

General conclusion

« Research is to see what everybody else sees, and think what nobody else has thought»

Albert Szent-Györgyi

General conclusion

The study of rotating flows is currently the subject of several works and constitutes a great phenomenological wealth, particularly in the occurrence of different instabilities, flow structures as well as the successive transitions to turbulence. Moreover, seldom does a physical system, particularly one as apparently simple as the flow between two concentric rotating bodies, known as Taylor-Couette flow, retain the interest of scientists, applied mathematicians and engineers for very long. This flow system can be regarded as part of the large domain of the flows in rotating systems. Indeed, the Taylor-Couette system shows a rich variety of interesting features and allows quantitative experimental, theoretical as well as numerical studies. Extensions of Taylor's fundamental work as combination of different geometries, effect of the working fluids, additional forces (imposed magnetic field, imposed axial flow and oscillation of inner or outer element of flow system) have discovered new flow patterns and different laminar-turbulent transition scenarios. However, the examination of these flows remains difficult to understand because of the three-dimensional and unsteady nature of the transition process.

In this thesis, the flow features and the instabilities between rotating bodies and combinations of them are investigated numerically using the simulation code Ansys-Fluent for three-dimensional and incompressible flows. Special emphasis is placed on the first onset and the further development of instabilities. All the bodies tested, cylinders, spheres, and cones and combination between them are bodies of revolutions with symmetry about the axis of rotation.

The modeling strategy has been developed in this thesis by studying 4 different fluid flow settings:

- Flow between two rotating sphero-cylinders (cylinders-spheres combination).
- Effect of the working fluid confined between two rotating cylinders on the onset of Taylor vortices.
- Flow between two rotating conical cylinders (cylinders-cones combination).
- Effect of imposed dipolar magnetic field on the stability of a conducting fluid contained between two rotating spheres.

Most of the results obtained can be summarized as follows:

The first part of the results is devoted to the effect of the cylinders-spheres combinations on the onset of different instabilities of a fluid confined between two concentric bodies. Particular attention was paid to the effects of axial confinement (end caps) on the onset of axisymmetric and wavy vortex flows between combinations of cylinders and sphero-cylinders by the study of the interaction

between terminal boundaries and centrifugal instability. Our results have shown how the end walls significantly modify the laminar-turbulent transition scenario predicted experimentally and numerically in the case of infinitely long cylinders. We have shown that the different combinations deeply affect the flow behaviour and the appearance of the instabilities. The transition from laminar Couette flow to Taylor vortex flow and then to wavy vortex flow in the combined flow systems is substantially retarded compared to the cylindrical Taylor-Couette flow system.

The second part of the results concerns the study of the influence of the working fluids confined inside an infinite aspect ratio Taylor-Couette system on the onset of cellular pattern. Four fluids have been used in the computations namely water, hydrogen, helium, and lithium. It is found that the number of toroidal rolls and the number of vortices for water and helium are the same, however for hydrogen and lithium are completely different to water and helium. Thus, we concluded that the physical properties of fluids play an important role on the stability of flow. The number of vortices occurring in the annulus and their wavelength are varied from one fluid to another. Water and helium have the same behaviour, while for hydrogen and lithium show significant changes on the number and shape of cellular patterns. For hydrogen liquid, the Ekman cells and the Taylor vortices are substantially elongated. However, for lithium liquid, the Ekman cells and the Taylor vortices are compressed.

In the third part of the results, we have presented the fluid motion in an annulus between cylinder-cone combinations. The transitional phenomena occurring in this flow are discussed under the effect of opening angles of the outer cylinder α ranging from 0 (classical case) up to 12°. We found that the first critical Taylor number, characterizing the occurrence of Taylor vortices in the flow, decreases drastically; the first instability mode of transition changes from Ta_{c1}=41.6, corresponding to the classical case to Ta_{c1}=20.3 when the apex angle reaches 12°. In addition, we shown a linear decrease of axial wavelength of vortices with decreasing width of the gap for which the gap width varies in height, and the Taylor vortices then vary in size, being large where the gap is wide and small where the gap is narrow.

Finally, the fourth part of results focuses on the flow behaviour and stability of an electrically conducting fluid confined between two concentric rotating spheres with an imposed dipolar magnetic field. We found that the imposed magnetic field radically alters the flow structures leading to significant topological changes on the flow patterns.

It was clear that even though great progress has been made in understanding some of the basic instabilities and resulting flow patterns in the Taylor-Couette system, there remains a great deal of work to be done.

This study has shown that the flow regime in the annular region of concentric bodies depends on the end-wall conditions, working fluids, geometry of flow problem and imposed extern forces . As

such, it was practically impossible to cover the full parameter space in this research work. Open questions, and what needs to be investigated further in future are detailed as follows:

- Is fully developed turbulence universal, or is it special in this system?
- What is the general relationship of the Taylor-Couette system to open flows, as well as to flows near rotating bodies (flow around or within cylinder, sphere and cone).
- Are the stability properties of the flow are modified if the two body axes do not coincide (axisymmetry of the flow system is broken)?
- What happens if a cylinder rotates in a conical container or a cone in a cylindrical shell? somewhat more complicated is the case of a rotating cone in a cylinder, where neither the radius nor the width of the gap remains constant.

The present CFD work could be extended to:

(1) A time-dependent simulation (second and third instabilities) and fully developed turbulent mode,

(2) The onset of the various instabilities between different rotating bodies (cylinder, sphere and cone) and combinations of them,

(3) The effect of oscillation motion on the onset of various flow modes in different rotating bodies,

(4) The influence of boundary conditions (lobed, grooved, tailored and ramped Taylor-Couette system),

(5) Flows between co and counter-rotating bodies,

(6) Effect of the working fluids on the pattern formation and stability in a Taylor-Couette system using non-Newtonian fluids,

(7) Taylor-Couette flows with axial and/or radial flow,

(8) Flow patterns at different geometries (between two rotating pentagons, hexagons and octagons)

(9) Transport phenomena in magnetic fluids in cylindrical, conical and spherical geometries,

(10) Thermal convective motions in spherical Couette flow,

(11) Superfluid Taylor-Couette flows,

(12) Hydrodynamic behaviour of granular flow in Taylor-Couette system,

(13) Effect of eccentricity on the stability of the Taylor-Couette flow: application to oil drilling,

(14) Compressible Taylor-Couette flow

References

« If we are uncritical we shall always find what we want: we shall look for, and find, confirmations, and we shall look away from, and not see, whatever might be dangerous to our pet theories.»

Karl Popper

REFERENCES

[1] E. Koschmieder, "Bénard Cells and Taylor Vortices", Cambridge, UK: Cambridge University Press, (**1993**).

[2] R. Tagg, "A guide to literature related to the Taylor-Couette problem," in Ordered and Turbulent Patterns in Taylor-Couette Flow, pp.303-354, New York, Plenum Press, (**1992**).

[3] R. Tagg, "The Couette-Taylor problem," Non-linear Sci. Today, vol.4, pp.1-25, (**1994**).

[4] R. Di Prima and H. L. Swinney, "Instabilities and transition in flow between concentric rotating cylinders," in Hydrodynamic Instabilities and the Transition to Turbulence, pp.139-180, New York, NY: Springer-Verlag, (**1985**).

[5] C. D. Andereck, S. S. Liu, and H. L. Swinney, "Flow regimes in a circular Couette system with independently rotating cylinders," J. Fluid Mech., vol.164, pp.155-183, (**1986**).

[6] I. Newton, "Philosophie Naturalis Principia Mathematica (trans. Andrew Motte)". New York, NY: Daniel Adee, (**1846**).

[7] G. G. Stokes, "On the theories of the internal friction of fluids in motion and of the equilibrium and motion of elastic solids," in Mathematical and Physical Papers, pp.102-104, Cambridge, UK: Cambridge University Press, (**1880**).

[8] R. Donnelly, "Taylor-Couette flow: The early days," Phys. Today, pp.32-39, (**1991**).

[9] A. Mallock, "Determination of the viscosity of water," Proc. R. Soc. London, vol.45, pp.126-132, (**1888**).

[10] A. Mallock, "Experiments on fluid viscosity," Phil. Trans. R. Soc. A, pp.41-56, (**1896**).

[11] M. Couette, "Etudes sur le frottement des liquides",Ann.Chim.Physi, pp.433-510, (**1890**).

[12] L. Rayleigh, "On the dynamics of revolving fluids," Proc. R. Soc. Lond. A, vol. 93, pp. 148-154, (**1917**).

[13] G. Taylor, "Experiments with rotating fluids," P. Camb. Philos. Soc., vol. 20, pp.326-329, (**1921**).

[14] G. Taylor, "Stability of a viscous liquid contained between two rotating cylinders," Phil. Trans. R. Soc. A, vol. 223, pp.289-343, (**1923**).

[15] F. Wendt, "Turbulente Strömungen zwischen zwei rotierenden konaxialen Zylindern," Ing.-Arch., vol. 4, pp.577-595, (**1933**).

[16] S. Chandrasekhar, "the stability of viscous flow between rotating cylinders, mathimatika," London, Press Clarendon Oxford, 1, pp.5-13, (**1954**).

[17] S. Chandrasekhar, "The stability of viscous flow between rotating cylinders," Proc. R. Soc. London, Ser. A 246, pp.301-311, (**1958**).

[18] D. Coles, "Transition in circular Couette flow", J. Fluid Mech.. 21, pp.385-425., (**1965**).

[19] J. P. Gollub and H. L. Swinney, "Onset of turbulence in a rotating fluid," Phys. Rev. Lett., vol. 35, pp.927-930, (**1975**).

[20] P. Fenstermacher, H. Swinney, and J. P. Gollub, "Dynamical instabilities and the transition to chaotic Taylor vortex flow," J. Fluid Mech., vol. 94, pp.103-128, (**1979**).

[21] Lathrop, D. P., J. Fineberg, and H. L. Swinney, "Transition to shear-driven turbulence in Couette-Taylor flow," Phys. Rev. A 46, 6390, (**1992b**).

[22] O. Czarny, E. Serre, P. Bontoux and R. M. Lueptow, "Interaction between Ekman pumping and the centrifugal instability in Taylor-Couette flow", Phys. Fluids, 15(2), (**2003**).

[23] Heise, M., Abshagen, J., Küter, D., Hochstrate, K., Pfister, G., and Hoffman, C., "Localized spirals in Taylor-Couette flow", Phys. Rev. E 77, 026202 (**2008**).

[24] Abshagen, J., Lopez, J., Marques, F., and Pfister, G., "Bursting dynamics due to a homoclinic cascade in Taylor-Couette flow", J. Fluid Mech. vol.613, pp.357-384, (**2008**)

[25] Manneville, P. and Czarny, O., "Aspect-ratio dependence of transient Taylor vortices close to threshold", Theor. Comput. Fluid Dyn. 23, 15 (**2009**).

[26] Abshagen, J., von Stamm, J., Heise, M., Will, Ch., and Pfister, G., "Localized modulation of rotating waves in Taylor-Couette flow", Phys. Rev. E 85, 056307 (**2012**).

[27] López, J. M. and Francisco, M., "Dynamics of axially localized states in Taylor-Couette flows", Phys. Rev. E 91(5), 053011 (**2015**).

[28] Martinand, D., Serre, E., and Lueptow, R. M., "Mechanisms for the transition to waviness for Taylor vortices", Phys. Fluids 26(9), 094102 (**2014**).

[29] M. A. Razzak, B. C. Khoo , and K. B. Lua., " Numerical study on wide gap Taylor-Couette flow with flow transition" Phys. Fluids 31, 113606 (**2019**).

[30] Jeffreys, H.: Some cases of instability in fluid motion. Proc. Roy. Soc. (London)A 118, pp.195-208, (**1928**).

[31] S. Chandrasekhar, "Hydrodynamic and Hydromagnetic Stability", London, Press Clarendon Oxford, (**1961**).

[32] R. C. Di Prima, "The Stability of Viscous Flow Between Rotating Cylinders with Axial Flow ", J. Fluid Mech. vol.9, 621 (**1960**).

[33] P.H. Roberts," The solution of characteristic value problem" Proc. Roy. Soc. Lond. A., 283, pp.550-556, **(1965).**

[34] Schmid, P. J. and Henningson, D. S., "Stability and transition in shear flows", New York, Springer, (**2001**).

[35] Betchov, R. and Criminale(Jr), W. O., "Stability of parallel flows", New York, Academic Press, (**1967**).

[36] Lin, C. C., "The theory of hydrodynamic stability", Cambridge Press, (**1955**).

[37] Joseph, D. D., "Stability of fluid motions", vol. 1 and 2, Berlin, Springer-Verlag, (**1976**).

[38] Drazin, P. G. and Reid, W. H., "Hydrodynamic Stability", Second edition, Cambridge, Cambridge University Press, (**2004**).

[39] Dou, H. S., "Mechanism of flow instability and transition to turbulence", Inter. J. Non-linear Mech, vol.41, pp.512-517, (**2006**).

[40] Dou, H. S., Khoo, B. C. and Yeo, K. S., "Instability of Taylor-Couette flow between concentric rotating cylinders", Inter. J. Ther. Scie, 47 (11), pp.1422-1435, (**2008**).

[41] Deng, D., "A numerical and experimental investigation of Taylor flow instabilities in narrow gaps and their relationship to turbulent flow in bearings", PhD thesis, The University of Akron, (**2007**).

[42] J.T Stuart, "On the non-linear mechanics of hydrodynamics stability", J. Fluid Mech. vol.4, pp.1-12, (**1958**).

[43] A. Davey, "The growth of Taylor vortices in flow between rotating cylinders" J. Fluid Mech., 14:336, (**1962**).

[44] Donnelly, R. J., "Experiments on the stability of viscous flow between rotating cylinders. Torque measurements", Proc. Roy. Soc. Lond. A, 246 (1246), pp.312-325, (**1958**).

[45] Jones, C. A., "Nonlinear Taylor vortices and their stability", J. Fluid Mech, vol.102, pp.249-261, (**1981**).

[46] Zarti, A. S. and Mobbs, F. R., "'Wavy Taylor vortex flow between eccentric rotating cylinders, Energy conservation through fluid film lubrication technology: Frontiers in research and design", Proc. winter annual meeting, New York, ASME, pp.103-116, (**1979**).

[47] Davey, A., Di Prima, R. C. and Stuart, J. T., "On the instability of Taylor vortices, J. Fluid Mech, vol.31, pp.17-52, (**1968**).

[48] Takeda, Y., "Quasi-periodic state and transition to turbulence in a rotating Couette system", J. Fluid Mech, vol.389, pp.81-99, (**1999**).

[49] Gorman, M. and Swinney, H. L., "Spatial and temporal characteristics of modulated waves in the circular Couette system", J. Fluid Mech, vol.117, pp.123-142, (**1982**).

[50] C-S. Yih, "Instability of a rotating liquid film with a free surface", Proc. R. Soc. London, Ser. A 258, 63 (**1960**).

[51] Snyder, H. A., and Karlsson S. K. F., "Experiments on the stability of Couette motion with a radial thermal gradient". Phys. Fluids 7, pp.1696-1706, (**1964**).

[52] Chen, J. C., and Kuo, J. Y., "The linear stability of steady circular Couette flow with a small radial temperature" Phys. Fluids A 2, pp.1585-1591, (**1990**).

[53] Ball, K. S., and Farouk, B., "Bifurcation phenomena in Taylor–Couette flow with buoyancy effects". J. Fluid Mech. 197, pp.479-501, (**1988**).

[54] Kuo, J. Y., and Ball, K. S., "Taylor- Couette flow with buoyancy: Onset of spiral flow". Phys. Fluids 9, pp.2872-2884, (**1997**).

[55] I. Mutabazi, A. Goharzadeh and F. Dumouche, "The circular Couette flow with a radial temperature gradient", 12th International Couette-Taylor Workshop (**2001**).

[56] K.S. Ball, B. Farouk, and V.C. Dixit., "An experimental study of heat transfer in a vertical annulus with a rotating inner cylinder". Int. J. Heat Mass Transfer, 32:1517-1527, (**1989**).

[57] M.E. Ali and P.D. Weidman., "On the stability of circular Couette flow with radial heating". J. Fluid Mech., 220: pp.53-84, (**1990**).

[58] D. Liu, S.H. Choi, and H.B. Kim., "Experiments on the stability of Taylor-Couette flow with radial temperature gradient". Moscow, FLUCOME (**2009**).

[59] V. Lepiller, A. Goharzadeh, A. Prigent, and I. Mutabazi., "Weak temperature gradient effect on the stability of the circular Couette flow". Eur. Phys. J. B, 61: pp.445-455, (**2008**).

[60] H.N. Yoshikawa, M. Nagata, and I. Mutabazi., "Instability of the vertical annular flow with a radial heating and rotating inner cylinder". Phys. Fluids, 25:114104, (**2013**).

[61] H. Rubin and C. Elata, "Stability of Couette flow of dilute polymer solutions", Phys. Fluids, 7, pp.1929-1933, (**1966**).

[62] R.G. Larson, E.S.G. Shaqfeh, and S.J. Muller, "A purely elastic instability in Taylor-Couette flow", J. Fluid Mech. 218, pp.573-600, (**1990**)

[63] A. Groisman, and V. Steinberg, "Solitary vortex pairs in viscoelastic Couette flow", Phys. Rev. Lett. 78, 1460 (**1997**).

[64] A. Groisman, and V. Steinberg, "Elastic turbulence in curvilinear flows of polymer solutions", New J. Phys. 6, 29 (**2004**).

[65] A.N. Morozov, and W. van Saarloos, "Subcritical finite-amplitude solutions for plane Couette flow of viscoelastic fluids", Phys. Rev. Lett. 95, 024501(**2005**).

[66] M. Lange, and B. Eckhardt, Vortex pairs in viscoelastic Couette-Taylor flow, Phys. Rev. E 64, 027301(**2001**).

[67] K. Kumar, and M.D. Graham, "Finite-amplitude solitary states in viscoelastic shear flow: computation and mechanism", J. Fluid Mech. vol.443, pp.301-328, (**2001**).

[68] D. Thomas, B. Khomami, and R. Sureshkumar, "Nonlinear dynamics of viscoelastic Taylor-Couette flow: effect of elasticity on pattern selection, molecular conformation and drag", J. Fluid Mech. vol.620, pp.353-382, (**2009**).

[69] N. Liu, and B. Khomami, "Polymer-induced drag enhancement in turbulent Taylor-Couette flows: Direct numerical simulations and mechanistic insight", Phys. Rev. Lett. 111, 114501, (**2013**).

[70] R.G. Larson, E. S. G. Shaqfeh, and S.J. Muller, "A purely elastic instability in Taylor-Couette system", J. Fluid Mech., 218, pp.573-600, (**1990**).

[71] A. Groisman, and V. Steinberg, "Mechanism of elastic instability in Couette flow of polymer solutions: experiment", Phys. Fluids, 10 (10), pp.2451-2463, (**1998**).

[72] G. S. Beavers, and D. D. Joseph, "Interfacial shapes between two superimposed rotating simple fluids," J. Fluid Mech. vol.145, pp.11-70, (**1984**).

[73] B. Martinez-Arias and J. Peixinho, "Torque in Taylor-Couette flow of viscoelastic polymer solutions", J. Non-Newt Fluid Mech. vol.247, pp. 221-228, (**2017**).

[74] M. Stockert and R.M Lueptow , "Velocity field in Couette-Taylor with axial flow", 10th International Couette-Taylor Workshop , Paris, France, (**1997**).

[75] R.M. Lueptow, "Stability and experimental velocity field in Taylor-Couette flow with axial and radial flow", Lecture Notes in Physics, vol. 549, pp. 137, (**2000**).

[76] Astill K. N. "Studies of the Developing Flow Between Concentric Cylinders with the Inner Cylinder Rotating", J. Heat Transfer 86, 383 (**1964**).

[77] Piva, M., Calvo, A., Aguirre, A., Callegari, G., Gabbanelli, S., Rosen, M., and Wesfreid, J. E. "Hydrodynamical Dispersion in Propagative Couette-Taylor Cells", Journal de Physique III 7 (4), pp.895-908, les éditions de physique (**1997**).

[78] Gu, Z. H., and Fahidy, T. Z., "The Effect of Geometric Parameters on the Structure of Combined Axial and Taylor Vortex Flow", Can. J. Chem. Eng. 64, (**1986**).

[79] Gu, Z. H., and Fahidy, T. Z., "Characteristics of Taylor Vortex Structure in Combined Axial and Rotating Cylinders", Can. J. Chem. Eng. 63, pp.710-715, (**1985**).

[80] N. Lancial, F. Torriano, F. Beaubert, S. Harmand, and G. Rolland, "Taylor-Couette-Poiseuille flow and heat transfer in an annular channel with a slotted rotor", International Journal of Thermal Sciences, 112. pp.92-103, (**2018**).

[81] G. Rudiger and D. Shalybkov, "Stability of axisymmetric Taylor-Couette flow in hydromagnetics", Phys. Rev. E 66, 016307, (**2002**).

[82] F. Stefani, T. Gundrum, G. Gerbeth, G. Rudiger, M. Schultz, J. Szklarski, and R. Hollerbach, "Experimental evidence for magnetorotational instability in a Taylor-Couette flow under the influence of a helical magnetic field", Phys. Rev. Lett. 97, 184502, (**2006**).

[83] A. P. Willis and C. F. Barenghi, "A Taylor-Couette dynamo", Astron. Astrophys. 393, 339, (**2002**).

[84] Donnelly, R. J. et M. Ozima, "Experiments on the stability of flow between rotating cylinders in the presence of a magnetic field," Proc. R. Soc. London, Ser. A 266, pp.272-286, (**1962**).

[85] P.H. Roberts, "The stability of hydromagnetic Couette flow", Proc. Camb. Phil. Soc., 60, pp.635-651, (**1964**).

[86] J .Singh and R. Bajaj, "Couette flow in ferrofluid with magnetic field", J. Magnetism and Magnetic Materials. vol. 294, Issue 1, pp.53-62, (**2005**).

[87] M. Kaneda, T. Tagawa, J. Noir and J .M Aurnau, "Variations in driving torque in Couette-Taylor flow subject to a vertical magnetic field, " Journal of Physics: Conference serie 14, 14th International Couette-Taylor Workshop, pp.42-47, (**2005**).

[88] S. Aberkane, M. Ihdene, M. Moderes and A. Ghezal., "Axial Magnetic Field Effect on Taylor-Couette Flow". J. Appl. Fluid Mech, vol. 8, No. 2, pp. 255-264, (**2015**).

[89] Y.E. Kamıs, K. Atalık., "Thermomagnetic effects on the stability of Taylor-Couette flow of a ferrofluid in the presence of azimuthal magnetic field", J. of Magnetism and Magnetic Materials, 454 pp.196-206, (**2018**).

[90] X. Leng, Y. B. Kolesnikov, D. Krasnov, and B. Li., "Numerical simulation of turbulent Taylor-Couette flow between conducting cylinders in an axial magnetic field at low magnetic Reynolds number", Phys Fluids 30, 015107, (**2018**).

[91] E. Adnane, A. Lalaoua and A. Bouabdallah., " Experimental Study of the Laminar-Turbulent Transition in a Tilted Taylor-Couette System Subject to Free Surface Effect ",J. Appl. Fluid. Mech, vol. 9, No. 3, pp.1097-1104, (**2016**).

[92] Snyder, H. A., "Wave-number selection at finite amplitude in rotating Couette flow", J. Fluid Mech, vol.35, pp.273-298, (**1969b**).

[93] A. Lorenzen et T. Mulin., "Anomalous modes and finite-length effects in Taylor-Couette flow", Phys. Rev. A, vol 31, pp.3463-3465, (**1985**).

[94] T. T. Lim, Y. T. Chew, and Q. Xiao, "A new flow regime in Taylor-Couette flow", Phys. Fluids, vol 10, 3233, (**1998**).

[95] Koschmieder, E.L., "Turbulent Taylor vortex flow", J. Fluid Mech, vol.93,3, pp.515-527, (**1979**).

[96] C.A Bielek and E.L Koschmieder, "Taylor vortices in short fluid columns with large radius ratio'", Phys. Fluids, A 2-9, pp 1557-1563 (**1990**).

[97] H. Furukawa, T. Watanabe and I. Nakamura, "Visual information of the mode formation in accelerating Taylor vortex flow with finite length", 9th. Inter. Symp on flow Visualisation, (**2000**).

[98] Snyder H. A., "Change in Wave-Form and Mean Flow associated with Wavelength Variations in Rotating Couette Flow", J. Fluid Mech, vol. 35, pp.337-352, (**1969**).

[99] Mahamdia, A. and Bouabdallah, A., "Effets de la surface libre et du rapport d'aspect sur la transition de l'écoulement de Taylor- Couette", CRAS -Paris Mécanique, vol 331, pp.245-252, (**2003**).

[100] Watanabe, T. and Y. Toya, "Vertical Taylor-Couette flow with free surface at small aspect ratio", Acta Mech (223), pp.347–353, (**2012**).

[101] Watanabe, T., Y. Toya and S. Hara, "Development and Flow Modes of Vertical Taylor-Couette System with Free Surface", World Journal of Mechanic. (4), pp.90-96, (**2014**).

[102] Wilcock, D. F., "Turbulence in High Speed Journal Bearings", Trans. ASME, Vol. 72, pp. 825-834, (**1950**).

[103] Smith, M. I. and Fuller, D. D., "Journal Bearing Operations at Superlaminar Speeds", Trans. ASME, vol. 78, pp.469-474, (**1956**).

[104] Di Prima, R. C., "A Note on the Stability of Flow in Loaded Journal Bearings", Tran. ASLE, vol. 6, pp. 249-253, (**1963**).

[105] Di Prima, R. C. and Stuart, J. T., "Non-local Effects in the Stability of Flow between Eccentric Rotating Cylinders", J. Fluid Mech., vol. 54, pp. 393-415, (**1972**).

[106] Constantinescu, V. N., "On Turbulent Lubrication", Proc. Inst. Mech. Eng., Vol.173, pp. 881-889, (**1959**).

[107] Ng, C. W. and Pan, C. H. T., "A Linearized Turbulent Lubrication Theory", Trans. ASME, Ser. D, Vol. 87, pp. 675-688, (**1965**).

[108] Hirs, G. G., "Bulk Flow Theory for Turbulence in Lubricant Films", Trans. ASME, Serie. F, Vol. 95, pp. 137-146, (**1973**).

[109] I. M. Dris and Eric S.G. Shaqfeh, "Experimental and theoretical observations of elastic instabilities in eccentric cylinder flows: local versus global instability". Journal of Non-Newtonian Fluid Mechanics, vol. 80, Issue 1, pp. 1-58, (**1998**).

[110] C. Shu, L. Wang, Y. T. Chew, and N. Zhao, "Numerical study of eccentric Couette-Taylor flows and effect of eccentricity on flow patterns", Theor. Comp. Fluid Dyn. 18 (1), pp. 43-59, (**2004**).

[111] Cadot, O., Couder, Y., Daerr, A., Douady, S. and Tsinober, A., "Energy injection in closed turbulent flows: stirring through boundary layers versus inertial stirring", Phys. Rev. E 56, pp.427-433, (**1997**).

[112] Van den Berg, T. H., Doering, C. R., Lohse, D. and Lathrop, D. P., "Smooth and rough boundaries in turbulent Taylor-Couette flow", Phys. Rev. E 68, 036307, (**2003**).

[113] C. Y. Wang et C. F. Tsai, "Torque and forces resulting from the rotation of two longitudinally cylinders separated by a viscous fluid", Phys. Fluids. vol.29, (**1986**).

[114] Zhu, X., Ostilla-mónico, R., Verzicco, R. and Lohse, D., "Direct numerical simulation of Taylor-Couette flow with grooved walls: torque scaling and flow structure", J. Fluid Mech. 794, pp.746-774, (**2016**).

[115] Zhu, X., Verschoof, R. A., Bakhuis, D., Huisman, S. G., Verzicco, R., Sun, C. and Lohse, D., "Wall roughness induces asymptotic ultimate turbulence", Nat. Phys. 14, pp.417-423, (**2018**).

[116] Berghout, P., Zhu, X., Chung, D., Verzicco, R., Stevens, R. J. A. M. and Lohse, D., "Direct numerical simulations of Taylor-Couette turbulence: the effect of sand grain roughness", J. Fluid Mech., vol. 873, pp.260-286, (**2019**).

[117] D. Bakhuis , R. Ezeta , P. Berghout , P. A. Bullee , D. Tai , D. Chung , R. Verzicco , D. Lohse , S. G. Huisman and C. Sun, "Controlling secondary flow in Taylor-Couette turbulence through spanwise-varying roughness", J. Fluid Mech., vol. 883, A15, (**2020**).

[118] Cole, J. A., "Taylor vortex instability and annulus-length effects", J. Fluid Mech, vol.75, pp.1-15, (**1976**).

[119] T. B. Benjamin and T. Mullin, "Anomalous modes in the Taylor experiment", Proc. R. Soc. London Ser. A 377, 221, (**1981**).

[120] A. Kageyama, H-T. Ji, J. Goodman, F. Chen, and E. Shoshan, "Numerical and experimental investigation of circulation in short cylinders", J. Phys. Soc. Jap. vol.73, pp.2424-2437, (**2004**).

[121] V. Sobolík, B. Izrar, F. Lusseyran, and S. Skali, "Interaction between the Ekman layer and the Couette-Taylor instability", Int. J. Heat. Mass. Transfer, 43: pp.4381-4393, (**2000**).

[122] Sparrow, E. M., W. D. Munro, and V. K. Jonsson, "Instability of the flow between rotating cylinder: the wide-gap problem," J. Fluid Mech, vol.20, pp.35-46 (**1964**).

[123] Q. Xiao, T. T. Lim, and Y.T. Chew, "Second Taylor vortex flow: Effects of radius ratio and aspect ratio", Phys. Fluids 14(4), pp.1537-1539, (**2002**).

[124] Biage, M., and Campos, J.C.C., "Visualization study and quantitative velocity measurements in turbulent Taylor-Couette flow tagging: a description of the transition to turbulence", J. Braz. Soc. Mech. Sci. Eng. 25 (4), pp.378-390, (**2003**).

[125] Benjamin, T. B., "Bifurcation Phenomena in Steady Flows of a Viscous Fluid. I. Theory", Proc. Roy. Soc. London A., vol. 359, pp. 1-26, (**1978a**).

[126] Benjamin, T. B., "Bifurcation Phenomena in Steady Flows of a Viscous Fluid. II. Experiments", Proc. Roy. Soc. London A., vol. 359, pp. 27-43, (**1978b**).

[127] Blennerhassett, P. J. and Hall, P., "Centrifugal Instabilities of Circumferential Flows in Finite Cylinders: Linear Theory", Proc. Roy. Soc. London A., vol. 365, pp. 191-207, (**1979**).

[128] Ohmura, N., Kataoka, K., Kataoka, T. and Naitoh, Y., "Numerical and Experimental Study of Bifurcation Phenomena in a Finite-Length Taylor-Couette Flow", ASME/STLE Tribology Conference, (**1994**).

[129] M. Douaya, "Analyse des transitions dans l'écoulement de Taylor-Couette à faible rapport d'aspect ", Doctorat de l'INPL, Nancy- France (**1989**).

[130] D. Walgraef, "Onset of wavy Taylor vortex flow in finite geometries", Phys. Rev. A 29, 1514-1519, (**1984**).

[131] P. Bontoux, "Spiral and wavy vortex flows in short counter- rotating Couette Taylor cells", 12th International Couette- Taylor Workshop, Evanston, USA, (**2001**).

[132] Donnelly, R.J., "Experiments on the stability of viscous low between rotating cylinder. III. Enhancement of stability by modulation", Proc. R. Soc. Lond. A 281:130-139, (**1964**).

[133] P. Hall, "The stability of unsteady cylinder flows", J. Fluid Mech, vol. 67, part 1.(**1975**).

[134] F. Marques and M. Lopez, "Taylor-Couette flow with axial oscillations of the inner cylinder; Floquet analysis of the basic flow", J. fluid Mech, vol.348, (**1997**).

[135] Lopez, J. M, and Marques, F., "Modulated Taylor-Couette flow: onset of spiral modes", Theor .Comput. Fluid. Dyn, 16(1):59-69, (**2002**).

[136] Lopez, J. M, and Marques, F., "Spatial and temporal resonances in a periodically forced hydrodynamic system", Phys D 136(3-4):340–352, (**2002**).

[137] Aouidef. A, "Centrifugal instability of pulsed flow", Phys Fluids 6: pp.3665-3676, (**1994**).

[138] Barenghi, C. F., Jones, C. A, "Modulated Taylor-Couette flow", J. Fluid Mech, vol.208, pp.127-160, (**2006**).

[139] Walsh, T. J., "The influence of external modulation on the stability of azimuthal Taylor-Couette flow: an experimental investigation". PhD. thesis University of Oregon, (**1988**).

[140] Walsh, T. J., Donnelly, R. J., "Stability of modulated Couette flow". Phys. Rev. Lett 58: pp.2543-2546, (**1988**).

[141] Feugaing, M. G., Crumeyrolle, O., and Mutabazi, I., "Etude expérimentale de l'écoulement de Couette-Taylor avec modulation de fréquence". 20eme CFM, (**2011**).

[142] M. Sinha, "Spatial response of wavy vortex flow to axial oscillations of the inner cylinder", 12th international Taylor-Couette workshop; USA (**2001**).

[143] Oualli, H., Lalaoua, A., Hanchi, S. and Bouabdallah, A., "Taylor-Couette flow control using the outer cylinder cross-section variation strategy", Eur. Phys. J. Appl. Phys, 61(1), (**2013**).

[144] Lalaoua, A., and Bouabdallah, A.,"On the onset of Taylor vortices in finite-length cavity subject to a radial oscillation motion", J. Appl. Fluid. Mech,9(4):pp.1887-1896, (**2016**).

[145] Khlebutin, G. N., "Stability of Fluid Motion Between a Rotating and Stationary Concentric Sphere", Fluid Dyn., 3(6), pp. 31, (**1968**).

[146] Nakabayashi, K., Tsuchida, Y., and Zheng, Z., "Characteristics of Disturbances in the Laminar Turbulent Transition of Spherical Couette Flow" Part 1: Spiral Taylor-Görtler Vortices and Travelling Waves for Narrow Gaps", Phys. Fluids, 14(11), pp.3963-3972, (**2002**).

[147] Marcus, P. S., and Tuckerman, L. S., “"Simulation of Flow Between Concentric Rotating Spheres-Part 2: Transitions", J. Fluid Mech., 185, pp. 31-65, (**1987**).

[148] Wimmer, M., "Viscous Flow and Instabilities Near Rotating Bodies", Prog. Aerosp. Sci., 25(1), pp. 43-103, (**1988**).

[149] Bühler, K., "Symmetric and Asymmetric Taylor Vortex Flow in Spherical Gaps", Acta Mech., 81(1), pp. 3-38, (**1990**).

[150] Egbers, C., and Rath, H. J., "The Existence of Taylor Vortices and Wide-Gap Instabilities in Spherical Couette Flow", Acta Mech., 111, pp. 125-140, (**1995**).

[151] Yuan, L., "Numerical Investigation of Wavy and Spiral Taylor-Görtler Vortices in Medium Spherical Gaps", Phys. Fluids, 24(12), pp. 124104, (**2012**).

[152] Tigrine, Z., Mokhtari, F., Bouabdallah, A., and Mahloul, M., "Experiments on Two Immiscible Fluids in Spherical Couette Flow", Acta Mech., 225(1), pp. 233–242, (**2014**).

[153] A., Lalaoua and A., Bouabdallah, "A Numerical Investigation on the Onset of the Various Flow Regimes in a Spherical Annulus", J. Fluids Eng, vol. 138, issue 11 (**2016**).

[154] M. N. Noui-Mehidi, N. Ohmura, and K. Kataoka., "Mechanism of Mode Selection for Taylor Vortex Flow between Coaxial Conical Rotating Cylinders", J. Fluids and Structures, 16: pp.247-262, (**2002**).

[155] M. N. Noui-Mehidi, N. Ohmura, and K. Kataoka., "Dynamics of the helical flow between rotating conical cylinders", J. Fluids and Structures, 20: pp.331-344, (**2005**).

[156] M. Wimmer., "An experimental investigation of Taylor vortex flow between conical cylinders", J. Fluid Mech, 292: pp.205-227, (**1995**).

[157] M. Wimmer., "Taylor vortices at different geometries". Lecture Notes in Physics (Springer-Verlag), 549: pp.194-212, (**2000**).

[158] Y. Yamada and M. Ito., "Frictional Resistance of Enclosed Rotating Cones With Superposed Through flow", J. Fluids Eng, 101: pp.259-264, (**1979**).

[159] Marcus, P. S., "Simulation of Taylor-Couette flow. Part 2. Numerical results for wavy vortex flow with one travelling wave", J. Fluid Mech, vol.146, pp.65-113, (**1984**).

[160] K. Avila and B. Hof, "High-precision Taylor-Couette experiment to study subcritical transitions and the role of boundary conditions and size effects," Rev. Sci. Instrum., vol. 84, pp.065106, (**2013**).

[161] Griffini, D., Insinna, M., Salvadori, S., Barucci, A., Cosi, F., Pelli, S., and Righini, G. C., "On the CFD Analysis of a Stratified Taylor-Couette System Dedicated to the Fabrication of Nanosensors", Fluids, 2, 8, (**2017**).

[162] Froitzheim , S. Merbold and C. Egbers., "Velocity profiles, flow structures and scalings in a wide-gap turbulent Taylor-Couette flow", J. Fluid Mech., vol. 831 , pp. 330-357, (**2017**).

[163] Brauckmann, H. J., Salewsky, M. and Eckhardt, B., "Momentum transport in Taylor–Couette flow with vanishing curvature", J. Fluid Mech., vol. 790, pp.419-452, (**2016**).

[164] Chouippe, A., Climent, E., Legendre, D. and Gabillet, C., "Numerical simulation of bubble dispersion in turbulent Taylor-Couette flow", Phys. Fluids, vol. 26, 043304, (**2014**).

[165] Grossmann S., Lohse D. and Sun C., "High-Reynolds number Taylor-Couette turbulence", Annu. Rev. Fluid Mech. vol. 48, pp.53-80, (**2016**).

[166] Mullin, T., Heise, M., and Pfister, G., "Onset of cellular motion in Taylor-Couette flow", Phys. Rev. Fluids, vol. 2, 081901(R), (**2017**).

[167] Yavorskaya, I. M., Belyaev, Yu.N. and Monakhov, A. A., "Investigation of the Stability and Secondary Flows in Rotating Spherical Fluid Layers at Arbitrary Rossby Numbers", Dokl. Akad. Nauk. SSSR. vol. 237 (4), 804 (**1977**).

[168] Nakabavashi, K., "Frictional Moment of Flow Between Two Spheres, one of which Rotates", ASME J. Fluids Eng., vol. 100, 97, (**1978**).

[169] Marcus, P. S., and Tuckerman, L. S., "Simulation of Flow Between Concentric Rotating Spheres, Part 1. Steady states", J. Fluid Mech., vol. 185, pp.1-30, (**1987a**).

[170] Hollerbach, R., "Time-Dependent Taylor Vortices in Wide-Gap Spherical Couette Flow", Phys. Rev. Lett; vol. 81: 3132 (**1998**).

[171] Peralta, C., Melatos, A., Giacobello, M. and Ooi, A., "Superfluid Spherical Couette Flow", J. Fluid Mech., vol. 609, pp.221-274, (**2008**).

[172] Bühler, K., "Pattern Formation in Rotating Fluids", J. Therm. Sci., vol. 18, pp.109-118, (**2009**).

[173] Wimmer, M., "Strömungen zwischen rotierenden Ellipsen", ZAMM, vol. 69, pp.616-619, (**1989**).

[174] Wimmer, M., "Vortex patterns between cones and cylinders", In Ordered and turbulent patterns in Taylor-Couette flow. Eds.: C. D. Andereck, F. Hayot. NATO ASI Series B. Physics 297, Plenum Press N. Y. pp. 205- 211, (**1992**).

[175] Abboud, M., "Numerical research into Taylor vortices in the cleft between a cone and a cylinder" Z. Angew. Math. Mech., vol. 70: T441-442, (**1990**).

[176] Ning, L., Ahlers, G., and Cannel, D.S., "Wave-number selection and traveling vortex waves in spatially ramped Taylor-Couette flow", Phys. Rev. Lett., vol. 64, pp. 1235-1238, (**1990**).

[177] Denne, B., and Wimmer, M., "Travelling Taylor vortices in closed systems" Acta Mech., vol. 133, pp. 69-85, (**1999**).

[178] Sprague, M. A., Weidman, P. D., Macumber, S., and Fischer, P. F., "Tailored Taylor vortices" Phys. Fluids, vol. 20, 014102 (**2008**).

[179] Parker, J., and Merati, P., "An Investigation of Turbulent Taylor-Couette Flow using Laser Doppler Velocimetry in a Refractive Index Matched Facility" Trans. ASME., vol. 118, pp.810-818, (**1996**).

[180] DiPrima, R.C., Eagles, P.M. and Ng, B.S., "The effect of radius ratio on the stability of Couette flow and Taylor vortex flow", Phys. Fluids, vol. 27(10): pp. 2403-2411, (**1984**).

[181] Tokgoz, S., Elsinga, G. E., Delfos, R., and Westerweel, J., "Spatial resolution and dissipation rate estimation in Taylor-Couette flow for tomographic PIV", Exp. Fluids, vol. 53: pp. 561-583, (**2012**).

[182] Viazzo, S., and Poncet, S., "Numerical simulation of the flow stability in a high aspect ratio Taylor-Couette system submitted to a radial temperature gradient", Computers & Fluids, vol. 101: pp. 15-26, (**2014**).

[183] Avgousti, M. and Beris, A. N., "Viscoelastic Taylor-Couette flow: bifurcation analysis in the presence of symmetries", Proc. R. Soc. London. Ser A 443, pp. 17-37, (**1993**).

[184] Batra, R. L. and Das, B., "Flow of a Casson fluid between two rotating cylinders", Fluid dynamics research, vol. 9: pp. 133, (**1992**).

[185] Baumert, B. M. and Muller, S. J., "Flow regimes in model viscoelastic fluids in a circular Couette system with independently rotating cylinders", Phys. Fluids, vol. 9: pp. 566, (**1997**).

[186] Groisman, A. and Steinberg, V., "Solitary Vortex Pairs in Viscoelastic Couette Flow" Phys. Rev. Lett., vol. 78: pp. 1460, (**1997**).

[187] Khayat, R. E., "Onset of Taylor vortices and chaos in viscoelastic fluids", Phys. Fluids, vol 7: pp. 2191, (**1995**).

[188] Kapitza, P.L., Journal of Physics, USSR 4, vol. 181: (**1941**).

[189] Chandrasekhar, S., and Donnelly, R.J., "The hydrodynamic stability of He II between rotating cylinders", I. Proc. Royal Society A 241, pp. 9-28, (**1957**).

[190] R. Donnelly, "Experiments on the hydrodynamic stability of helium II between rotating cylinders," Phys. Rev. Lett., vol. 3, pp.507-508, (**1959**).

[191] R. Donnelly and M. LaMar, "Flow and stability of helium II between concentric cylinders," J. Fluid Mech., vol. 186, pp.63-198, (**1988**).

[192] Barenghi, C.F., and Jones, C.A., "The stability of the Couette flow of helium II", J. Fluid. Mech, vol. 197: pp. 551-569, (**1988**).

[193] Swanson, C.J., and Donnelly, R.J., "Instability of Taylor-Couette flow of helium II", Phys. Rev. Lett., vol. 67: pp. 1578-1581, (**1991**).

[194] Barenghi, C.F., "Vortices and the Couette flow of helium II", Physical Review B 45, pp. 2290-2293, (**1992**).

[195] Henderson, K.L., and Barenghi, C.F., "Calculation of the torque in nonlinear Taylor vortex flow of helium II", Physics Letters A 191, pp. 438-442, (**1994**).

[196] Henderson, K.L., Barenghi, C.F., and Jones, C.A., "Nonlinear Taylor-Couette flow of helium II", J. Fluid Mech, vol. 283: pp. 329-340, (**1995**).

[197] Henderson, K.L., and Barenghi, C.F., "Numerical methods for helium's two fluid model", J. Low Temperature Physics, vol. 98: pp. 351-381, (**1995**).

[198] Donnelly, R.J., and Barenghi, C.F., "The observed properties of liquid helium at the saturated vapour pressure", J. Phys. and Chem. Ref. Data, vol. 27: pp. 1217-1274, (**1998**).

[199] Henderson, K.L., and Barenghi, C.F., "The anomalous motion of superfluid helium in a rotating cavity", J. Fluid Mech, vol. 406: pp. 199-219, (**2000**).

[200] Henderson, K.L., and Barenghi, C.F.," Superfluid Couette flow in an enclosed annulus", Theoret. Comput. Fluid Dynamics, vol. 18: pp. 183-196, (**2004**).

[201] Henderson, K.L., and Barenghi, C.F., "Transition from Ekman flow to Taylor vortex flow in superfluid helium", J. Fluid Mech, vol. 508: pp. 319-331, (**2004**).

[202] Stewart, R.B., and Roder, H. M., "Properties of Normal and Parahydrogen. In Technology and uses of Liquid Hydrogen", Pergamon Press, New York, pp. 379-404, (**1964**).

[203] Webeler, R., and Bedard, F., " Viscosity Difference Measurements for Normal and Para Liquid Hydrogen Mixtures", Phys. Fluids 4, pp. 159-60, (**1961**).

[204] Beattie, J.A., "The Physical and Thermodynamic Properties of Helium", J. Am. Chem. Soc., vol. 80 (1): pp. 252-252, (**1958**).

[205] Carty, R. D. Mc, "Thermodynamic Properties of Helium 4 from 2 to 1500 K at Pressures to 10^8 Pa" Journal of Physical and Chemical Reference Data 2, vol. 923: (**1973**).

[206] Davison, H.W., "Compilation of thermophysical properties of liquid lithium", Scientific and technical information division, NASA TN D-4650. Washington, D.C. (**1968**).

[207] Jeppson, D. W., Ballif, J. L., Yuan, W. W., and Chou, B. E., "Lithium literature review: lithium's properties and interactions", Hanford Engineering Development Laboratory (**1978**).

[208] Crane, N. T., "Physical and Thermodynamic Properties of Lithium", Rep. FXM-4986, Pratt & Whitney Aircraft, (**1961**).

[209] Ahlers, G., Cannell, D.S., Dominguez-Lerma, M.A., Heinrichs, R., "Wavenumber selection and Eckhaus instability in Couette-Taylor flow", Physica D; 23: pp.202-219, (**1986**).

[210] Dominguez-Lerma, M.A., Cannell, D.S., Ahlers, G., "Eckhaus boundary and wave-number selection in rotating Couette-Taylor flow", Phys. Rev A; 34: pp. 4956-4970, (**1986**).

[211] Paap, H.G and Riecke, H., "Drifting vortices in ramped Taylor vortex flow: Quantitative results from phase equation", Phys. Fluids; A 3:1519, (**1991**).

[212] Cannel, D.S., Dominguez-Lerma, M.A., Ahlers, G., "Experiments on wave number selection in rotating Couette-Taylor flow", Phys Rev Lett; 50: pp. 1365-1368, (**1983**).

[213] Noui-Mehidi, M.N., Ohmura, N., Nishiyama, K., Takigawa, T., "Effect of wall alignment in a very short rotating annulus", Comm. Nonlinear. Sci. Num. Simulat; 14: pp. 613-621, (**2009**).

[214] Sprague, M.A., Weidman, P. D., "Continuously tailored Taylor vortices", Phys. Fluids; 21:114106, (**2009**).

[215] Savin. L., and Kornaeva. E., "Modeling of Fluid Flow in the Cone Seal", Procedia Engineering; 39: pp. 132-139, (**2012**)

[216] Raju, V.R.K., "Taylor vortices in the flow between two coaxial cylinders one of which has a step change in radius", Fluid. Dyn. Res; 46: 015506, (**2014**).

[217] Wimmer, M., "Experiments on a Viscous Fluid Flow Between Concentric Rotating Spheres", J. Fluid Mech, vol. 78: 317, (**1976**).

[218] Hollerbach, R., "A spectral solution of the magneto-convection equations in spherical geometry", Int. J. Numer. Meth. Fluids, vol. 32: pp. 773-797, (**2000**).

[219] Hollerbach, R. and Skinner, S., "Instabilities of magnetically induced shear layers and jets", Proc. R. Soc. London A, vol. 457: pp. 785–802, (**2001**).

[220] Schmitt, D., Alboussiere, T., Brito, D., Cardin, P., Gagnière, N., Jault, D., and Nataf, H.-C., "Rotating spherical Couette flow in a dipolar magnetic field: Experimental study of magneto-inertial waves", J. Fluid Mech, vol. 604: pp. 175-197, (**2008**).

[221] Nataf, H.-C., Alboussiere, T., Brito, D., Cardin, P., Gagnière, N., Jault, D. and Schmitt, D., "Rapidly rotating spherical Couette flow in a dipolar magnetic field: An experimental

study of the mean axisymmetric flow", Physics of the Earth and Planetary Interiors, vol.170: pp. 60-72, (**2008**).

[222] Travnikov, V., Eckert, K., and Odenbach, S., "Influence of an axial magnetic field on the stability of spherical Couette flows with different gap widths", Acta Mech, vol. 219: pp. 255-268, (**2011**).

[223] Gissinger, C., Ji, H., and Goodman, J., "Instabilities in magnetized spherical Couette flow", Phys. Rev. E, vol. 84: 026308, (**2011**).

[224] Kaplan, E., "On the saturation of non-axisymmetric instabilities of magnetized spherical Couette flow", Phys. Rev. E, vol. 89: 063016, (**2014**).

[225] Lalaoua, A. and Bouabdallah, A., "Effect of a dipolar magnetic field on the stability of spherical Taylor vortex flow", 8th Inter. Conf. on Elec. Proce. Materials, EPM (**2015**).

[226] Dormy, E., Jault, D. and Soward, A. M., "A super-rotating shear layer in magnetohydrodynamic spherical Couette flow", J. Fluid Mech., vol. 452: pp. 263-291, (**2002**).

[227] Hollerbach, R., Canet, E. and Fournier, A., "Spherical Couette flow in a dipolar magnetic field", European Journal of Mechanics B/Fluids, vol. 26: pp. 729-737, (**2007**).

[228] Cardin, P., Brito, D., Jault, D., Nataf, H.-C. and Masson, J.-P." Towards a rapidly rotating liquid sodium dynamo experiment", Journal of MHD, vol. 38: pp. 177-189, (**2002**).

[229] Kelley, D. H., Triana, S. A., Zimmerman, D. S., Tilgner, A., and Lathrop, D. P., "Inertial waves driven by differential rotation in a planetary geometry", Geophysical and Astrophysical Fluid Dynamics, vol. 101: pp. 469-487, (**2007**).

[230] Sisan, D. R., Mujica, N., Tillotson, W. A., Huang, Y.-M., Dorland, W., Hassam, A. B., Antonsen, T. M., and Lathrop, D. P., "Experimental Observation and Characterization of the Magnetorotational Instability", Phys. Rev. Lett., vol. 93: 114502, (**2004**).

Résumé

L'étude des écoulements rotatifs fait actuellement l'objet de plusieurs travaux et constitue une grande richesse phénoménologique, notamment dans l'apparition des différentes instabilités, des motifs d'écoulement ainsi que de la transition laminaire-turbulent. Parmi les systèmes d'écoulement rotatif les plus largement utilisés, le dispositif connu sous le nom de Taylor-Couette, fluide évoluant dans un espace annulaire entre deux corps rotatifs, qui est surtout connu pour son rôle dans le développement de la théorie de la stabilité hydrodynamique. En effet, l'examen des écoulements entre deux corps coaxiaux rotatifs tels que cylindres, sphères, cônes ou combinaison entre eux reste difficile à appréhender en raison du caractère tridimensionnel et instable du processus de transition.
Dans ce travail, les structures d'écoulement et l'apparition des différentes instabilités entre deux corps rotatifs (cylindres, sphères, cônes) et les combinaisons entre eux sont étudiés numériquement à l'aide du code de simulation Ansys-Fluent pour des écoulements tridimensionnels et incompressibles. Un accent particulier est mis sur la première apparition et le développement ultérieur des instabilités. Le but de l'étude dans cette thèse est de fournir plus de détails sur les caractéristiques d'écoulement dans l'anneau entre les différents corps coaxiaux. Tous les corps testés, cylindres, sphères et cônes et combinaison entre eux sont des corps de révolutions symétriques autour de l'axe de rotation.

La stratégie de modélisation a été développée dans ce travail en étudiant 4 paramètres d'écoulement de fluide différents :

- Écoulement entre deux sphéro-cylindres rotatifs (combinaison cylindres-sphères).
- Écoulement entre deux cylindres coniques rotatifs (combinaison cylindres-cônes).
- Effet du fluide de travail confiné entre deux cylindres en rotation sur l'apparition des tourbillons de Taylor.
- Effet du champ magnétique dipolaire sur la stabilité d'un fluide conducteur contenu entre deux sphères en rotation.

Abstract

The study of rotating flows is currently the subject of several works and constitutes a great phenomenological wealth, particularly in the occurrence of different instabilities, flow patterns as well as the laminar-turbulent transition. Among the most widely used rotating flow systems, the device known as Taylor-Couette, fluid evolving in an annular gap between two rotating bodies, which is most famous for its role in the development of hydrodynamic stability theory. Indeed, the examination of flows between two rotating coaxial bodies such as cylinders, spheres, cones or combination between them remain difficult to understand because of the three-dimensional and unsteady nature of the transition process.
In this work, the flow patterns and the onset of various instabilities between two rotating bodies and combinations between them are investigated numerically using the simulation code Ansys-Fluent for three-dimensional and incompressible flows. Special emphasis is placed on the first onset and the further development of instabilities. The aim of the study in this thesis is to provide further details on the flow features in the annulus between different coaxial bodies. All the bodies tested, cylinders, spheres, and cones and combination between them are bodies of revolutions with symmetry about the axis of rotation.

The modeling strategy has been developed in this work by studying 4 different fluid flow settings:

- Flow between two rotating sphero-cylinders (cylinders-spheres combination).
- Flow between two rotating conical cylinders (cylinders-cones combination).
- Effect of the working fluid confined between two rotating cylinders on the onset of Taylor vortices.
- Effect of dipolar magnetic field on the stability of a conducting fluid contained between two rotating spheres.

ملخــص

تعد دراسة التدفقات الدوارة حاليًا موضوعًا للعديد من الأعمال وتشكل ثروة ظاهرية كبيرة ، لا سيما في ظهور العديد من حالات عدم الاستقرار وأنماط التدفق وكذلك الانتقال المضطرب. من بين أنظمة التدفق الدوراني الأكثر استخدامًا ، الجهاز المعروف باسم Taylor-Couette ، وهو سائل يتحرك في فراغ حلقي بين جسمين في حالة الدوران ، والذي اشتهر بدوره في تطوير نظرية الاستقرار. في الواقع ، لا يزال من الصعب فهم فحص التدفقات بين جسمين محوريين دائريين مثل الأسطوانات أو الكرات أو المخاريط أو الجمع بينهما بسبب الطبيعة ثلاثية الأبعاد وغير المستقرة لعملية الانتقال .في هذا العمل ، تمت دراسة طبيعة التدفق وظهور حالات عدم استقرار مختلفة بين جسمين في حالة الدوران (أسطوانات ، كرات ، مخاريط) والتوليفات بينهما باستخدام برنامج محاكاة Ansys-Fluent للتدفقات ثلاثية الأبعاد وغير القابلة للضغط. يتم التركيز بشكل خاص على الظهور الأول والتطور اللاحق لحالة عدم الاستقرار.

الهدف من الدراسة في هذه الأطروحة هو تقديم مزيد من التفاصيل حول خصائص التدفق في الحلقة بين الأجسام المحورية المختلفة. جميع الأجسام والأسطوانات والأشكال الكروية و المخاريط المختبرة والجمع بينها عبارة عن أجسام متناظرة حول محور الدوران.

تم تطوير إستراتيجية المحاكاة في هذا العمل من خلال دراسة 4 نماذج مختلفة لتدفق السوائل:

- التدفق بين أسطوانتين كرويتين في حالة الدوران (تركيبة كروية أسطوانية).
- التدفق بين أسطوانتين مخروطيتين في حالة الدوران (تركيبة أسطوانة مخروطية).
- تأثير سائل العمل المحصور بين أسطوانتين في حالة الدوران على ظهور دوامات تايلور.
- تأثير المجال المغناطيسي ثنائي القطب على ثبات مائع موصل محصور بين كرتين في حالة الدوران.